Investigating the effects of varying levels of EB2 expression on migration in cancer cells

Jasmine Render
100205070

i. Abstract

Metastasis is the process whereby cancer cells migrate from the primary tumour to other tissues and organs where they colonise and form new tumours and metastasis is responsible for the majority of cancer associated deaths. End-binding protein 2 (EB2) is a microtubule (MT) associated protein that associates with the plus-end of MTs. EB2 has been shown to play a role in MT organisation and contributes to efficient cell migration, however its full functional role is currently unknown. EB2 is overexpressed in a variety of cancer types and therefore it is essential that the effects of varying EB2 expression be investigated. Additionally, the mechanism by which EB2 expression is regulated has not yet been identified and it has been suggested that fibroblast growth factor receptor 3 (FGFR3) promotes MT associated protein 2 (MAPRE2) expression. Therefore, the objective of this investigation was to further investigate the functional role of EB2 in cell migration and determine whether FGFR3 effects EB2 expression. Two cell lines were used in this study, the pancreatic cancer cell line PANC1 and the breast cancer cell line MDA-MB-231. PANC1 cells were subcloned for increased and decreased EB2 expression ($PANC1^{EB2Hi}$ and $PANC1^{EB2Low}$ cells) and MDA-MB-231 cells with a partial EB2 knockout (MDA^{EB2KO}) in addition to wildtype MDA-MB-231 cells (MDA^{WT}) were used. To determine whether EB2 expression is affected by FGFR3, $PANC1^{EB2Hi}$ and $PANC1^{EB2Low}$ cells were treated with an FGFR inhibitor. Fluorescence intensity analysis of EB2 determined that there was no significant difference in EB2 fluorescence following FGFR inhibition in $PANC1^{EB2Low}$ cells and a significant decrease in EB2 fluorescence in FGFR inhibited $PANC1^{EB2Hi}$ cells. However, as the significant decrease in intensity in $PANC1^{EB2Hi}$ cells was only slight and there was no change in $PANC1^{EB2Low}$ cells, it was concluded that FGFRs do not affect the expression of EB2 in PANC1 cells, suggesting that EB2 expression must be regulated through a different mechanism. Immunofluorescence labelling for MTs in $PANC1^{EB2Hi}$ and $PANC1^{EB2Low}$ cells demonstrated that $PANC1^{EB2Hi}$ cells have a more polarised MT organisation and thus a more migratory phenotype. This is supported by time-lapse imaging of MDA^{WT} and MDA^{EB2KO} cells that showed that MDA^{WT} cells had a higher migration velocity. Furthermore, immunolabelling for proteins involved in cell migration (GEF-H1, pMLC, mDia1, dynamin2) as well as the cytoskeleton (MTs and actin) determined the effects of varying EB2 expression on cell migration. The organisation and localisation of these proteins in migrating $PANC1^{EB2Hi}$ cells suggests that these proteins are essential for cell migration and that EB2 may have an effect on these proteins. It was found that dynamin2 localises along the leading edge of migrating cells and strongly appears to co-localise with EB2, which builds off of previous work in the Mogensen lab to suggest that these two proteins interact. While the function of this co-localisation is unknown, it appears from the immunofluorescence labelling that these proteins may interact at focal adhesions. Additionally, migrating $PANC1^{EB2Hi}$ and $PANC1^{EB2Low}$ cells were treated with the ROCK inhibitor, Y27632, and the fluorescence intensity of GEF-H1 significantly increased. Therefore, in $PANC1^{EB2Hi}$ cells, when ROCK is inhibited, it appears that the concentration of GEF-H1 increases, suggesting that ROCK inhibition leads to an increase in MT dynamics. In conclusion, this study contributes to the growing literature on the role of EB2, particularly in cell migration, and highlights several avenues for further investigation.

ii. Acknowledgements

I would like to thank Dr Mette Mogensen and Dr Jelena Gavrilovic for their invaluable support, guidance and feedback that she has provided throughout the project. In addition, I would also like to express my gratitude towards Benjamin Rix for all the help they gave me in the lab. Figure 7 was created with BioRender.com.

iii. Table of contents

iv. List of figures

v. List of tables

vi. Abbreviations

ADP - Adenosine diphosphate
AMT - Amoeboid-to-mesenchymal
Arp2/3 - Actin-related protein 2/3
ATP - Adenosine triphosphate
CDKL5 - Cyclin-dependent kinase-like 5
CH - Calponin homology
CSC-KT - Circumferential skin creases Kunze type
CTCF - Corrected total cell fluorescence
DMSO - Dimethyl sulfoxide
EB - End binding protein
EBH - End binding protein homology
ECM - Extracellular matrix
EGFR - Epidermal growth factor receptor
EMT - Epithelial-mesenchymal transition
ER - Estrogen receptor
FA - Focal adhesion
FAK - Focal adhesion kinase
FGF - Fibroblast growth factor
FGFR - Fibroblast growth factor receptor
FBS - Foetal bovine serum
G-actin - Globular actin
GAS2 - Growth arrest specific protein 2
GDP - Guanosine diphosphate
GEF - Guanine nucleotide exchange factor
G.S. - Goat serum
GTP - Guanosine triphosphate
HAX1 - HCLS1-associated protein X-1
HER2 - Human epidermal growth factor receptor 2
HCC - Hepatocellular carcinoma
HDAC6 - Histone deacetylase 6
IF - Intermediate filaments
IL - Interleukin
KD - Knockdown
KO - Knockout
MAPRE2 - Microtubule associated protein 2
MAP4K4 - Mitogen-activated protein kinase kinase kinase kinase 4
MAT - Mesenchymal-to-amoeboid
mDia1 - Diaphonous-related formin 1
MCP-1 - Monocyte chemotactic protein 1
MLC - Myosin light chain
MLCK - Myosin light chain kinase
MT - Microtubule
MTOC - Microtubule organising centre
PBS - Phosphate Buffered Saline

PDA - Pancreatic ductal adenocarcinoma
pMLC - Phosphorylated myosin light chain
PR - Progesterone receptor
RhoA - Ras homolog family member A
ROCK - Rho-associated coiled coil-containing kinase
RTK - Receptor tyrosine kinase
TNFα - Tumour necrosis factor α
VASP - Vasodilator-stimulated phosphoprotein
WASP - Wiskott-Aldrich syndrome protein
WAVE - WASP-family verpolin-homologous protein
WDHD1 - WD repeat and HMG-box DNA binding protein 1
γ-TuRC - Gamma-tubulin ring complex

Chapter 1.
Introduction

1.1 The cytoskeleton in cell migration and cancer

The cytoskeleton is composed of three types of structure (actin filaments, microtubules (MTs) and intermediate filaments (IFs)) and is responsible for several key functions, including connecting the cell to its external environment, maintaining cell morphology, and cell migration (Fletcher and Mullins, 2010). IFs are a family of proteins that share a common primary structure, an N-terminal, a central conserved α-helical rod domain and a C-terminal domain; both the N- and C-terminal domains vary considerably in their structure and composition (Parry et al., 2007). One of the primary functions of IFs is structural – providing mechanical support and cytoarchitecture – but other roles for IFs have been elucidated, including in cell migration (Coulombe and Wong, 2004). However, the focus of this investigation was on the other two cytoskeletal elements, actin and MTs, and the roles these structures play in cell migration.

Cell migration is vital for a number of processes including morphogenesis, wound healing and immune response; however, cell migration also contributes to a multitude of pathologies, including cancer (Trepat et al., 2012). The migration of cancer cells from the primary tumour to other tissues and organs is known as metastasis, and this migration allows cancer cells to colonise in these areas and form secondary tumours (Lawrence, 2016). The vast majority of cancer-associated deaths (~90%) are a result of metastasis as opposed to the primary tumour (Lambert et al., 2017) and thus this highlights the importance of research on cell migration. Two types of cancer that have been shown to be highly metastatic are breast and pancreatic cancer.

Globally, female breast cancer is the most frequently diagnosed form of cancer, accounting for 11.7% of cancer cases, and is the fourth leading cause of cancer death (6.9% of cases) – although it is the leading cause of cancer death in women (Sung et al., 2021). Despite this, the mortality rate from breast cancer has been decreasing, and it is expected that by 2025 pancreatic cancer will surpass breast cancer to become the third leading cause of cancer death in the European Union (Ferlay et al., 2016). Based on gene expression, breast cancer has been classified into four main molecular subtypes (although some further subtypes have been identified): luminal A, luminal B, HER2-enriched and basal/triple negative (the molecular characteristics of these subtypes can be seen in Table 1.) (Johnson et al., 2021; Dai et al., 2016). Breast cancer subtypes behave differently, notably in the metastatic progression of the disease; for example, in breast cancer patients who developed metastatic disease, patients with luminal A or luminal B less frequently had brain metastases (7.6% and 10.8% respectively) compared to HER2-enriched (28.7%) and basal-like (25.5%) (Kennecke et al., 2010).

Breast cancer subtype	**Expression profile**
Luminal A	ER and PR positive, HER2 and Ki67 negative
Luminal B	ER and PR positive, HER2 positive or negative, Ki67 positive
HER2-enriched	ER and PR negative, HER2 positive
Basal/triple negative	ER, PR and HER2 negative

Table 1. Breast cancer subtypes. ER = estrogen receptor, PR =progesterone receptor, HER2 = human epidermal growth factor receptor 2.

According to GLOBOCAN, pancreatic cancer had the seventh highest mortality rate from cancer worldwide, with 466,003 deaths and 495,773 new cases in 2020; rates of mortality and incidence of pancreatic cancer have remained stable or marginally increased (Sung et al., 2021). Additionally, as of 2020, the 5-year survival rate for pancreatic cancer was reported to be 9% (Siegel et al., 2020). The primary form of pancreatic cancer is pancreatic ductal adenocarcinoma (PDA), accounting for 95% of cases, and PDA has a multitude of genetic and lifestyle risk factors including, but not limited to, Lynch syndrome (8.6-fold increased risk), hereditary pancreatitis (69-fold increased risk), smoking (1.7–2.2-fold increased risk), type 2 diabetes (1.8-fold increased risk) and a high body mass index (1.5-fold increased risk for males and 2.8-fold for females) (Becker et al., 2014).

Cytoskeleton proteins are significantly involved in cell migration processes and in this study we investigated the effects of the MT associated protein, end-binding protein 2 (EB2), on cell migration. To do this two cancer cell lines were used, a pancreatic cancer cell line (PANC1) and a breast cancer cell line (MDA-MB-231). To investigate cell migration, live cell imaging and immunofluorescence techniques were used to examine how several proteins, including pMLC, GEF-H1, ROCK and dynamin2 contribute to migration processes in PANC1 and MDA-MB-231 cells with varying EB2 expression levels.

1.2 Microtubule structure, dynamics and function

Microtubules (MTs) are composed of heterodimers of α- and β-tubulin arranged linearly in polymers called protofilaments; 13 protofilaments associate laterally to form a hollow tube (Goodson and Jonasson, 2018). The tubulin dimers are arranged in a head-to-tail way, which provides MTs with intrinsic polarity; the α-tubulin exposed end is the minus-end and the β-tubulin exposed is the plus-end (Teixidó-Travesa et al., 2012). The minus end of MTs frequently associate to MT organising centres (MTOCs), which anchor, stabilise and nucleate these structures (Sanchez and Feldman, 2017). While the most common MTOC is the centrosome, which generates a radial MT organisation, other non-centrosomal MTOCs have been identified that are responsible for alternative MT organisations, such as the Golgi body which typically arranges MTs asymmetrically (Vinogradova et al., 2012) and, in skeletal muscle, the nuclear membrane organises MTs into parallel fibres (Sulimenko et al., 2017). However, despite the different MTOCs, all of these rely on a third type of tubulin, γ-tubulin, for MT nucleation (Kollman et al., 2011). In higher eukaryotes γ-tubulin forms a complex with several associated proteins to form the γ-tubulin ring complex (γ-TuRC). MTs are nucleated by the γ-TuRC; 13 γ-tubulin molecules bind to α- and β-tubulin dimers present in the cytosol which promotes lateral associations between the heterodimers to form 13 protofilaments (Tovey and Conduit, 2018; Böhler et al., 2021). In this way the γ-TuRC acts as a template for new MTs and allows them to bypass the lag phase and rapidly polymerise (Kollman et al., 2011).

MTs undergo a process called dynamic instability where the minus-end of MTs are anchored at MTOCs, while the plus-end is continually growing and shrinking. Dynamic instability is the process by which MTs undergo growth interrupted by a state of rapid shrinkage (MT catastrophe), which is subsequently followed by changing back to the growth phase (MT rescue) (Gardner et al., 2013) – this process is driven by GTP hydrolysis and is highlighted further in figure 1. Dynamic instability occurs primarily at the plus-end of MTs as the minus-ends are anchored at MTOCs (Goodson and Jonasson, 2018).

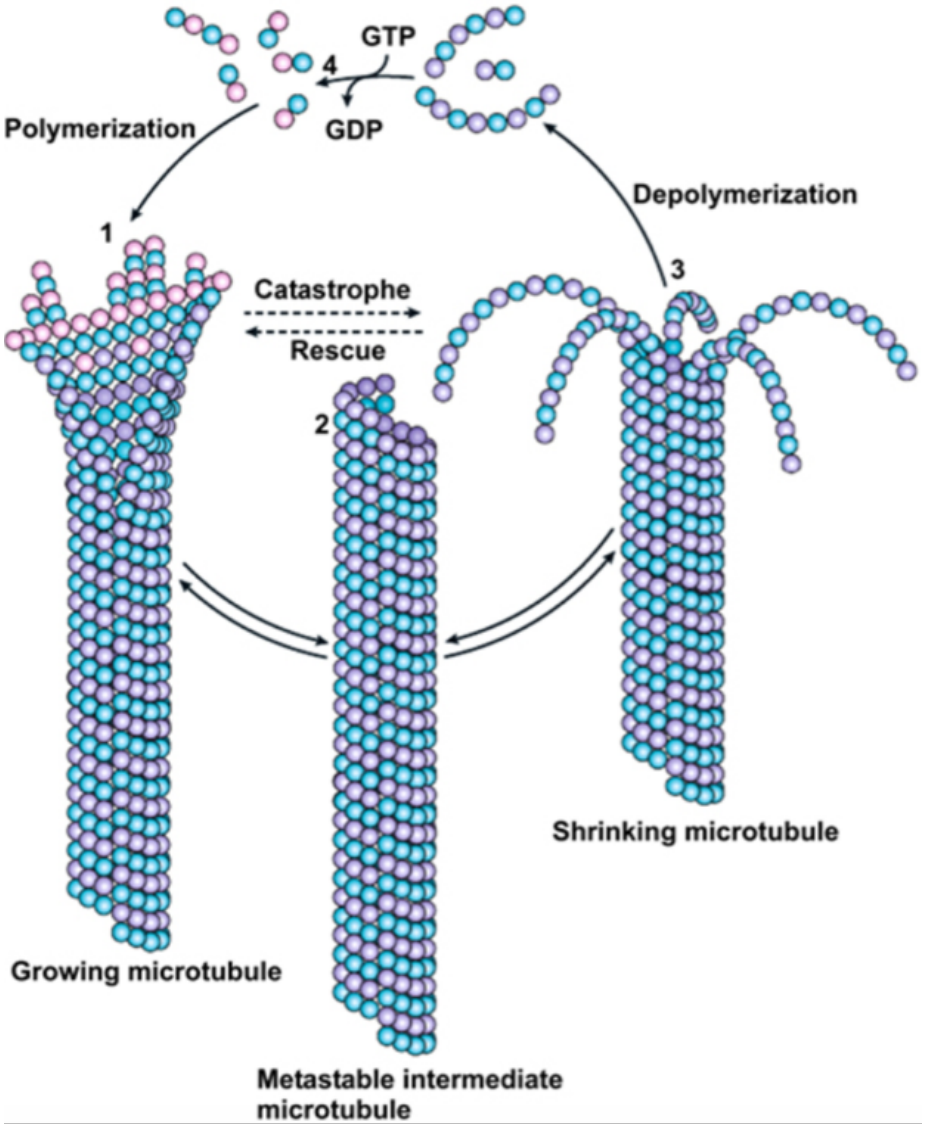

Figure 1. Microtubule (MT) dynamic instability. Structurally, the αβ-tubulin heterodimers contain a nonexchangeable site (N-site) located between the two monomers that constantly consists of GTP, and an exchangeable site (E-site) found on the β-tubulin subunit that catalyses GDP to GTP (van Haren and Wittmann, 2019). A delay in GTP hydrolysis occurs following MT assembly which causes the formation of a GTP cap at the plus-end and the loss of the GTP cap causes MTs to rapidly depolymerise as the unstable GDP-bound lattice is exposed (Mitchison and Kirschner, 1984) and thus the MT 'shrinks'. (Figure adapted from (Akhmanova and Steinmetz, 2008).)

1.3 End-binding proteins (EB1, EB2 and EB3) and MT dynamics

Microtubule associated proteins (MAPs) influence MT dynamics and especially the plus-end tracking proteins (+TIPs) which accumulate at the plus-end of growing MTs (Akhmanova and Hoogenrad, 2005). MT +TIPS are a diverse group of proteins that can be categorised according to their structural elements that allow them to interact with MTs and other +TIPs (Akhmanova and Steinmetz, 2010). End binding proteins (EBs) are a highly conserved family of +TIPs that consists of EB1, EB2 and EB3, which are encoded for by the genes MAPRE1, MAPRE2 and MAPRE3 respectively (Su and Qi, 2001). While many structural elements are consistent across all EB proteins, three structural differences have been identified in EB2, one in the C-terminal, an internal region near the coiled-coil domain and

a 42-amino acid N-terminal extension (Yue et al., 2014; Roth et al., 2018). Figure 2 further outlines the structure of EB proteins. The differences in the domains of the EB proteins affect their function, which is important as EB2 has a different function to EB1 and EB3.

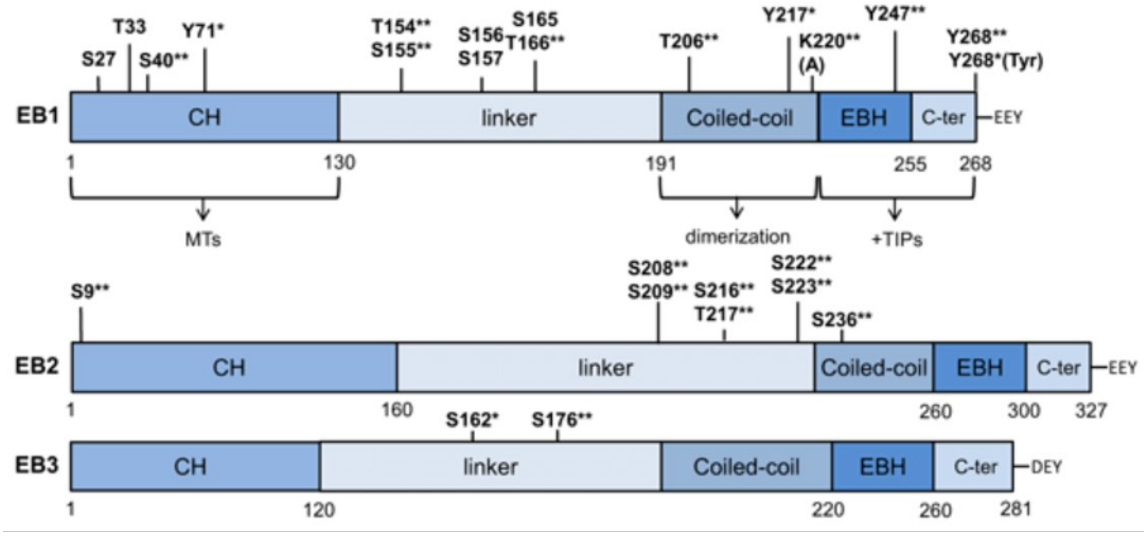

Figure 2. Structural domains of the EB family of +TIPs. Broadly the EB proteins are composed of the same domains, a calponin homology (CH) domain responsible for MT binding, a coiled-coil domain that mediates subunit oligomerisation, an end binding protein homology (EBH) domain located at the C-terminus and has a hydrophobic cavity that binding partners interact with, and a highly conserved EEY/F sequence motif that is targeted by the CAP-Gly domain proteins (Akhmanova and Steinmetz, 2008). (Figure adapted from (Nehlig et al., 2017))

In addition to differences in structure, the EB proteins are differentially distributed. EB1 and EB3 accumulate at the MT plus-end, which is due to EB1 having a ~10-fold higher binding affinity for GTP-bound tubulin which is found at the plus-end of MTs (GTP cap), compared to the GDP-tubulin lattice (Maurer et al., 2011; Roostalu et al., 2020). This contrasts with EB2, which is mainly found to associate along the MT lattice and has an affinity for GDP-tubulin (Roth et al., 2018). Moreover, EB1 knockdown has been shown to result in an upregulation of EB3, and vice versa, suggesting that these proteins have similar functions (Goldspink et al., 2013). This evidence suggests that EB2 has a functional role distinct from EB1 and EB3.

Treatment of glioblastoma cells with vorinostat, a histone deacetylase inhibitor, decreased the EB1 expression level while EB2 expression increased (Perez et al., 2021), which is further evidence that these proteins have different functions. EB2 has also been implicated in actin organisation. In highly nerve invasive pancreatic cancer cells with increased MAPRE2 expression, it was found that MAPRE2 colocalised with F-actin and that these cells had increased actin organisation, as well as an increase in the formation of stress fibres (Abiatari et al., 2009b). It has also been indicated that EB2 is involved in MT stabilisation; EB2 upregulation was found to be associated with increased histone deacetylase 6 (HDAC6), a tubulin deacetylase that decreases MT acetylation, thus causing MT destabilisation (Zhong et al., 2021).

EB2 in disease

Aberrations in MAPRE2 expression have been found to be the cause of some diseases.
In four unrelated individuals with cause circumferential skin creases Kunze type (CSC-KT), Isrie et al. identified two heterozygous nonsense mutations and two homozygous missense mutations in MAPRE2, and it is thought that these mutations may affect apical-basal epithelial differentiation through enhanced binding to MT plus-ends, therefore affecting MT reorganisation during this differentiation (Isrie et al., 2015). There has also been some indication that mutations in MAPRE2 are also associated with West syndrome (homozygous missense mutation in exon 4) (Gowda et al., 2021) and Brugada syndrome (Barc et al., 2022).

Moreover, EB2 has been found to be involved in several forms of cancer. Resistance to cisplatin, a chemotherapy drug used in the treatment of lung cancer, is a problem that has been investigated. It was found that the ubiquitin ligase WD repeat and HMG-box DNA binding protein 1 (WDHD1) is involved in cisplatin sensitivity in lung cancer (Gong et al., 2020). Gong et al. observed interaction between WHDHD1 and MAPRE2 in the nucleus; WHDHD1 promotes MAPRE2 ubiquitination, which results in increased cisplatin resistance in lung cancer (Gong et al., 2020). Therefore, as MAPRE2 seems to be involved in several aspects of cancer, it is important that the roles and mechanisms of action of this protein be elucidated.

Alternative splicing of MAPRE2 has been identified as a key splicing event in colon adenocarcinoma, and this splicing was found in three different colon cancer cell lines as well as determined to be involved in the immunity stage (Wu et al., 2020). The finding that the MAPRE2 alternative splicing had a strong association with T cell CD4 memory resting (Wu et al., 2020) is supported by a previous finding by Renner et al. that MAPRE2 is differentially expressed in activated T cells, but specifically MAPRE2 cDNA is highly expressed in activated CD4 and CD8 T cells and MAPRE2 was suggested to be involved in the control of the T cell receptor downstream signaling cascade (Renner et al., 1997). Additionally, one case of melanoma with a *MAPRE2-RAF1* fusion has been reported; oncogene fusion identification and targeting has been used to successfully treat several types of cancer, however, in this case treatment was unsuccessful (Lee et al., 2020).
Recently, EB2 has been shown to be upregulated in hepatocellular carcinoma (HCC) and that this overexpression was correlated with poor patient overall survival (Zhong et al., 2021). Zhong et al., indicated that EB2 may increase HDAC6 activity to destabilise MTs (Zhong et al., 2021).

High levels of EB2 expression have been linked to increased cell invasion in pancreatic cancer. Highly invasive pancreatic cancer nerve-invasive clones displayed upregulated MAPRE2 expression in three cell lines (PANC1, Colo357 and T3M4) (Abiatari et al., 2009a). Furthermore, EB2 upregulation promotes cell migration in hepatocellular carcinoma (HCC) and has been correlated with poor patient overall survival (Zhong et al., 2021).

1.4 Actin and Myosin II structure and function

Globular actin (G-actin) is a 42 kDa monomer that can bind to ATP and G-actin undergoes cycles of self-assembly to form actin filaments (F-actin) (Campellone and Welch, 2010). Actin polymerisation is tightly controlled and therefore the majority of G-actin monomers are bound to actin binding proteins, a diverse group of proteins that, dependent upon the protein family, preferentially bind to either ADP-G-actin or ATP-G-actin in order to prevent spontaneous actin polymerisation and

maintain a high concentration of G-actin (Xue and Robinson, 2013). The formation of F-actin is initiated by actin nucleators of which there are three classes: Arp2/3 complex, formins and tandem actin-binding domain nucleators (Rottner et al., 2017) (discussed further in section 1.5). Each G-actin monomer is organised in one direction which gives the filament polarity, with a myosin-coated barbed plus end and a pointed minus end (Higgs, 2013). Additionally, F-actin has a two-chained helical structure that has 13 subunits between every cross-over point with a 166° twist and 2.76 nm rise per molecule (Dominguez and Holmes, 2011).

A main function of actin is in several stages of cell migration, and parts of this function involves a member of the myosin superfamily, non-muscle myosin II (Conti and Adelstein, 2008). Structurally, non-muscle myosin II is a hexamer composed of three types of peptides that are arranged in pairs; these are two heavy chains, two regulatory light chains and two essential light chains (Vicente-Manzanares et al. 2009) - the regulatory and essential light chains together are called the myosin light chains (MLCs) (Brito and Sousa, 2020). Myosin II has been described as having two primary functions: 1) structural (through the formation of filaments myosin heads are able to hold tension for a long duration, and 2) as a motor, which is involved in several functions such as generating cell polarity through its distribution inside cells, and also in cell migration (Conti and Adelstein, 2008).

Myosin II activity is regulated via reversible phosphorylation of Ser19 and Thr18 of the regulatory light chain, which, when in the presence of actin, increases myosin II Mg^{2+}-ATPase activity; additionally, diphosphorylation can occur at both Ser19 and Thr18, however, while this does serve to further increase the myosin II Mg^{2+}-ATPase activity, it doesn't have an effect on the V_{max} of myosin II (Umemoto et al., 1989; Vicente-Manzanares et al. 2009). Several kinases have been identified that are able to phosphorylate the regulatory light chain, such as MLC kinase (MLCK) and Rho-associated coiled coil-containing kinase (ROCK) (Vicente-Manzanares et al. 2009). MLCK and ROCK differentially phosphorylate the light chain; when MLCK was inhibited in gerbil fibroma cells light chain phosphorylation was found to only be reduced at the periphery of the cells and not at the centre, whereas inhibition of ROCK found the reverse and, in addition, when both MLCK and ROCK were inhibited no enrichment of light chain phosphorylation was detected, indicating that MLCK and ROCK are the primary myosin kinases (Totsukawa et al., 2004). MLCK activity is regulated by Ca2+/calmodulin (Hartsthorne et al., 1998) while ROCK is activated by RhoA (Hartmann et al., 2015).

Rho GTPase signalling is initiated through plasma membrane receptors which activate guanine nucleotide exchange factors (GEFs); Rho is inactive in the GDP-bound form and GEFs catalyse the GDP to GTP exchange resulting in Rho activation (Bos et al., 2007). Conversely, GTPase activating proteins (GAPs) induce GTP hydrolysis to terminate Rho signalling (Bos et al., 2007).
The switch I and II regions of active GTP-RhoA bind to the ROCK Rho-binding domain (Dvorsky et al., 2004) and this results in an increase in ROCK activity through a conformational change in the kinase domain by the C-terminal (Hartmann et al., 2015). One of the substrates of ROCK is the MLC, and the phosphorylation of MLC allows myosin II to interact with F-actin and culminates in actomyosin contractility (Amano et al., 1996). In addition, ROCK stabilises F-actin via phosphorylating LIM kinase-1 and –2, which therefore inhibits cofilin activation and prevents cofilin-mediated F-actin disassembly (Amin et al., 2013). Moreover, RhoA also controls actin polymerisation through activation of the actin nucleation factor diaphonous-related formin 1 (mDia1) (Watanabe et al., 1999).

1.5 Actin filament nucleation and the role of Arp2/3 and formins

Actin filaments undergo a process called treadmilling, wherein ATP-bound G-actin monomers are added to the barbed end, while ADP-monomers dissociate from the filament at the pointed end (Fujiwara et al., 2007). The barbed ends of actin filaments have a 10 times higher affinity for phosphate than the pointed ends and therefore the monomers associate/dissociate slower at this end of the filament and, in addition, are more likely to hydrolyse the bound ATP to ADP before which then leaves ADP-actin exposed at the pointed end (Pollard, 2016). However, the treadmilling rate is gradual (<1 subunit/second) and thus isn't very involved in F-actin turnover (Pollard, 2016) and therefore cannot be responsible for the cellular F-actin assembly (Dominguez and Holmes, 2011).

As mentioned in section 1.4. actin polymerisation is a tightly controlled process. G-actin monomers undergo cycles of self-assembly to form F-actin, and this process is initiated by actin nucleators, primarily the actin-related protein 2/3 (Arp2/3) complex and formins (Campellone et al., 2010). Actin nucleators have roles in the formation of different types of actin structures, with formins assembling linear actin networks and the ARP2/3 complex involved in the formation of branched F-actin (Carlier and Shekhar, 2017).

Arp2/3 complex

The Arp2/3 complex is an actin nucleator that has been identified in a number of eukaryotic organisms, including humans, and it is composed of seven subunits (Arp2, Arp3, p14, p18, p19, p35 and p41) (Mullins and Pollard, 1999). The complex is activated by the Wiskott-Aldrich syndrome protein (WASP) and WASP-family verpolin-homologous protein (WAVE) families; the VCA domain of these proteins contains a central/connecting sequence and an acidic sequence that are responsible for Arp2/3 complex interaction, and also a WH2 and central C domain that binds to actin (Kurisu and Takenawa, 2009; Kelly et al., 2006). Upon binding of ATP, WASP/WAVE factors and F-actin, the Arp2 and Arp3 subunits form a dimer which acts as a template for the polymerisation of the new filament (Pizarro-Cerdá et al., 2017).

The Arp2/3 complex nucleates actin in a dendritic formation – the new actin filament is nucleated at a 70° angle from the side of an existing F-actin stucture – and this formation is essential for assembling several actin structures such as focal adhesions (FAs) and lamellipodia (Chesarone and Goode, 2009). These new F-actin structures elongate rapidly before a capping protein binds to the barbed end of the filament (Zigmond, 2004). Additionally, another actin nucleator, diaphonous-related formin 1 (mDia1), works alongside the Arp2/3 complex to initiate the formation of lamellipodia (Isogai et al., 2015).

mDia1

Formins are a family of proteins that have a highly conserved structure that contains two formin homology domains, FH1 and FH2, that are involved in actin assembly (Evangelista et al., 2003). mDia1 is a formin that in its native state has a molecular weight of ~267-282 kDa, however mDia1 is activated by RhoA and forms autoinhibited dimers with a weight of ~134-139 kDa; RhoA has a high affinity for the N-terminus of mDia1 and is able to activate mDia1 for actin assembly (Maiti et al.,

2012). The N-terminal Rho-binding domain selectively binds with GTP-bound RhoA, RhoB and RhoC (but not Rac1 or Cdc42) (Watanabe et al., 1999).

The FH2 domain of formins enhances actin nucleation by binding with the barbed end of F-actin and 'capping' the structure, which decreases actin monomer dissociation and increases the critical concentration of actin assembly (Shimada et al., 2004; Wear et al., 2003). The FH2 domain has been described as a 'leaky cap' as F-actin polymerisation occurs at the barbed end in contrast to tight capping proteins which prevent all actin dynamics (Zigmond, 2004). mDia1 remains bound to the growing end of actin throughout elongation and mDia1 FH1 and FH2 processively associates to the barbed end of F-actin (Higashida et al., 2004).

In addition to actin assembly, mDia1 has been found to be involved in a number of processes in cell migration. mDia1, which is involved in coordinating MTs and the actin cytoskeleton (Ishizaki et al., 2001), has been shown to accumulate at the leading edge of migrating cells, for example in T-cells (Heasman et al., 2010), fibroblasts (Goulimari et al., 2005; Brandt et al., 2007) and dendritic cells (Tanizaki et al., 2010). Furthermore, mDia1 knockout neutrophils were unable to form a distinct leading or tail edge and instead formed multiple unstable psuedopodia and failed to undergo directional cell migration (Shi et al., 2009).

Moreover, mDia1 knockdown also impairs focal adhesion turnover, as shown in rat C6 glioma cells (Yamana et al., 2006) and further, co-expression of ROCK and mDia1 is required for evenly distributed FAs at the leading edge of HeLa cells but expression of mDia1 alone was sufficient to marginally restore FAs in Rho inhibited HeLa cells (Watanabe et al., 1999). As actin stress fibres display a variety of morphologies and have differing associations with FAs they can be separated into four categories: dorsal, ventral, transverse arcs and perinuclear actin cap (Tojikander et al., 2012). Human osteosarcoma mDia1 knockdown cells exhibited a reduction in dorsal stress fibre elongation as well as abnormal dorsal morphology (Hotulainen and Lappalainen, 2006), demonstrating the mDia1 is essential for the assembly of actin stress fibres. Additionally, Hotulainen and Lappalainen also found an accumulation of α-actinin, a protein initially responsible for cross-linking stress fibre bundles before being displaced by myosin II, which would further indicate the lack of proper stress fibre assembly in mDia1 knockdown cells (Hotulainen and Lappalainen, 2006).

1.6 Modes of migration in cancer

Cellular migration is a vital process that occurs in multicellular organisms for a variety of functions including organogenesis, homeostasis, immune response and wound healing (Vicente-Manzanares et al., 2005; Trepat et al., 2012). Cells can either migrate via mesenchymal migration, wherein cells crawl across a 2D structure (e.g. basal lamina), or through a 3D environment (Etienne-Manneville, 2013). Many tumour cells can transition between mesenchymal and amoeboid migration, allowing these cells to respond to their microenvironments (e.g. to adapt to matrix stiffness and elude anticancer treatments) and thus are more highly invasive (Taddei et al., 2014). The mechanisms of 2D and 3D migration mechanisms are outlined below.

2D cell migration

The general process of 2D mesenchymal migration involves five steps: establishment of front-rear polarity, protrusion of the lamellipodium, focal adhesion (FA) formation, contraction of the cell body and retraction of rear attachments (Figure 3.) (Seetharaman and Etienne-Manneville, 2020).

Dendritic nucleation activity by the Arp2/3 complex polymerises a new F-actin at a 70° angle from the side of an existing filament, generating a branched structure – this form of nucleation is used to assemble lamellipodia (Chesarone and Goode, 2009). Lamellipodia are formed near the plasma membrane and contain a crosslinked mesh of F-actin; that is pushed outwards at the leading edge of the cell as a result of the force of actin polymerisation (Alberts et al., 2008). Physical crosslinking between actin stress fibres and growing MTs by spectraplakins and growth arrest specific protein 2-like (GAS2-like) proteins is essential for guiding MTs towards FAs (Dogterom and Koenderink, 2019). Spectraplakin and GAS2-like proteins have binding sites for F-actin in the calponin homology domain as well as a MT binding site, meaning they can bind to both structures simultaneously and link them together (Stroud et al., 2014; Nazgiewicz et al., 2019).

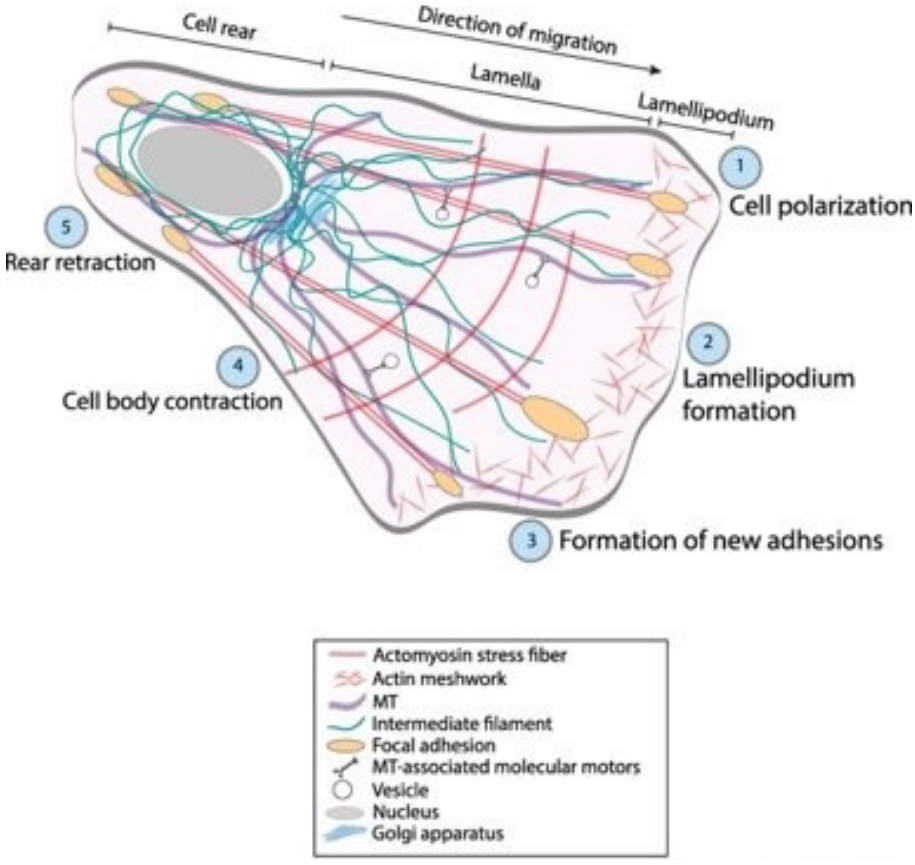

Figure 3. The five stages of 2D mesenchymal cell migration. 1) and 2) Cell migration begins with an external signal that the cell responds to, leading to the polarisation and extension of a protrusion at the leading edge. 3) Focal adhesions then form, which attaches the protrusion onto the surface that the cell is migrating across. These adhesions act as traction points for migration and initiate signals that regulate protrusion activity and adhesion dynamics. 4) Next, contraction occurs, wherein the cell body moves forward and, 5) the rear attachments retract (Horowitz and Webb, 2003). (Figure reused from (Seetharaman and Etienne-Manneville, 2020) with appropriate permissions)

Moreover, Rho-GTPases are key regulators of cell migration. These molecules function as molecular switches by transmitting intracellular signals as a result of cycling between GDP-bound inactive forms and GTP-bound active forms (Watanabe et al., 2005). Rac1 is a Rho-GTPase that is particularly important in mesenchymal cell migration. The growth phase of MTs promotes the generation of Rac1-GTP, which competes with tubulin for the same binding sites on MTs – when tubulin is added to the plus-end of the MT during growth, Rac1-GTP is displaced and thus is present on the leading edge of migrating cells (Waterman-Storer et al., 1999). Rac1 activation (along with Cdc42, whose activation is independent from Rac1) causes the lamellipodia and filopodia to protrude at the leading edge in cell migration (Kurokawa et al., 2004).

3D cell migration

The majority of studies on cell migration have been conducted using 2D migration techniques, however, when moving through tissues, most cells migrate using 3D migration mechanisms. There are three distinct modes of 3D cell migration: amoeboid, mesenchymal and lobopodial (Figure 4.). Lobopodial migrating cells have an elongated morphology and along the leading edge have large cylindrical protrusions in addition to small blebs present along the lateral sides of the cell (Petrie et al., 2012). More importantly for this report, are mesenchymal and amoeboid mechanisms. 3D mesenchymal migration is similar to its 2D counterpart, however the cells in 3D have a more elongated morphology and use proteases to remodel the extracellular matrix (ECM) to create gaps in which to migrate through (Yamada and Sixt, 2019). Conversely, amoeboid migration differs considerably from the 2D migration model outlined in the previous section (Yamada and Sixt, 2019). The amoeboid mode of migration has been identified in leukocytes and certain types of cancer cells, and tumour cells that migrate in this way are characterised by a spherical cell morphology in 3D substrates (Paňková et al., 2010). Furthermore, amoeboid migration doesn't require FAs as there is no need for cells to adhere to a substrate (Paluch et al., 2016). In amoeboid migration, the cell body undergoes successive rapid cycles of expansion and contraction with the cell membrane developing 'bleb-like' protrusions, which enable the tumour cell to explore its microenvironment to determine the best migration path (Krakhmal et al., 2015). These 'bleb-like' protrusions drive amoeboid migration and they are mediated by RhoA. Activation of RhoA/ROCK leads to cortical actomyosin contraction and increased hydrostatic pressure that drives the cytoplasm forward producing the bleb-like protrusions that allow tumour cells to move through gaps in the ECM (Spano et al., 2012). In amoeboid migration, RhoA is activated, while Rac1 is inhibited and the expression of proteases and integrins is decreased (Krakhmal et al., 2015).

Theoretically, high levels of EB2 expression could lead to an increase of amoeboid movement by increasing MT dynamics, thereby leading to the release of GEF-H1 (a RhoA-activating factor) from the MTs. GEF-H1 is inactive when bound to MTs but is activated upon release from MTs. This will result in RhoA activation, causing actomyosin contraction in the cortex and thus increased amoeboid migration. Conversely, EB2 knockdown would lead to increased MT stability and therefore Rho inhibition, Rac will then be activated, and this will result in mesenchymal motility.

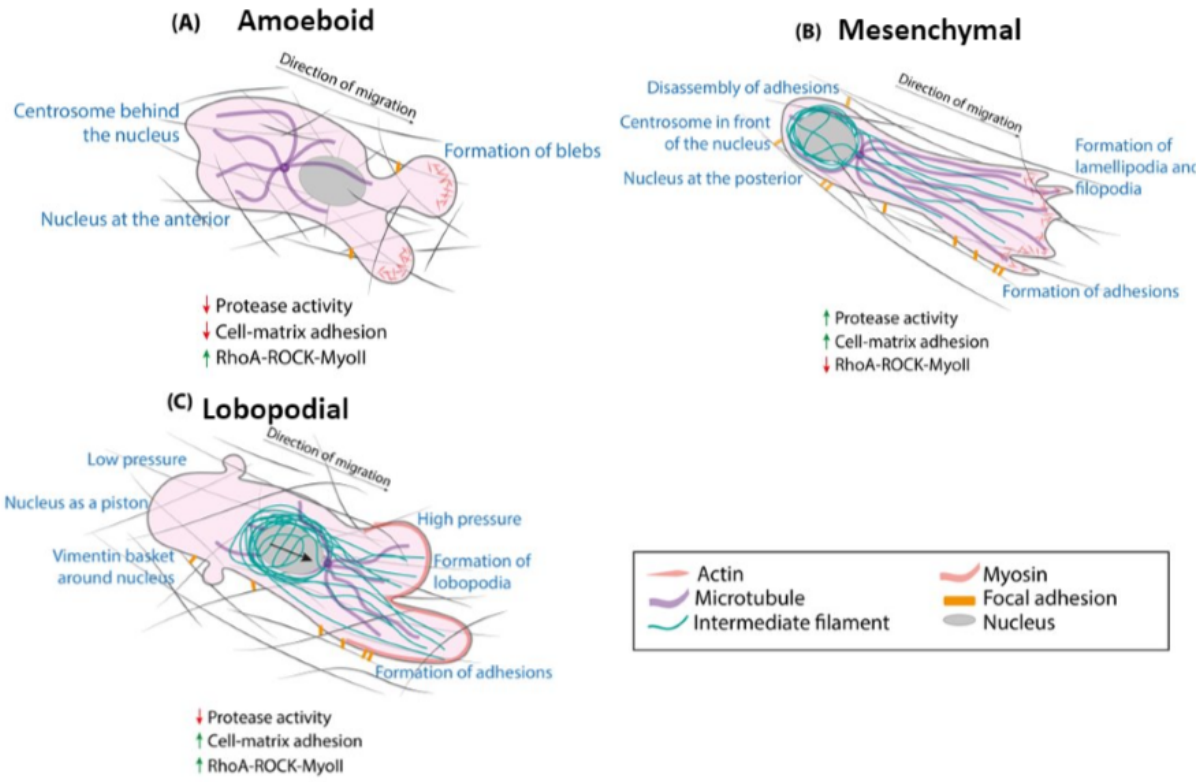

Figure 4. 3D modes of migration. A) amoeboid migration, B) mesenchymal migration and C) lobopodial migration. There are key differences between these migration mechanisms, such as centrosome positioning, which, in 3D mesenchymal migrating cells is positioned in front of the nucleus, but is found behind the nucleus in amoeboid migration (Seetharaman and Etienne-Manneville, 2020). Additionally, RhoA-ROCK is activated in amoeboid migration, but not in mesenchymal migration (Sahai and Marshall, 2003). Other key differences between amoeboid and 3D mesenchymal include migration speed, polarisation, presence of focal adhesions and actin cytoskeleton organisation (Bear and Haugh, 2014). (Figure reused from (Seetharaman and Etienne-Manneville, 2020) with appropriate permissions).

1.7 Fibroblast growth factors

Receptor tyrosine kinases (RTKs) are one class of cell-surface receptors for a variety of extracellular ligands, including growth factors, and are key for mediating intracellular signalling (Östman and Böhmer, 2001). There are 58 known RTKs in humans, organised into 20 subfamilies, all of which have a molecular similar structure: an extracellular domain containing a ligand-binding region, a single transmembrane helix, a protein tyrosine kinase (TK) domain in the cytoplasmic region, juxtamembrane regulatory regions and a carboxy (C-) terminal (Lemmon and Schlessinger, 2010). One family of RTKs are fibroblast growth factors (FGFs), and their receptors, fibroblast growth factor receptors (FGFR).

There are 23 FGFs (although only 18 of these bind to FGFRs) and they are present in both vertebrates and invertebrates; in vertebrates the molecular weight of FGFs are 17-34 kDa and they all share a 120 amino acid sequence that displays 16-65% sequence identity (Yun et al., 2010). FGFs were originally classified into 7 subfamilies, however, the intracellular FGF11 – FGF14, also known as FGF homology factors 1-4 (FHF1 – FHF4), despite having considerable sequence homology to FGFs, are no longer considered FGFs as they are not able to activate FGFR's (Olsen et al., 2003). This means

that FGF11 – FGF14 do not share a common functionality with this family of growth factors and therefore it is now generally accepted that there are only 6 FGF subfamilies. These subfamilies, each containing 2 – 4 members (shown in Figure 6.) are arranged based on sequence similarity and phylogenetic differences (Itoh and Ornitz, 2004).

The subfamily genes, Fgf1, Fgf4, Fgf7, Fgf8 and Fgf9, encode for canonical FGFs that can be secreted and then activate their respective FGFR isoform with heparin or heparin sulphate (HS) as a cofactor, whereas Fgf15/19 subfamily genes encode for endocrine FGFs that use either the αKlotho or βKlotho protein as a cofactor to bind and activate FGFRs (Ornitz and Itoh, 2015).
Four FGFRs have been identified, FGFR1 – FGFR4, serving 22 FGF ligands, and one factor that contributes to the diversity of FGF signalling is the existence of multiple FGFR isoforms that arise due to alternative splicing variants (Gong, 2014).

FGF subfamily	FGF	Cofactor	Receptor specificity
FGF1 subfamily	FGF1 FGF2		All FGFRs FGFR 1c, 3c > 2c, 1b, 4Δ
FGF4 subfamily	FGF4 FGF5 FGF6		FGFR 1c, 2c > 3c, 4Δ
FGF7 subfamily	FGF3 FGF7 FGF10 FGF22	+ Heparin or Heparan sulfate	FGFR 2b > 1b
FGF8 subfamily	FGF8 FGF17 FGF18		FGFR 3c > 4Δ > 2c > 1c >> 3b
FGF9 subfamily	FGF9 FGF16 FGF20		FGFR 3c > 2c > 1c, 3b >> 4Δ
FGF15/19 subfamily	FGF15/19 FGF21 FGF23	+βKlotho +αKlotho	FGFR 1c, 2c, 3c, 4Δ FGFR 1c, 3c FGFR 1c, 3c, 4

Figure 5. Table summarising FGF receptor specificity of both canonical and endocrine FGFs, the subfamilies they are divided in to and the cofactors required for receptor binding (Figure from (Ornitz and Itoh, 2015)).

Figure 5. shows the FGF8 subfamily, importantly FGF18, which can activate FGFR1c, FGFR2c, FGFR3c and both FGFR4 isoforms, with the highest activity observed on cells expressing FGFR3c (additionally no activity was detected in cell lines expressing the FGFR3b isoforms) (Zhang et al., 2006).

FGF18 and FGFR3

The general structure of FGFR3 is similar to the other members of the FGFR family, however, FGFR3 has two separate exons (exons 8 and 9) that encode for the IgG-like domain III and therefore FGFR3-

IIIb and FGFR3-IIIc isoforms arise due to the alternate usage of these exons – IIIb is a binding site for FGF1 and FGF9, while, in addition, IIIc can bind to FGF2, FGF4, FGF8, FGF17, FGF18 as well as the endocrine FGFs: FGF19, FGF21 and FGF23 (Paur et al., 2015). Tissue-specific expression of these two isoforms has been observed, with FGFR3-IIIb expression seemingly associated with epithelial cells (L'Hôte and Knowles, 2005), and, upon FGF binding, exon switching can occur that causes the FGFR-IIIb to be reversibly switched to FGFR3-IIIc, possibly correlated with a loss of epithelial properties (Scotet and Houssaint, 1998).

Generation of FGF18 knockout mice highlight the importance of FGF18, as loss of Fgf18 was shown to be embryonic lethal just before or at birth (Ohbayashi et al., 2002). A lot of research has been conducted into the role of FGF18 in embryonic development, where it has been demonstrated to be involved in multiple developmental processes, including playing a role in remodelling the distal lung and lung cell proliferation in embryonic lung development (Usui et al., 2004) and in skeletal development through osteogenesis and chondrogenesis (Ohbayashi et al., 2002).
FGFR3 and FGF18 have been implicated in a wide variety of cancers, however, only those in which these proteins have been shown to influence migration/metastasis will be discussed.

FGFR3 and FGF18 in cancer
Breast cancer: An immunohistochemistry analysis of 50 specimens of invasive ductal carcinoma of the breast observed FGFR3 expression in a third of these patients and indicated that this expression may be useful as a prognostic tool in invasive breast cancer (Kuroso et al., 2010). Additionally, numerous studies have reported that FGF18 expression is increased in breast cancer, with allusions to a potential use as a biomarker (Mustacchi et al., 2013). A recent study analysing the blood serum of healthy patients and patients with breast cancer observed a significantly higher concentration of FGF18 in breast cancer, concluding that FGF18, along with the cytokines interleukin-19 (IL-19) and IL-23, represent good potential biomarkers for detecting this disease (Rafiq et al., 2020). Furthermore, breast cancer cells treated with recombinant FGF18 had a higher migration velocity and distance as well as increased expression levels of TGF-β, MMP-2 and MMP-9 - genes which are involved in activities relating to tumour migration (Song et al., 2018). Interestingly, in breast cancer, MMP-2 and MMP-9 have been found to be highly expressed, in addition to being linked with tumour staging and lymph node metastasis; MMP-2 and MMP-9 destroy tissue barriers by degrading type IV collagens in the basement membrane and ECM, thereby promoting metastasis and invasion (Li et al., 2017). Therefore, this suggests that FGF18 may promote metastasis in breast cancer via increasing the expression levels of MMP-2 and MMP-9.
Recently, microRNA-99a (miRNA-99a) was overexpressed in breast cancer cells and it was observed that FGFR3 is a target gene for miRNA-99a, in addition to observing that this overexpression had an inhibitory effect on proliferation, invasion and migration of breast cancer cells (Long et al., 2020). Similar effects have also been observed in overexpression of miRNA-99a in prostate cancer (Wu et al., 2015), bladder cancer (Wu et al., 2014) and ovarian cancer (Jiang et al., 2014).
Pancreatic cancer: One study forced expression of FGFR3 in pancreatic cancer cells and observed that, in epithelial-like cells, FGFR3 supressed tumour growth, whereas in mesenchymal-like cells it had oncogenic properties, thus leading to the development of the proposed model (Figure 6.) of FGFR3 action in pancreatic cancer (Lafitte et al., 2013).

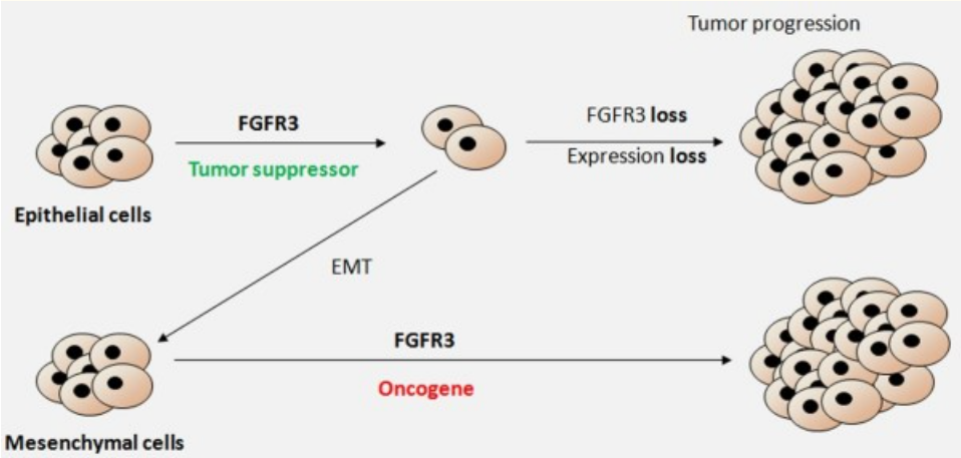

Figure 6. Proposed working model of the action of FGFR3 in pancreatic cancer. FGFR3 acts as a tumour suppressor in epithelial cells, however, if FGFR3 expression is lost or disrupted during pancreatic tumour progression, then there is an increase in cell growth. If EMT occurs, FGFR3 will then act as an oncogene in the mesenchymal cells, promoting tumour progression (Lafitte et al., 2013). (Figure from (Lafitte et al., 2013)

Melanoma: Melanoma tissues highly express FGFR3, which has been shown to promote the growth and migration of melanoma cells through the epithelial-mesenchymal transition (EMT) pathway and phosphorylation of AKT, ERK and EGFR (Li et al., 2019). This was established by FGFR3 knock-down in melanoma cells, which leads to increased levels of E-cadherin (an epithelial marker) and a reduction in N-cadherin and vimentin (mesenchymal markers) (Li et al., 2019).

Ovarian cancer: Evidence suggests that FGF18 is a good therapeutic and prognostic biomarker for use in ovarian cancer. Analysis determined that chromosome segment 5q31 – 5q35.3 amplification was associated with poor overall survival in ovarian cancer and from this, FGF18 (chromosome 5q35.1) was found to be the gene from this amplicon possessing the best prognostic value; in addition, FGF18 overexpression is present in ~50% of high-grade ovarian serous tumours (Wei et al., 2013). Ectopic overexpression of FGF18 increased migration and invasion in A224 and OVCA429 cells and was also found to influence the tumour microenvironment via activation of several signalling events and angiogenic factors, and by promoting the production of cytokines (Wei et al., 2013). Furthermore, FGF18 expression is significantly increased in ovarian cancer tumours ranging from benign to borderline and malignant type I, regardless of tumour histological type (serous or mucinous) (El-Gendi et al., 2015). It has been suggested that, in both serous and mucinous ovarian tumours, FGF18 expression may be involved in the adenoma-carcinoma sequence (El-Gendi et al., 2015).

Hepatocellular carcinoma: One study observed that in 82% HCC cases, at least one member of the FGF8 subfamily was upregulated and/or an FGFR. Furthermore, pronounced FGF18 upregulation was identified in a subset of HCC cases, possibly due to disruptions in the wnt signalling cascade, as well as FGF18 (along with FGF8 and FGF17) seemingly acting as a key driving forces for neoangiogenesis and malignant behaviour (Gauglhofer et al., 2011).

FGFR3 has been shown to promote the metastatic potential of HCC cells through targeting of monocyte chemotactic protein 1 (MCP-1), a protein that has been identified to have pro-angiogenic properties in other cancers, thus suggesting that through MCP-1 targeting, FGFR3 may regulate angiogenesis-dependent tumour metastasis (Liu et al., 2016).

MAPRE2 and fibroblast growth factor signalling

EB2 expression has been linked to several MT dependent processes including cell division, differentiation and migration. For example, depletion of EB2 causes a reduction in cell migration while its upregulation promotes migration and invasion. However, little is known about how EB2 expression is controlled. One possibility is through FGF signalling, which has been linked to *MAPRE2* expression.

FGFR3 knockout (FGFR3-/-) mice were observed to have inner ear defects, one of which being aberrant pillar cells that had a decreased size and decreased MT bundles (Szarama et al., 2012). Additionally, cochlear explants treated with an FGFR inhibitor lead to a significant increase in *MAPRE2* expression (Szarama et al., 2012). This would indicate that FGFR3 activation leads to EB2 downregulation and vice versa. However, this is currently the only paper that links FGFR3 and EB2.

1.8 Immunofluorescence

In this study immunofluorescence was the primary technique used to determine protein localisation and expression in cells. Immunofluorescence is an immunochemical technique that uses antibodies conjugated with a fluorophore to target specific antigens. When excited with a shorter wavelength of light fluorophores emit light and thus the proteins that the antibodies have bound to can be visualised (Im et al., 2018). Immunofluorescence can be direct or indirect; direct immunofluorescence staining involves the use of an antibody conjugated with a fluorophore that can directly bind to the antigen of interest, while indirect immunofluorescence uses a secondary antibody conjugated to a fluorophore which binds to a primary antibody specific for the antigen (Joshi and Yu, 2017). Here, indirect immunolabelling was used, and while there are advantages to using this technique, there are also many limitations. The disadvantages of antibodies in immunofluorescence have been discussed in several papers; Griffiths and Lucocq highlighted many problems with the antibodies including secondary antibody interspecies cross-reactivity, issues with sensitivity (particularly when labelling for a protein that has been overexpressed) and that antibodies lose activity over time (Griffiths and Lucocq, 2014). Additionally, as fluorescence tags are used, photobleaching is another limitation of this technique, wherein the fluorescence is lost over time due to exposure to light (Odell and Cook, 2013). Thus, while every effort was made to ensure that these issues were minimised in this study, they are important to note as the limitations of immunofluorescence could have impacted the results.

1.9 Hypothesis, aims and objectives

Based on current published data and previous research in the Mogensen lab, certain aspects of EB2 have been elucidated. We know that EB2 preferentially associates with the MT lattice rather than the MT plus-end, and that its downregulation results in increased MT stability while EB2 upregulation is predicted to increase MT dynamics. Additionally, EB2 expression has been shown to be important for apico-basal epithelial differentiation with depletion inhibiting MT reorganisation and cell elongation, while its downregulation is associated with fully differentiated epithelial cells containing stable MT bundles. EB2 is also important for cell migration, most likely through its role in FA turnover. EB2 depletion results in a reduction in cell migration while its upregulation has been associated with increased migration and invasion in pancreatic and hepatocellular carcinoma.

Based on this it seems that EB2 may be involved in cell migration and this investigation aimed to further elucidate the functional role of EB2 and highlight its involvement in the process of migration.

Additionally, it is suggested that EB2 affects the mode of cell migration. Theoretically, high levels of EB2 expression could lead to an increase in amoeboid movement by increasing MT dynamics, thereby leading to the release of GEF-H1 from MTs. GEF-H1 is inactive when bound to MTs, but is activated upon its release and this will result in RhoA activation, causing actomyosin contraction in the cortex of the cell and thus increased amoeboid migration. Conversely, a reduction in EB2 would lead to increased MT stability and therefore Rho inhibition and Rac activation which would result in mesenchymal motility. Due to time constraints no analysis of cells in a 3D environment could be conducted, however, analysis of the proteins involved in mesenchymal and amoeboid migration modes could provide an insight in to this theory.

Therefore, the following hypotheses are proposed:

1. EB2 upregulation or overexpression will lead to increased cell invasion.
2. EB2 upregulation or overexpression will lead to an increased in actomyosin contraction.
3. FGF18 binding to FGFR3 promotes EB2 expression.

The aims and objectives of this study are thus to:

1. Determine the relationship between FGF18/FGFR3 and EB2 expression in PANC1 cells.
2. Determine the consequences of increased and decreased EB2 expression in the PANC1 clones, $PANC1^{EB2Hi}$ and $PANC1^{EB2Low}$.
3. Determine the consequences of increased and decreased EB2 expression in WT MDA-MB-231 breast cancer cells and EB2 knockdown MDA-MB-231 cells.
4. Determine the possible mechanism by which high or low EB2 expression may influence switching in modes of migration between amoeboid and mesenchymal.

Chapter 2.
Materials and Methods

2.1. Cell culturing

2.1.1. Cells from frozen

Vials containing 1 ml of cells with culture media + 10% DMSO were removed from either –80 °C or liquid nitrogen dry store and the cells were transferred to a T25 flask with 5 ml of medium + 10% FBS. The flasks were placed in the 37 °C 5% CO2 incubator overnight and the medium was changed. Once the cells were ~70% confluent, a 2 ml trypsin wash was carried out followed by incubation in 3 ml trypsin at 37 °C 5% CO2 for the appropriate time depending on the cell line (Table 2). Next, 3 ml of medium was added to neutralise the trypsin and the contents of the flask were transferred to a 15 ml Falcon tube and centrifuged at 10,000 rpm for 5 mins. The supernatent was removed and the pellet was resuspended in 5 ml medium. The cell resuspension was transferred to a T75 flask containing 5 ml medium and placed in the 37 °C 5% CO_2 incubator.

Cell Line	Split ratio	Trypsin
PANC1 Clone 3	1:4	10 mins
PANC1 Clone 26	1:4	10 mins
MDA-MB-231	1:8 – 1:10	5 mins
MDA-MB-231 EB2 KD (Clone 6)	1:2 – 1:5	5 mins

Table 2. The split ratio and trypsinisation time for each cell line used. Split ratio refers to the volume of the cell resuspension that needs to be added to the fresh medium (volume of cell resuspension : volume of medium).

2.1.2. Passaging cells

Once cells reached ~70% confluency the medium was removed, and the cells were washed with 2 ml of pre-warmed trypsin, which was then removed, and 3 ml of trypsin was added. This was then incubated in 37 °C 5% CO_2 for 10 mins. Once the cells had detached from the surface of the flask, 3 ml of pre-warmed medium was added, and the contents of the flask were transferred to a 15 ml falcon tube.

(At this stage a cell count is conducted if seeding cells, see section 2.1.3.)

The falcon tube was centrifuged for 5 mins at 1,000 rpm. The supernatant was removed and the pellet was resuspended in 2 ml of medium. The split ratio (Table 2) of cell resuspension was then removed and added to a new T75 flask containing 10 ml of medium. This was placed into a 37 °C 5% CO_2 incubator.

2.1.3. Seeding cells

A cell count was conducted using a haemocytometer and from this, the number of cells required per ml was determined. The quantity of cells required per ml was then removed from the cell resuspension and suspended in the desired volume of medium.

For immunolabelling: to a 35 mm dish, 3 x 13 mm glass coverslips were added, and 2 ml of the new cell suspension was added. The dish was then placed in a 37°C 5% CO_2 incubator.

For scratch assay: inserts (ibidi, 80209) were placed into a 24 well plate and 100 µl of the new cell suspension was pipetted into each side of the insert. The place was then placed in a 37°C 5% CO_2 incubator.

2.2. Collagen-coated coverslips for random migration

Rat tail collagen I was diluted in sterile PBS to 5 µg/cm^2 of the surface to be coated. For 13 mm coverslips in 24 well plates, 60 µl of the collagen solution was pipetted across the surface and for wells in 24 well plates, 88 µl was used. The coated surfaces were left to set at room temperature for

~2 h before being washed with sterile PBS. Cells were seeded at 10,000 cells per well which were then placed in the 37 °C 5% CO_2 incubator for ~24 h.

2.3. Random migration imaging

Cells seeded 10,000 cells per well in a collagen I coated 24 well plate were left to migrate for ~24 h. The media was then removed and replaced with phenol-free medium + 10% FBS and a green fluorescent nuclear dye (1:1000) was added. The cells were then placed in the 37 °C 5% CO_2 incubator for at least 10 mins before being moved to the incubation chamber of the Observer 7 microscope where they were left to settle for at least 30 mins before imaging. Images were taken every 10 mins at x10 for 16-20 h. The live migration movies were analysed with ImageJ using the Trackmate plugin.

2.4. Scratch assay

To create a scratch PANC1 cells were seeded in two cell inserts (ibidi, 80209) in a 24 well plate (Figure 7) and left in the 37 °C 5% CO_2 incubator overnight. The medium was then removed and replaced with medium + 0.5% FBS and placed back in the incubator overnight. The inserts were removed and the cells were washed with media + 10% FBS before adding in 500 µl media + 10% FBS and placing the 24-well plate back in the incubator for 6 h or 8h. The cells were then immunolabelled according to section 2.5.

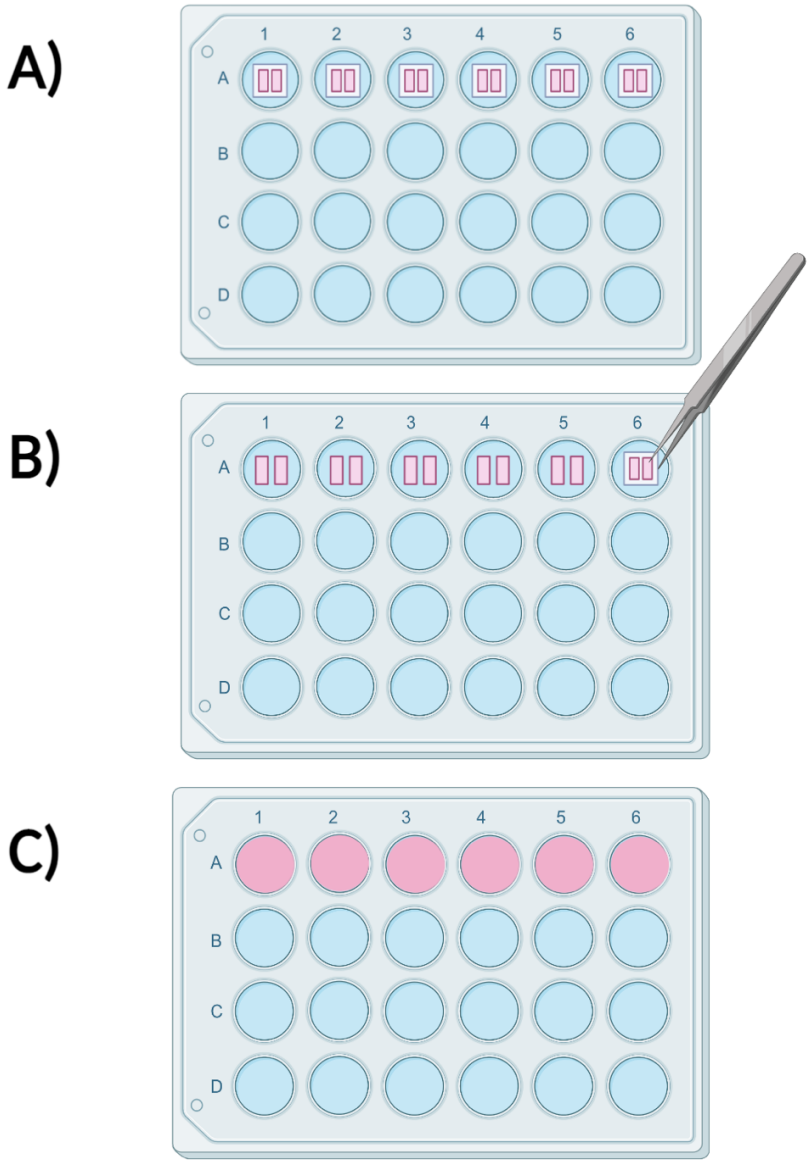

Figure 7. Using inserts to create a cell free gap for a scratch assay.
A) The cells were seeded in inserts with two chambers.
B) After overnight incubation the inserts were removed with tweezers. By growing the cells in two separate chambers a gap containing no cells is created once the insert is removed. Using the inserts means that there is less cell debris and all 'scratches' are the same size (~500 µm).
C) The cells were covered with media + 10% FBS and placed in an 37 °C 5% CO2 incubator and left to migrate for 6 or 8 h before fixation and immunolabelling.

2.5. Immunolabelling

Once cells were ready for immunolabelling, they were removed from the 37 °C 5% CO_2 and immediately fixed with -20 °C methanol. The cells were then placed on ice for 5-6 mins before the methanol was subsequently removed. The cells were then washed with phosphate buffered saline (PBS) for 10 mins and subsequently washed in PBS + 1% goat serum (G.S.) 2 x 10 mins. This was followed by an incubation in PBS + 1% NP-40 for 3 mins and then the cells were blocked in PBS + 10% G.S. for 30-45 mins. The primary antibody solution was then made up by diluting the relevant primary antibodies (Table 3) in PBS + 1% G.S and the cells were incubated in an incubation chamber in 50 µl drops of this solution at 4 °C overnight.

Primary Antibody	Dilution Ratio	Species Origin	Manufacturer	Catalogue Code	Polyclonal or Monoclonal
α-tubulin	1:300	Rabbit	Abcam	Ab15246	Polyclonal
YL1/2 (α-tubulin/ tyrosinated-tubulin)	1:150	Rat	Thermo	MA1-80017	Monoclonal
Acetylated tubulin	1:200	Mouse	Sigma	T6793	Monoclonal
β-tubulin	1:300	Mouse	Sigma	T4026	Monoclonal
β-actin	1:2000	Mouse	Sigma	A1978	Monoclonal
EB1	1:600	Rat	Absea	010811B11	Monoclonal
EB2	1:300	Rat	Absea	010614A11	Monoclonal
FGFR3	1:300	Rabbit	Abcam	Ab180906	Polyclonal
GEF-H1	1:500	Rabbit	Abcam	Ab201687	Monoclonal
Myosin light chain (phospho S20)	1:300	Rabbit	Abcam	Ab2480	Polyclonal
Dynamin 2	1:300	Rabbit	Abcam	Ab3457	Polyclonal
mDia1	1:200	Mouse	BD	610849	Monoclonal
Paxillin	1:200	Mouse	BD	610620	Monoclonal

Table 3. Primary antibodies

The cells were removed from 4 °C and left to warm up at room temperature for at least 1 h and then washed in PBS + 1% G.S. 4 x 10 mins. The secondary antibody solution was prepared by diluting the relevant secondary antibodies (Table 4) in PBS + 1% G.S. The cells were then incubated in 30 µl drops of the solution in an incubation chamber for 30 mins.

Fluorophore	Target Species	Species Origin	Dilution	Manufacturer	Catalogue Code	Polyclonal or Monoclonal
Alexa 488	Rat IgG	Goat	1:1000	Thermo Fisher	A11006	Polyclonal
Alexa 488	Rabbit IgG	Goat	1:1000	Thermo Fisher	A11034	Polyclonal
Alexa 488	Mouse IgG	Goat	1:1000	Thermo Fisher	A11001	Polyclonal
Alexa 568	Rat IgG	Goat	1:1000	Thermo Fisher	A11077	Polyclonal
Alexa 568	Rabbit IgG	Goat	1:1000	Thermo Fisher	A11036	Polyclonal

Table 4. Secondary antibodies

Following secondary antibody incubation, the coverslips were washing in PBS 3 x 10 mins then incubated in DAPI diluted in PBS (1:10,000) for 10 mins. The cells were then washed in PBS 3 x 5 mins before being mounted onto microscope slides and placed in the fridge.

2.6. Drug treatments

Y27632 treatment

Cells were seeded on collagen coverslips in a 24-well plate and placed in the 37 °C 5% CO_2 incubator overnight. The medium was then removed from the wells and replaced with either medium + 1% FBS (MDA^{WT} and MDA^{EB2Low}) or medium + 0.5% FBS ($PANC1^{EB2Hi}$) and placed back in the incubator overnight. Cells were removed from the incubator and treated with one of the following: 2% DMSO,

10 µM Y27632 or 20 µM Y27632. The cells were then placed in the 37 °C 5% CO2 incubator for ~8 h. The fixed cells were then immunolabelled according to Section 2.5.

SU5402 treatment

Cells were seeded 100,000 cells per 2 ml of media on 35 mm glass coverslips and placed in the incubator overnight. The cells were then removed from the incubator and 2 ml of either 10 µM DMSO, 10 µM SU5402 or media were added. The cells were then incubated for 18 h before immunolabelling for EB2.

2.7. Fluorescence microscopy

Immunolabelled cells were imaged either using a Ziess Axioplan 2 microscope with a Zeiss AxioCam HRm camera or with the Observer 7.

2.8. Manual Fluorescence intensity analysis

Images of immunolabelled cells were taken using a set exposure and intensity setting. The images were analysed in ImageJ. Individual cells were traced using the 'Freehand selection' tool and the area and integrated density were recorded. Measurements of the background fluorescence were taken at various points surrounding each cell and the corrected total cell fluorescence (CTCF) was then calculated using the following equation:

$$CTCF = integrated\ density - (cell\ area\ \times\ mean\ background\ fluorescence)$$

2.9. CellProfiler

CellProfiler is a software tool that can analyse a number of cell characteristics such as size, shape and intensity in a high throughput manner (Carpenter et al., 2006). Here, fluorescence intensity and cell shape was analysed in CellProfiler using the following pipeline:

1. ColorToGrey
2. IdentifyPrimaryObject (nuclei) – Typical diameter of objects in pixel units: 10-200, Threshold strategy: Adaptive, Otsu, Three classes, Threshold correction factor: 1.25
3. IdentifySecondaryObject – Method to identify the secondary objects: Propagation, Threshold strategy: Adaptive, Otsu, Three classes
4. MeasureObjectSizeShape
5. MeasureObjectIntensity

2.10. Data analysis

Statistical analysis was conducted on all the results using IBM SPSS software. Initially, the Kolmogorov-Smirnov or Shapiro-Wilk test for normal distribution and the Levene's test for equal variance were conducted for all datasets. If the data was normally distributed and had equal variance, one-way ANOVA test was performed; if homogeneity of variance could not be assumed, the post hoc Games-Powell test was used. Additionally, when data was not normally distributed the Mann-Whitney U test was used. For all tests a significance level of $P < 0.05$ was used. Graphs were created in Microsoft Excel. Microsoft PowerPoint and Adobe Photoshop were used to edit the images and figures. ImageJ was used to analyse time-lapse movies using the TrackMate plugin as well as manual fluorescence intensity analysis. CellProfiler was also used to analyse fluorescence intensity and cell morphology.

Chapter 3.

Results

3.2 Model systems

PANC1

PANC1 is an epithelial cell line originating from a human pancreatic carcinoma in the ductal cells (Lieber et al., 1975). Mutations in the tumour suppressor genes *p53*, *p16* and K-*ras* have been identified in this cell line, which are genes frequently mutated in pancreatic cancer (Sun et al., 2001). As PDA is a highly invasive form of cancer, pancreatic cancer cells are a good model to study cell migration, with PANC1 being ideal as they have been shown to migrate as single cells (Stähle et al., 2003) as well as collectively (Stähle et al., 2003) (Deer et al., 2010).

MAPRE2, the gene which encodes for EB2, was reported to be highly expressed in PANC1 cells and EB2 is localised to the cytoplasm in these cells (Abiatari et al., 2009b). Abiatari et al. generated highly invasive nerve PANC1 cells expressing increasing levels of MAPRE2 and found that cells overexpressing MAPRE2 had increased actin organisation and cortical and transverse stress fibres, while the invasive nerve clones with comparatively lower levels of MAPRE2 had apical actin expression condensed at filopodia (Abiatari et al., 2009b). This strongly suggests that EB2 is involved in cytoskeletal organisation and the level of EB2 expression can affect the actin organisation, which could have an impact on several factors of cell migration, including cell migration mode.

While Abiatari et al. determined that MAPRE2 was overexpressed in PANC1 cells, further analysis in the Mogensen lab found that EB2 expression was found to vary across a population of PANC1 cells. PANC1 cells expressing either high levels of EB2 ($PANC1^{EB2Hi}$) or low levels of EB2 ($PANC1^{EB2Low}$) were generated through subcloning (Gadsby – Mogensen Lab). Preliminary data from the Mogensen lab verified the increased and decreased EB2 expression levels in these two PANC1 clones with a Western blot (see Appendix).

MDA-MB-231

MDA-MB-231 is an epithelial cell line originating from an invasive ductal carcinoma and this cell line is estrogen receptor, progesterone receptor and HER2 negative, thus representing a good model for studying triple-negative breast cancer (Welsh, 2013). MAPRE2 has been found to be highly expressed in MDA-MB-231 (Heiser et al., 2012), indicating that MDA-MB-231 is a good cell line to study the effects of EB2 expression. This study used a wildtype MDA-MB-231 (MDA^{WT}) cell line in addition to a partial EB2 knockout MDA-MB-231 (MDA^{EB2KO}) line, generated using CRISPR/Cas9 by Ben Rix (Mogensen lab).

3.3 Role of FGF signalling in EB2 expression

FGFR3 Localisation in PANC1 Cells

FGF18 binds to FGFR3 to activate the downstream signalling pathway and therefore the distribution of FGFR3 within $PANC1^{EB2Hi}$ and $PANC1^{EB2Low}$ cells may indicate the involvement of these proteins in EB2 expression. $PANC1^{EB2Hi}$ and $PANC1^{EB2Low}$ cells were seeded on glass coverslips and grown to ~80% confluency before fixation and immunolabelling for FGFR3 and MTs. $PANC1^{EB2Hi}$ and $PANC1^{EB2Low}$ cells showed FGFR3 localisation primarily in the cell cytoplasm, with some peripheral FGFR3 dots evident in single cells without neighbours (Figure 8). More distinct cortical localisation is evident in cells in confluent regions (Figure 9). Interestingly, it appears as though FGFR3 localises along MTs (Figure 8), although it is possible that the FGFR3 could be localised close to MTs, but along actin filaments. To

determine whether FGFR3 does associate with the MT network, labelling for FGFR3 and actin needs to be conducted. Nocodazole can also be used to depolymerise MTs and see if the linear alignment of FGFR3 dots remain or not. Additionally, it appears that the cells express differing levels of FGFR3 (Figure 9). The localisation of FGFR3 to the cytoplasm and cell cortex and potentially along MTs contradicts previous findings where it was reported that FGFR3 has nuclear localisation in PANC1 cells (Lafitte et al., 2013).

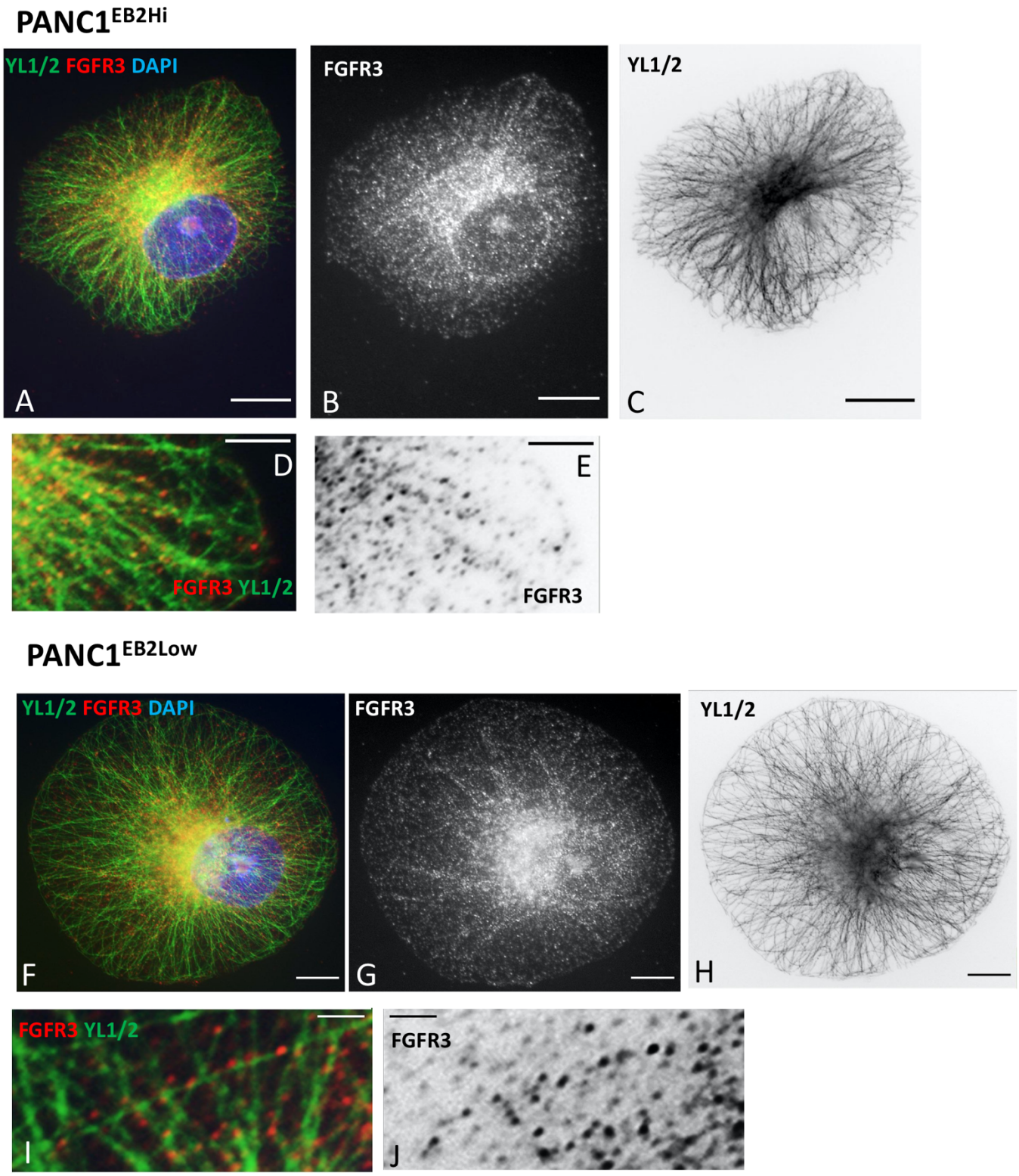

Figure 8. PANC1^{EB2Hi} and PANC1^{EB2Low} cells fluorescently labelled for MTs (YL1/2. green), FGFR3 (red) and the nucleus (DAPI) (blue). MTs in PANC1^{EB2Hi} cells have a more polarised organisation, which can be seen in panels A and C, where the majority of MTs are organised on one side of the nucleus, as opposed to PANC1^{EB2Low} cells which have a more radial organisation. Panels F and H show that the MTs in the cells are distributed evenly throughout the PANC1^{EB2Low} cell. In single cells, localisation of FGFR3 seems to correspond to MT distribution, with abundant staining for both MTs and FGFR3 found at the centre of cells (A, B, F and G), and FGFR3 was found to be present along MTs (D, E, I and J). (A-C, F-H scale bar = 10 µm) (D-E, I-J scale bar = 5 µm).

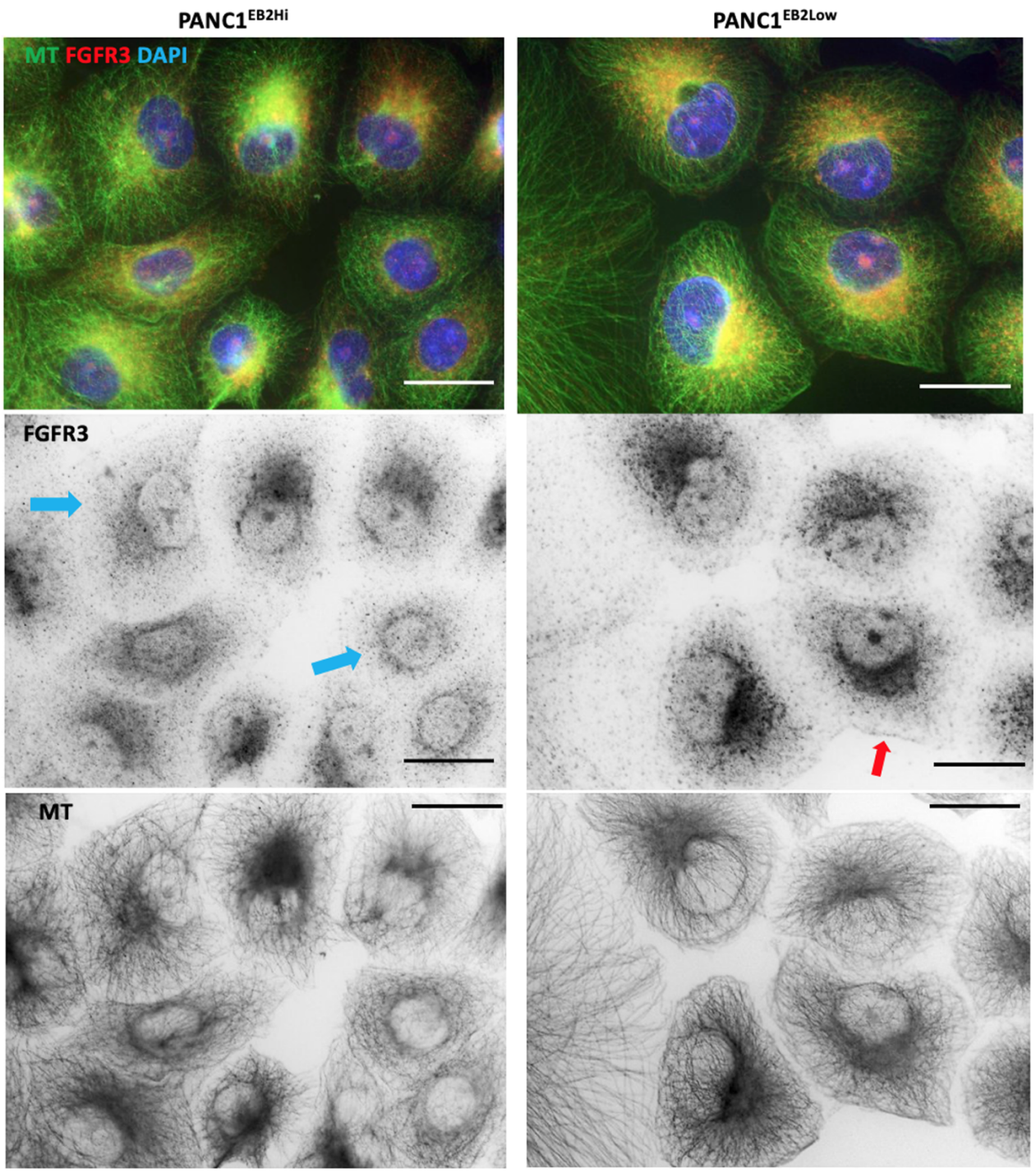

Figure 9. PANC1^{EB2Hi} and PANC1^{EB2Low} cells fluorescently labelled for MTs (green), FGFR3 (red) and the nucleus (DAPI, blue). It appears that cells can have different levels of FGFR3 expression in the same population, highlighted by the blue arrows, which indicate cells that possibly have less FGFR3 expression the rest of the cells in the same environment. Although less FGFR3 distribution towards the periphery of cells is observed, some FGFR3 localisation is found right at the cell edge, highlighted by the red arrow (scale bar = 20 µm).

The effect of FGFR inhibition on EB2 expression in PANC1^{EB2Hi} and PANC1^{EB2Low} cells

PANC1^{EB2Hi} and PANC1^{EB2Low} cells seeded on glass coverslips were treated with either media, 10 µM DMSO or 10 µM SU5402 and incubated for 18 h before fixation and immunolabelling. SU5402 is a known FGFR inhibitor that has been previously used to investigate the effects of FGFR3 inhibition (Ishibe et al., 2005). Examples of images taken with fixed exposures are shown in Figure 10.

EB2 fluorescence intensity was analysed in ImageJ by manually drawing around each cell and measuring the integrated intensity, followed by measurements of the background. The corrected total cell fluorescence (CTCF) was then calculated using the following equation and the results are shown in Figures 10 and 11:

$$CTCF = Integrated\ intensity - (Area\ of\ cell\ \times\ mean\ background\ fluorescence$$

A Shapiro-Wilk test determined that the results were not normally distributed ($P < 0.001$ for all treatments for both PANC1^{EB2Hi} and PANC1^{EB2Low}), so a non-parametric Games-Howell test was used. For PANC1^{EB2Hi}, a significant decrease in EB2 fluorescence intensity was found between SU5402 and DMSO treatments ($P = 0.004$), but no difference was found between SU5402 and media ($P > 0.05$). However, in PANC1^{EB2Low}, no difference in fluorescence intensity was found between any of the treatments ($P > 0.05$). It is important to note that the number of cells analysed here for PANC1^{EB2Hi} was a lot higher than PANC1^{EB2Low} and that these results are only based on one repeat, so it is possible that these results may change with the addition of more data.

Although the difference in fluorescence intensity between media and DMSO was determined not to be significant, it is interesting that, in PANC1^{EB2Hi} cells, SU5402 treatment significantly decreased EB2 fluorescence intensity compared to DMSO, but not media. It is possible that the DMSO had an effect on the cells, as it has been reported that DMSO can impact PANC1 growth rate, attachment to collagen and alkaline phosphate activity (MacIntyre and Kim, 1984) and it is known to have a stabilising effect on MTs (Katsuda et al., 1988).

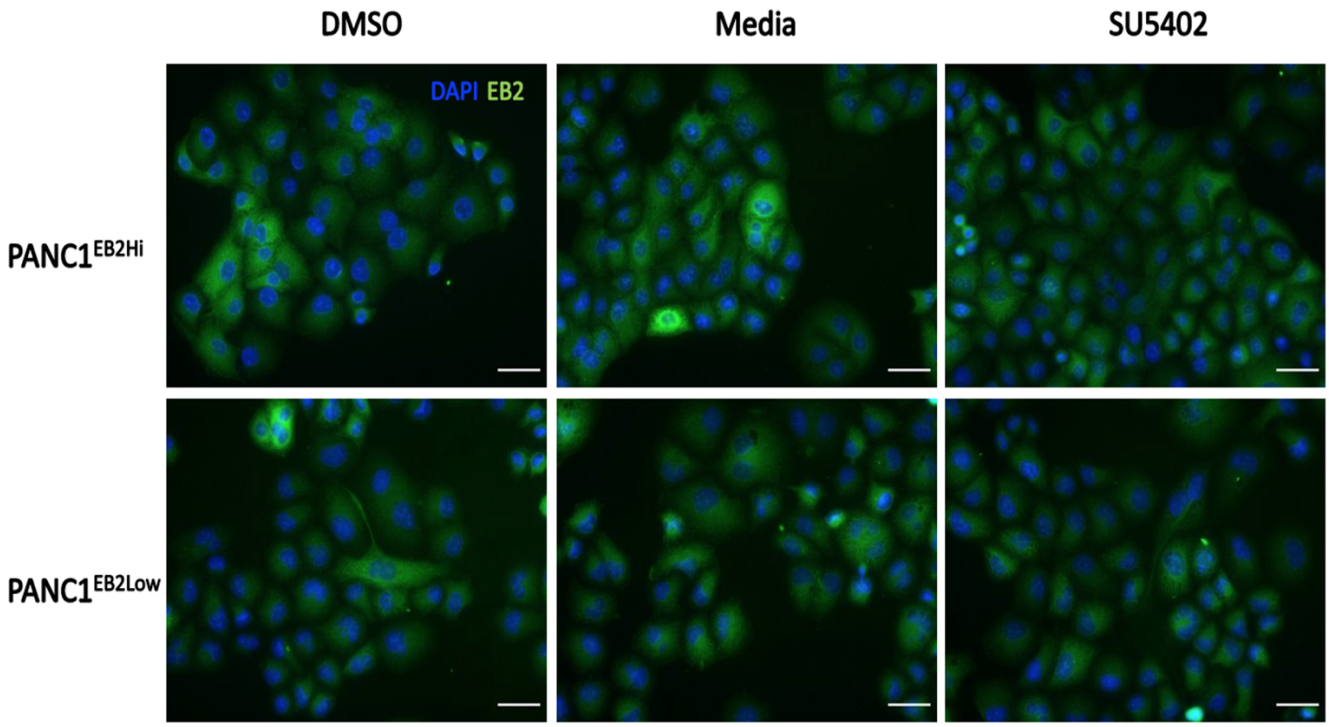

Figure 10. PANC1^{EB2Hi} and PANC1^{EB2Low} cells treated with either DMSO, media or SU5402 and fluorescently labelled for EB2 (green) and DAPI (blue). In the images it appears that there are no differences in EB2 fluorescence in all PANC1^{EB2Low} cells and a slight decrease in fluorescence in the PANC1^{EB2Hi} cells treated with SU5402. Fluorescence intensity cannot be compared between subclones as different set exposures were used when taking the images for PANC1^{EB2Hi} (3198 ms) and PANC1^{EB2Low} (4331 ms). Cells undergoing mitosis were not included in the fluorescence intensity analysis as these cells have a higher level of fluorescence and would skew the results. (Scale bar = 50 µm)

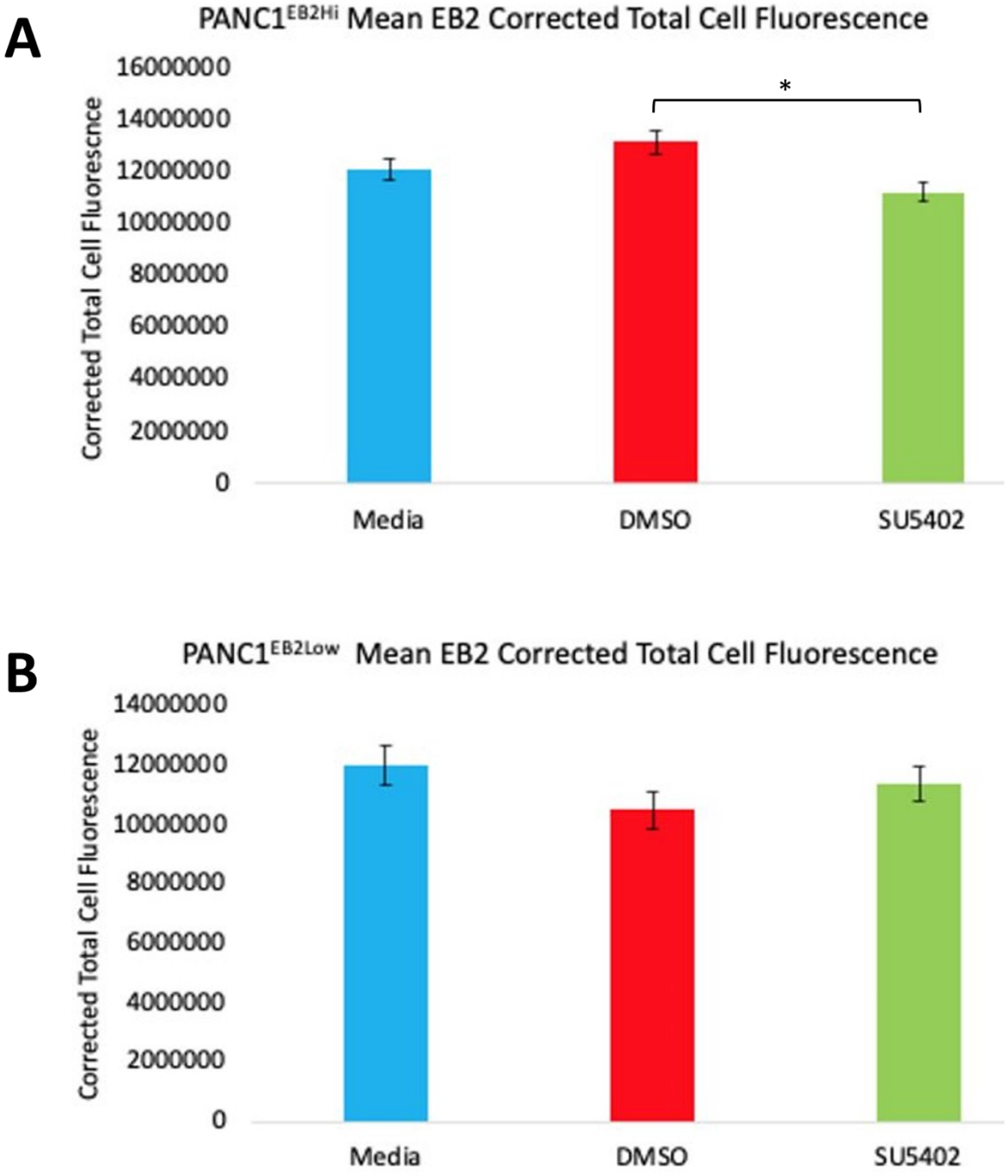

Figure 11. EB2 fluorescence intensity analysis of PANC1^{EB2Hi} and PANC1^{EB2Low} cells immunolabelled following 18 h treatment with either media, 10 µM DMSO or 10 µM SU5402. A) PANC1^{EB2Hi} cells displayed a significant decrease in EB2 fluorescence intensity in cells treated with SU5402 compared to DMSO treated with SU5402 (Games-Howell, P = 0.004), but no significant difference was detected between media and SU5402 or media and DMSO treatments. (Based on a total of 979 cells (media = 351 cells, DMSO = 311 cells and SU5402 = 317 cells)) B) PANC1^{EB2Low} cells showed no significant difference in EB2 fluorescence intensity was found between any of the treatments (Games-Howell, P > 0.05). (Based on a total of 336 cells (media = 114 cells, DMSO = 117 cells and SU5402 = 105 cells))

3.4 Effects of varying EB2 expression levels on cell migration

3.4.1 Elevated EB2 expression in PANC1 migrating cells

Microtubule organisation in PANC1^{EB2Hi} and PANC1^{EB2Low} cells

Differences in cytoskeleton organisation are frequently characterised by changes in cell morphology. To investigate the effects of different EB2 expression levels, PANC1^{EB2Hi} and PANC1^{EB2Low} cells were fluorescently labelled for MTs to observe differences between the two cell lines.

Figure 8. shows a representative of the PANC1^{EB2Hi} and PANC1^{EB2Low} cell populations and from this figure the differences in morphology between the two cell lines can be seen. PANC1^{EB2Low} have a larger and more rounded morphology compared to the PANC1^{EB2Hi} cells, which are frequently smaller. The differences in morphology can be linked to MT organisation, where the PANC1^{EB2Low} MTs have an unpolarised radial organisation compared to the PANC1^{EB2Hi} cells, which have a polarised MT organisation (Figure 8). This suggests that PANC1^{EB2Hi} cells have a more migratory phenotype compared to the PANC1^{EB2Low} cells.

Supporting this, there are distinct differences in MT organisation between the two cell lines. PANC1^{EB2Low} cells have a radial MT organisation whereas the MTs in PANC1^{EB2Hi} cells are organised in a more polarised way (Figure 8). MT organisation is defined as radial if the cell is unpolarised and the MTs are anchored at a central MTOC (centrosome), while in migrating cells, the MT array is polarised, meaning that the MTOC has been repositioned to one side of the nucleus, which orients the MTs in the direction of migration (Meiring et al., 2020). Therefore, differences in EB2 expression seems to affect MT organisation and cell morphology.

Localisation of the Rho effector GEF-H1, phosphorylated myosin light chain (pMLC) and the formin mDia1 in migrating PANC1^{EB2Hi} cells.

To determine the effect of elevated EB2 on migration in PANC1 cells a number of proteins known to be involved in migration were fluorescently labelled for in migrating PANC1^{EB2Hi} cells to determine their localisation. A combination of scratch assays and random migration assays were used, and the images were analysed by visually determining the protein localisation. Additionally, Adobe Photoshop was used to view the images in black and white, which made the localisation easier to assess as details that were lost in the colour images were clearer in black and white.

GEF-H1

GEF-H1 is involved in MT dynamics and is localised along MTs while inactivate, and when released from MTs is in its active form (Krendel et al., 2002). To determine the localisation of GEF-H1, migrating PANC1^{EB2Hi} cells were fluorescently labelled for GEF-H1 and MTs. As expected, labelling in randomly migrating PANC1^{EB2Hi} cells showed evidence of GEF-H1 localisation along MTs (Figure 12). Additionally, in the scratch assay, there is evidence of GEF-H1 accumulation at the leading edge of migrating cells. However, GEF-H1 is not only found at the leading edge, but is present throughout the cells (Figure 13).

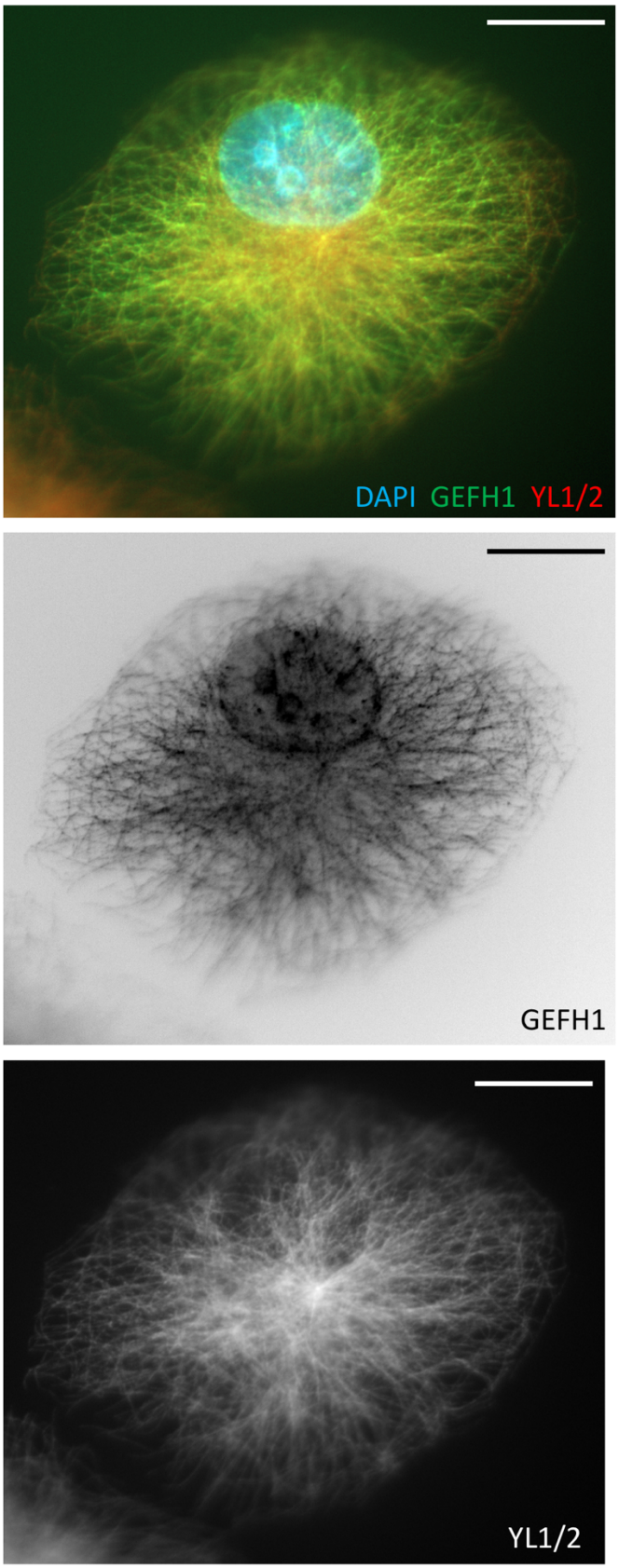

Figure 12. PANC1^{EB2Hi} cell labelled for microtubules (YL1/2, red), GEF-H1 (green) and the nucleus (DAPI, blue). The fluorescence images show that GEF-H1 is expressed throughout PANC1^{EB2Hi} cells and appears to localise to MTs. (Scale bar = 20 µm).

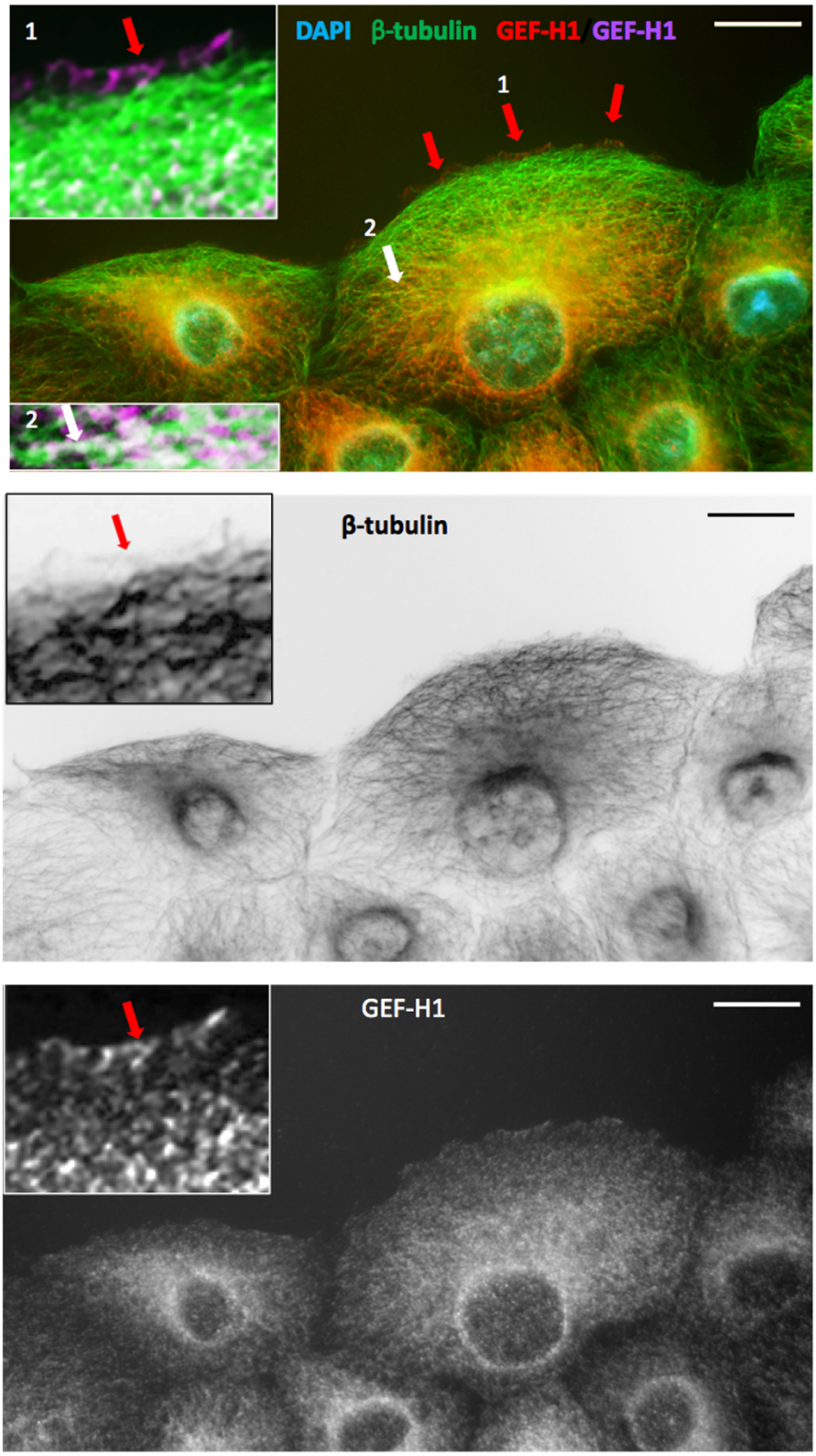

Figure 13. GEF-H1 is evident at the leading edge of PANC1^{EB2Hi} cells. PANC1^{EB2Hi} cells were labelled for MTs (β-tubulin, green), GEF-H1 (red/purple in insert) and the nucleus (DAPI, blue) after 8 h of wound healing. MTs are concentrated at the leading edge while the nucleus is located towards the rear. Some GEF-H1 is apparent along the MT lattice at the leading edge (red arrows and insert 1) as well as further back (white arrow and insert 2) (Scale bar = 20 µm).

pMLC

The phosphorylation of non-muscle myosin II regulatory light chain regulates cell migration in a variety of ways including actin reorganisation, protrusion generation and FA formation and disassembly (Vicente-Manzanares et al., 2009). In the randomly migrating PANC1^{EB2Hi} cells it can be seen that these cells have several cell body extensions and, while some of these contain both MTs and pMLC, some of these do not contain MTs (Figure 14). Additionally, from the images of the scratch assay of PANC1^{EB2Hi} cells, pMLC seems to localise to the leading edge of migrating cells and extend beyond MTs at the leading edge (Figure 15). Furthermore, PANC1^{EB2Hi} migrating cells labelled for EB2 and pMLC show evidence of possible colocalization between the two proteins (Figure 16). However, this potential colocalization seems to only appear in certain places along the leading edge, which could potentially indicate that the localisation of both of these proteins is to FAs.

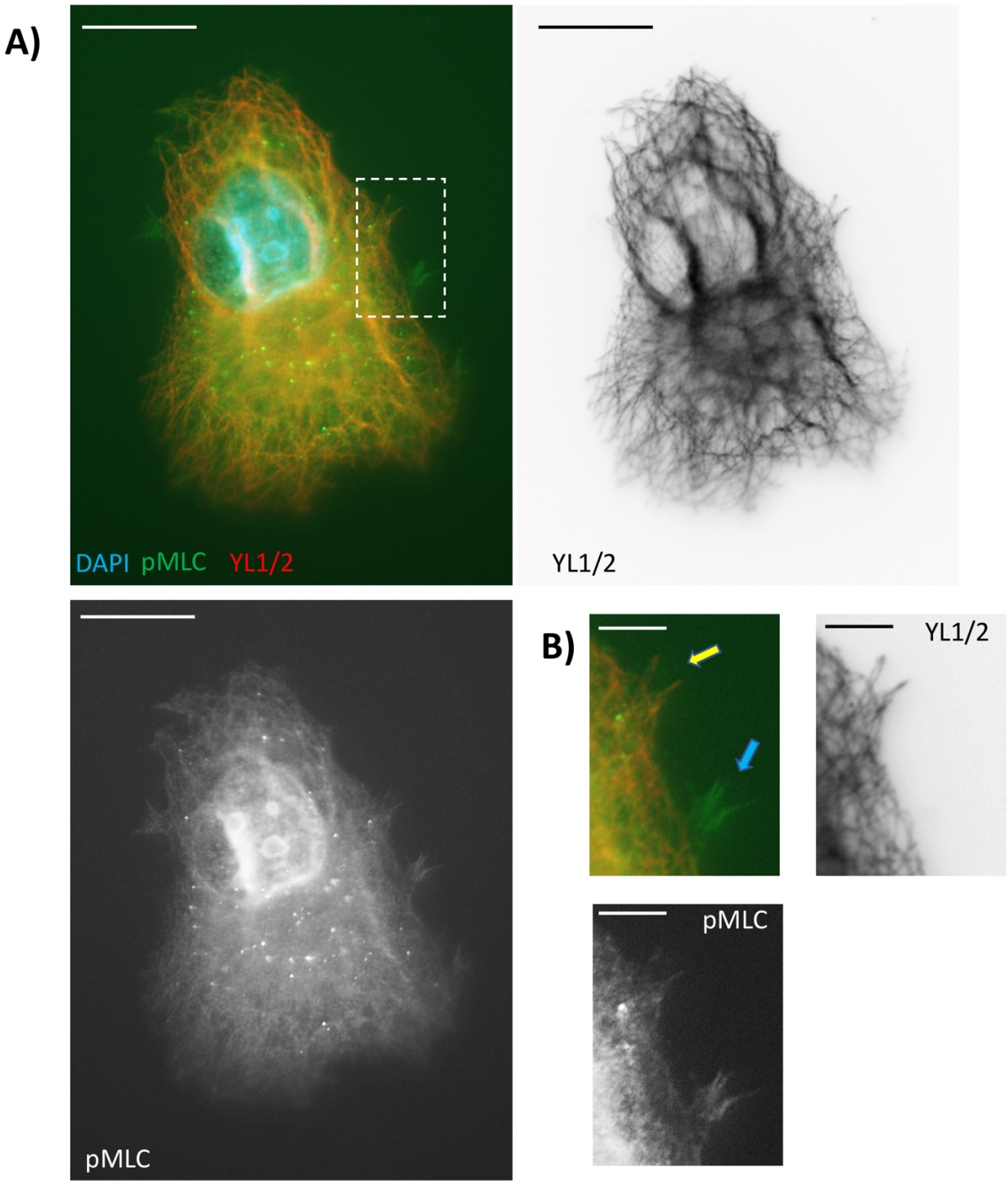

Figure 14. pMLC localisation in a randomly migrating PANC1^{EB2Hi} cell. A) A migrating PANC1^{EB2Hi} cell labelled for MTs (YL1/2) (red), pMLC (green) and the nucleus (DAPI) (blue). Several cell body extensions can be identified, some of which contain both MTs and pMLC and some that don't contain MTs. (Scale bar = 20 µm) B) Englarged section of an area of the cell body showing an extension that contains both MTs and pMLC (yellow arrow) and an extension containing no MTs (blue arrow) (Scale bar = 5 µm).

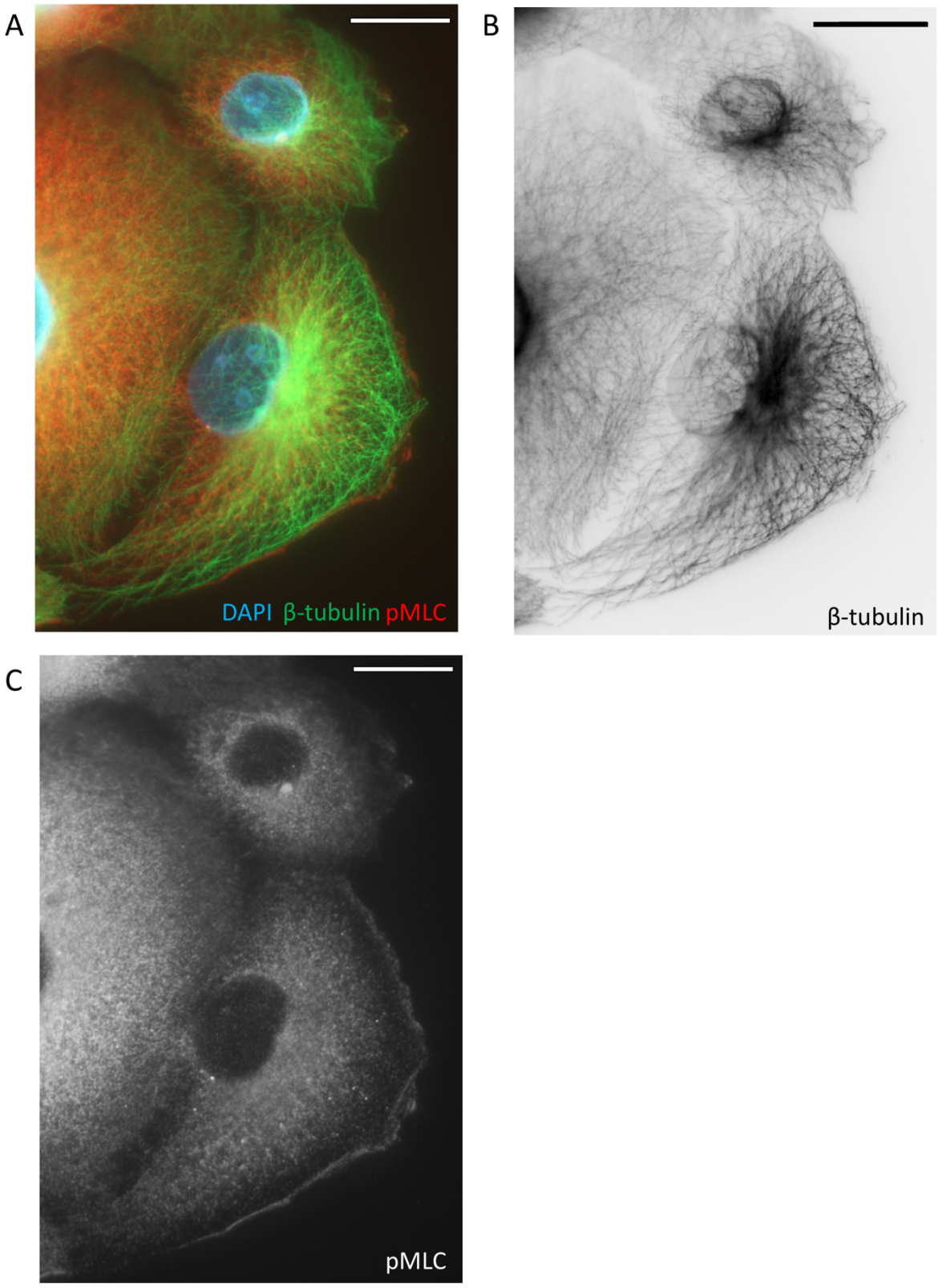

Figure 15. Scratch assay of PANC1^{EB2Hi} cells left to migrate for 8 h before labelling for MTs (β-tubulin) (green) and pMLC (red). The PANC1^{EB2Hi} cells shown in the figure display a migratory phenotype as the MTs are organised at the front of the cell in the direction of migration (panel B). In panels A and C accumulation of pMLC can be seen at the leading edge of cells and this accumulation extends beyond MTs (Scale bar = 20 µm).

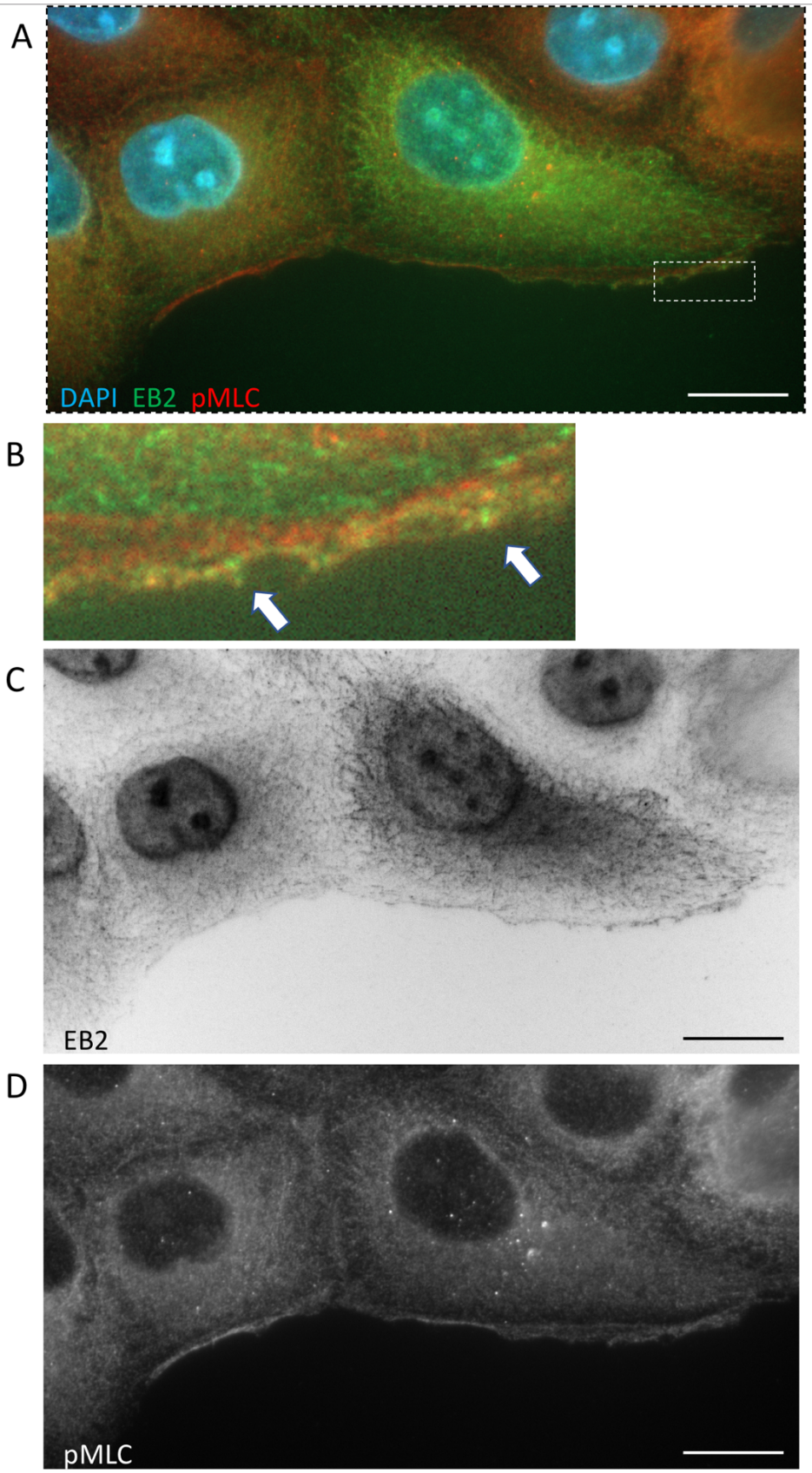

Figure 16. EB2 and pMLC in collectively migrating PANC1^{EB2Hi} cells. Following 8 h of migration, a scratch assay of PANC1^{EB2Hi} cells was labelled for EB2 (green), pMLC (red) and the nucleus (DAPI) (blue). Panels A and B show that in the migrating PANC1^{EB2Hi} cells on the edge of the scratch, both EB2 and pMLC accumulate at the leading edge and there appears to be colocalisation between these proteins (white arrows). Additionally, it seems that migrating cells have increased EB2 expression compared to the cells not on the leading edge of the scratch (panel C). pMLC accumulation at the leading edge appears to be very strong but there is a gap in fluorescence directly behind this localisation (panel D) (Scale bar = 20 µm).

mDia1

mDia1 interacts with the barbed ends of F-actin to increase F-actin nucleation (Mizuno and Watanabe, 2012). Fluorescence staining of mDia1 and MTs of collectively migrating PANC1^{EB2Hi} cells (scratch assay) shows evidence that mDia1 and MTs colocalise, particularly along the leading edge (Figure 17). In addition, while MTs also localise along the leading edge, mDia1 localisation extends beyond the MTs, suggesting that it associates with the actin cytoskeleton as opposed to MTs.

Furthermore, it appears that migrating cells may have a higher level of mDia1 than non-migrating cells, as seen in Figure 17, where the cells along the leading edge of the scratch seem to show more fluorescence. However, this wasn't investigated in this study and cannot be analysed from the images, so no conclusions can be made on this. However, this would correlate with previous findings that mDia1 is required for cell migration (Yamana et al., 2006; Thompson et al., 2018; Klein et al., 2019;) and that cells expressing mDia1 have increased invasiveness (Kim et al., 2016).

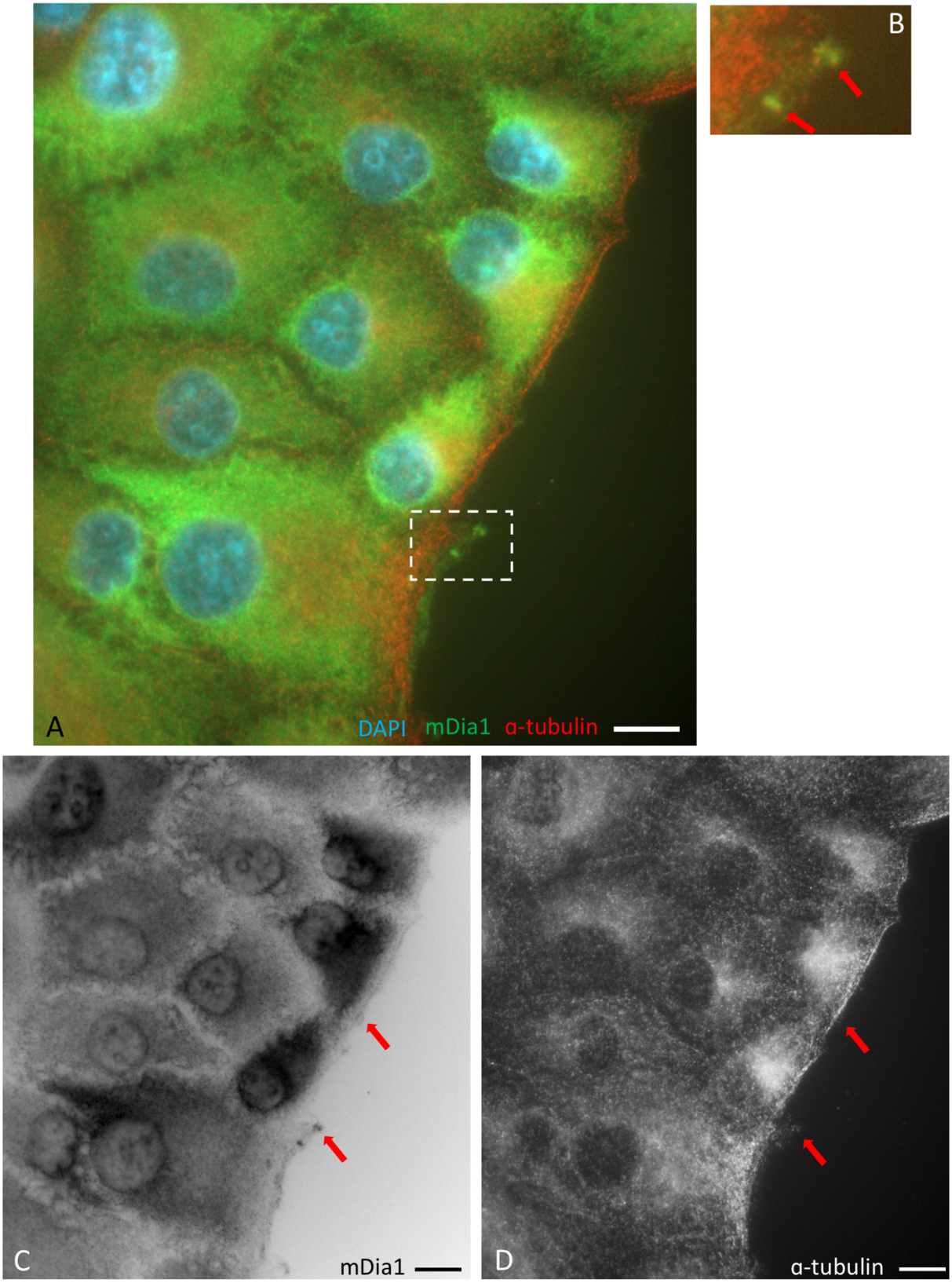

Figure 17. PANC1^{EB2Hi} scratch after 8 h migration fluorescently labelled for mDia1 (green), microtubules (α-tubulin, red) and nuclei (DAPI, blue). Panels A and C show that mDia1 appears to be localised primarily in the cell body and it appears that cells along the leading edge have increased levels of mDia1. However, as panel B shows, there is evidence of mDia1 expression along the leading edge of migrating cells and this seems to be localised with MTs (red arrows) (scale bar = 10 µm).

Localisation of EB2 in relation to dynamin2 and focal adhesions in PANC1^{EB2Hi} cells

Previous studies have shown that EB2 localises to FAs (Yue et al., 2014; Liu et al., 2015) and previous work in the Mogensen lab has suggested that EB2 co-immunoprecipitates with dynamin2. Based on these findings, labelling of migrating PANC1^{EB2Hi} cells was conducted using scratch assays to investigate whether dynamin2 colocalises with EB2 and localises to FAs. The images indicate that EB2 and dynamin2 does colocalise, particularly along the leading edge of migrating cells (Figure 18).

While staining of PANC1^{EB2Hi} cells for dynamin2 and the FA marker paxillin does show some association between dynamin2 and FAs, this association doesn't appear to be very strong in these cells (Figure 19). This finding is in contrast with previous studies that have reported that dynamin2 localises to FAs (Yoo et al., 2005). However, this study utilises a different cell line and, additionally, uses a cell line that has an overexpression of EB2, which may account for the different results.

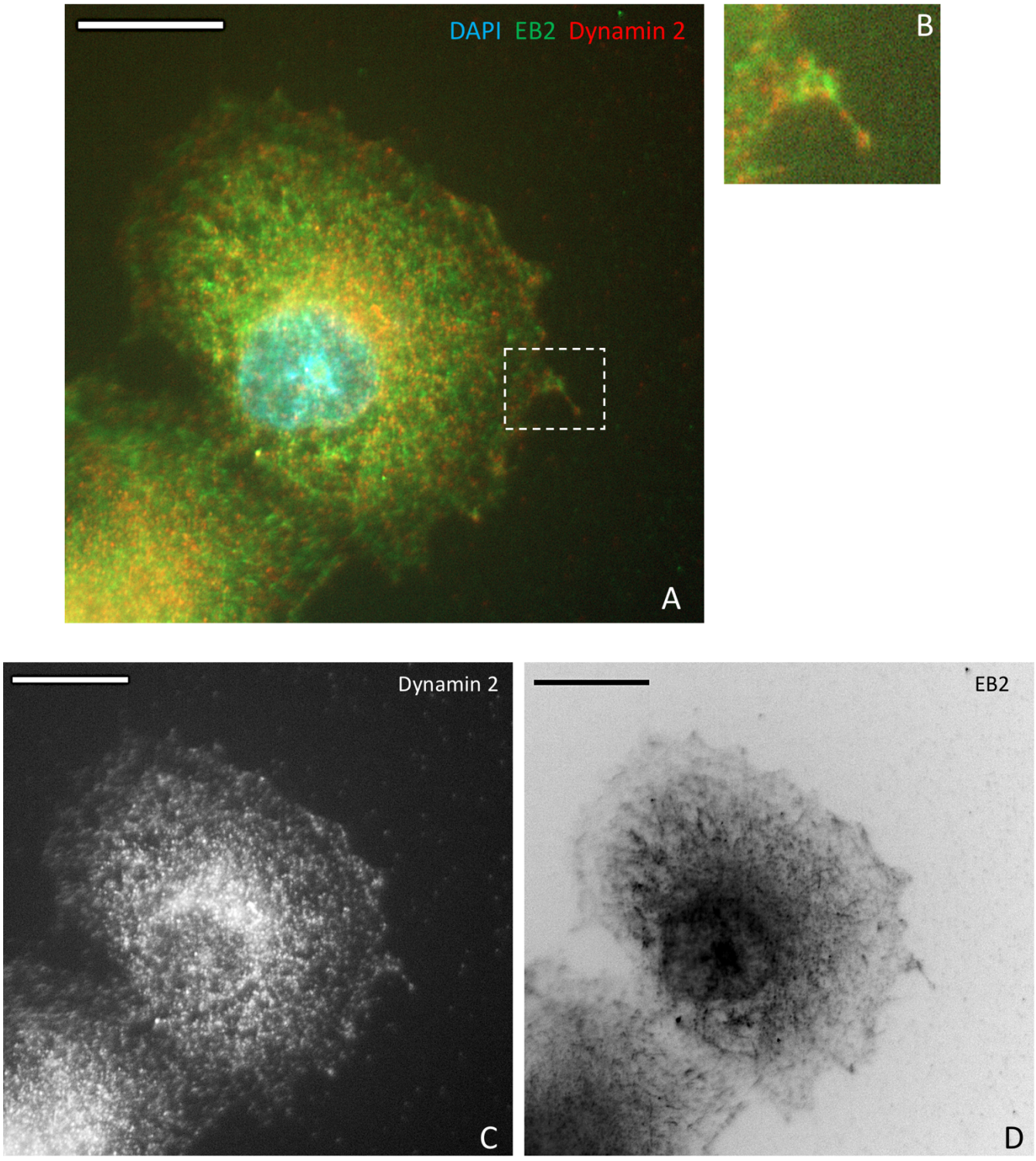

Figure 18. EB2 and dynamin2 in PANC1^{EB2Hi} migrating cells. Cells were left to migrate for 8 h following the creation of a scratch and were then fixed and labelled for EB2 (green), dynamin2 (red) and the nucleus (DAPI, blue). Both EB2 and dynamin2 accumulate at the leading edge of migrating PANC1EB2Hi cells (panels A, C and D) and enlargement of a section along the leading edge strongly suggests that these proteins colocalise (scale bar = 20 µm).

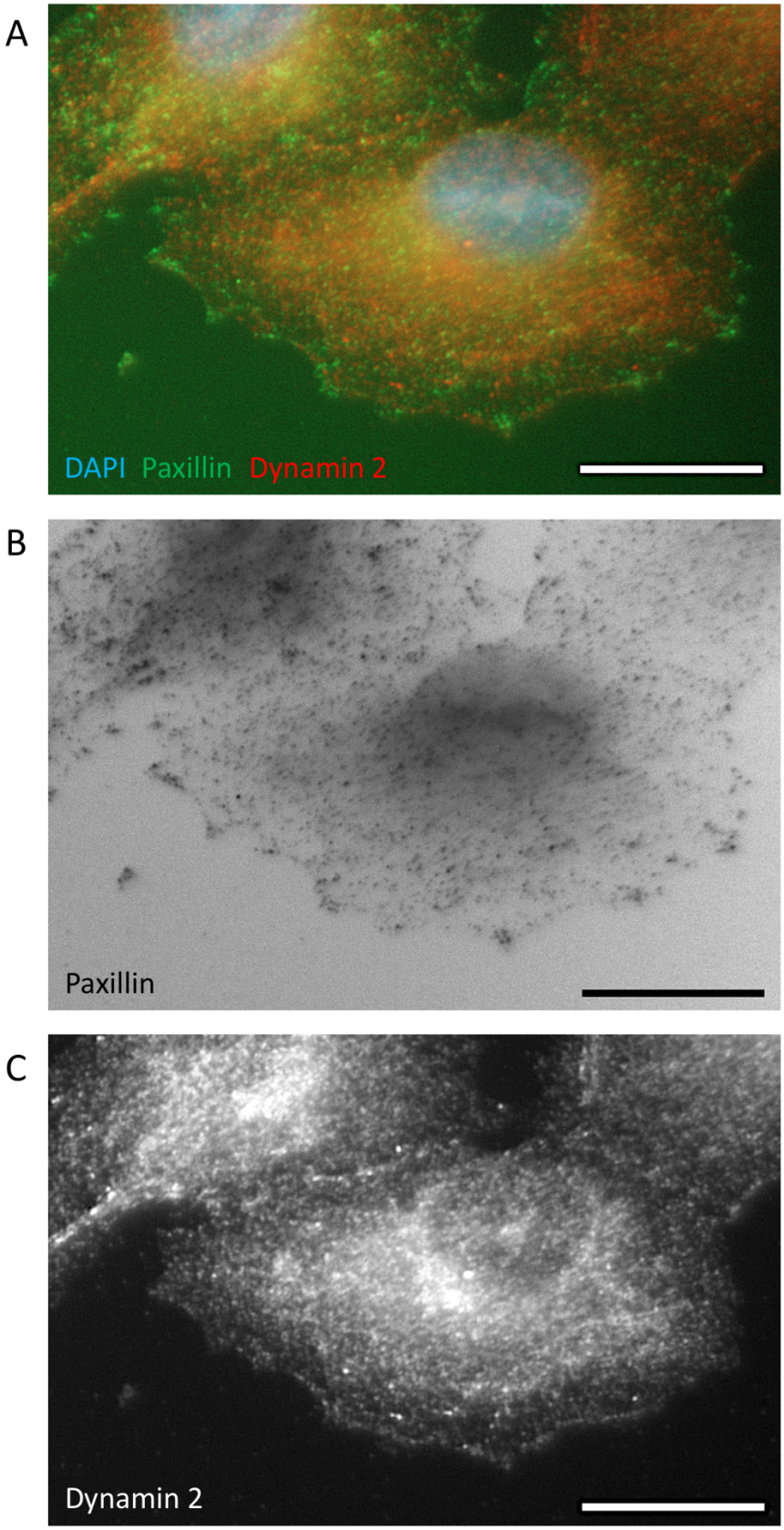

Figure 19. Dynamin2 and FAs in migrating PANC1^{EB2Hi} cells. PANC1^{EB2Hi} cells were left to migrate for 8 h following the creation of a scratch and then labelled for paxillin (green), dynamin2 (red) and the nucleus (DAPI, blue).
Panel A and C show that dynamin2 localises along the leading edge of migrating cells but is also distributed throughout the cell. In panel B it can be seen that paxillin is present in large spots at the leading edge (FAs), which indicates that there may be colocalisation between paxillin and dynamin2 (panel A) (scale bar = 20 µm).

Inhibition of ROCK with Y27632 in PANC1^{EB2Hi} cells

Following treatment with the ROCK inhibitor Y27632 for 8 h, PANC1^{EB2Hi} cells were fixed with methanol and fluorescently labelled for different proteins to investigate the effects that ROCK inhibition has on migrating PANC1^{EB2Hi} cells.

β-actin + pMLC

As pMLC is a substrate of ROCK, labelling for pMLC was conducted as a control to confirm ROCK inhibition following treatment with Y27632. Figure 20 shows PANC1^{EB2Hi} cells fluorescently labelled for β-actin and pMLC. Fluorescence intensity analysis showed a significant decrease in pMLC following treatment with the ROCK inhibitor (one-way ANOVA, $p < 0.05$).

Moreover, using the cells labelled for β-actin, the morphology of migrating cells following ROCK inhibition was investigated. This was analysed in CellProfiler using the eccentricity parameter, wherein 0 is a perfect circle and 1 is a line, and therefore allows us to determine how 'round' the cells are. It was found that PANC1^{EB2Hi} cells treated with Y27632 had an increased eccentricity and thus had a more elongated morphology (Figure 21).

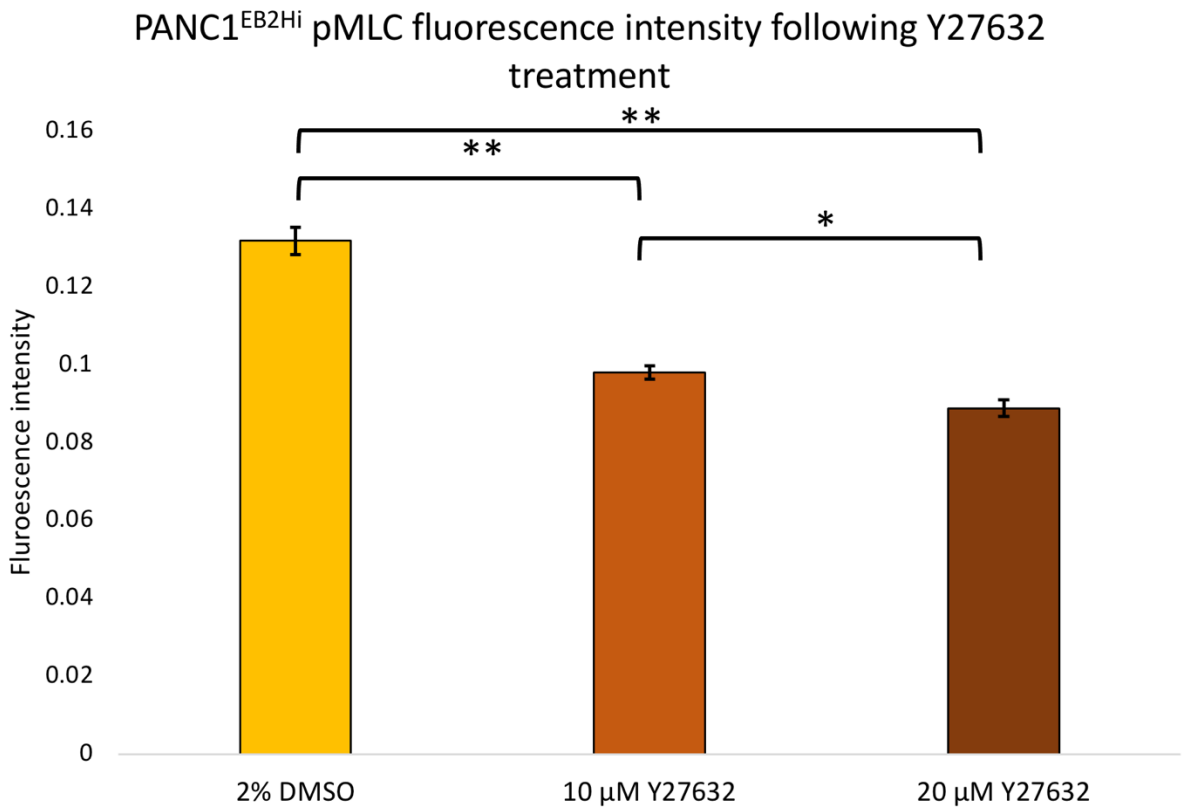

Figure 20. Migrating PANC1^{EB2Hi} cells incubated with the ROCK inhibitor Y27632 for 8 h before fixation and fluorescent immunolabelling for pMLC. One-way ANOVA showed that there was a statistically significant difference in pMLC fluorescence intensity between all treatments (* = $p < 0.05$, ** = $p < 0.01$) (based on 289 cells for 2% DMSO, 413 cells for 10 µM Y27632 and 245 cells for 20 µM Y27632).

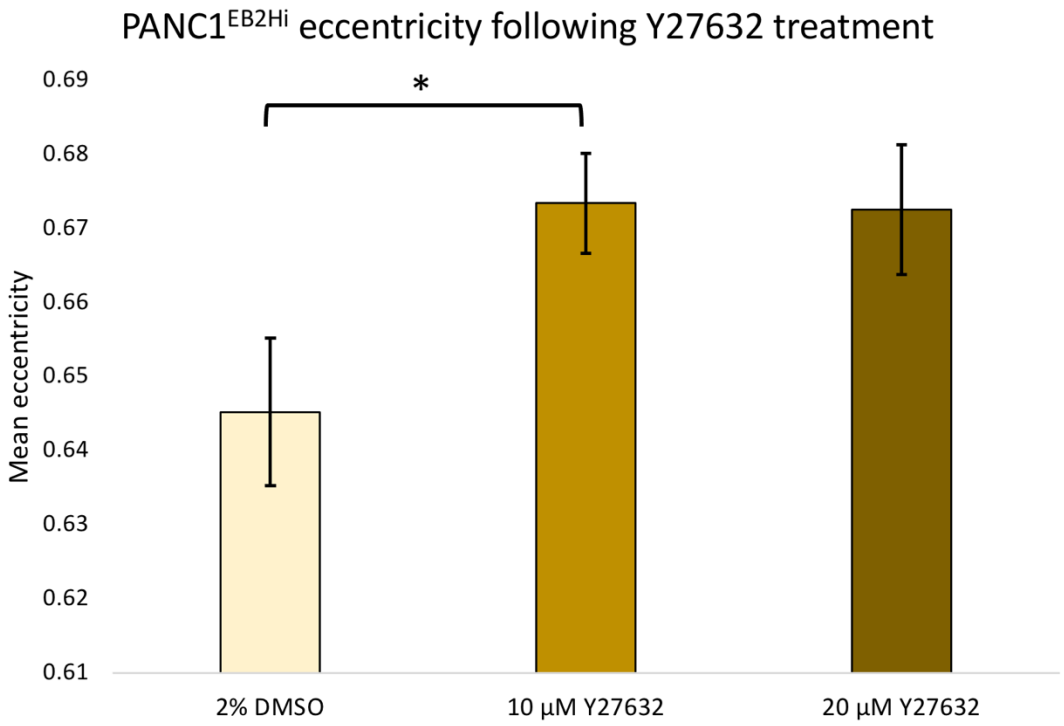

Figure 21. Migrating PANC1^{EB2Hi} cells were treated with either 2% DMSO (control) or 10 µM or 20 µM Y27632 for 8 h. The cells were then fixed and labelled for β-tubulin before being analysed in CellProfiler to determine the eccentricity of the cell shape. A significant increase in eccentricity was found in cells treated with 10 µM Y27632 compared to the control (one-way ANOVA, $p < 0.05$) (based on 305 cells for 2% DMSO, 459 cells for 10 µM Y27632 and 265 cells for 20 µM Y27632).

GEF-H1 + acetylated tubulin + Beta-tubulin

While treatment with 10 µM Y27632 decreased the fluorescence intensity of GEF-H1 in migrating PANC1^{EB2Hi} cells, this decrease was not significant (one-way ANOVA, $p > 0.05$). However, treatment with 20 µM Y27632 resulted in a significant increase in GEF-H1 compared to the control (2% DMSO) and 10 µM Y27632 (one-way ANOVA, $p < 0.01$) (Figure 22). Thus, indicating that when ROCK is inhibited, the concentration of GEF-H1 increases.

Furthermore, in Figure 23 it appears that the GEF-H1 in the DMSO control is present throughout the cell, whereas in the cells treated with the ROCK inhibitor it seems that the GEF-H1 is localised in a slightly more linear formation. This could indicate that there is more inactive GEF-H1 still associated with the MTs following Y27632 treatment. However, due to time constraints, staining was only done with acetylated tubulin and so this can't be confirmed in the present study. Interestingly, it appears as though the amount of acetylated tubulin also decreased (Figure 23), however this cannot be compared as the images were not taken on fixed settings for acetylated tubulin.

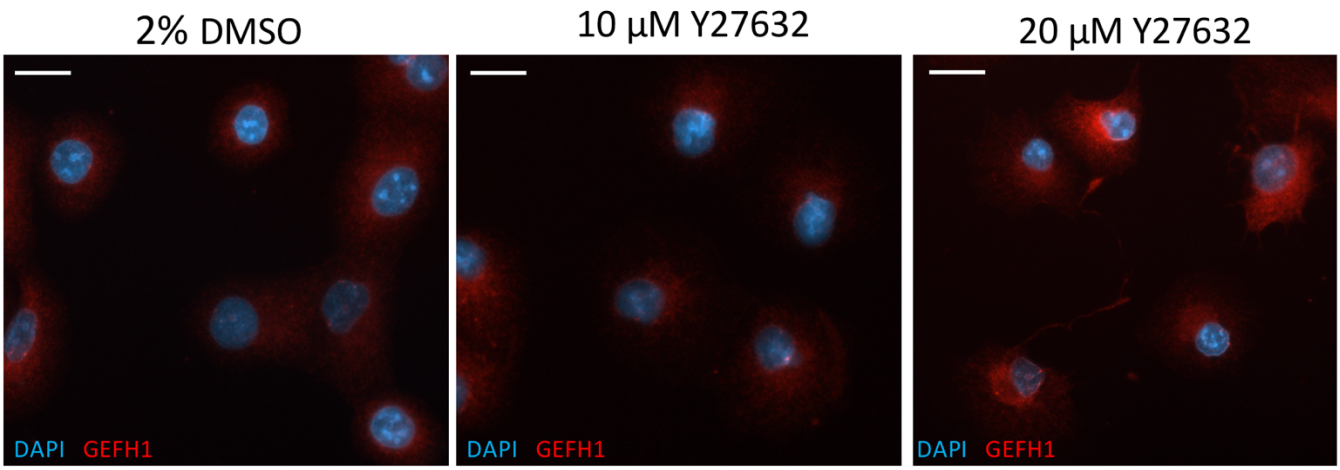

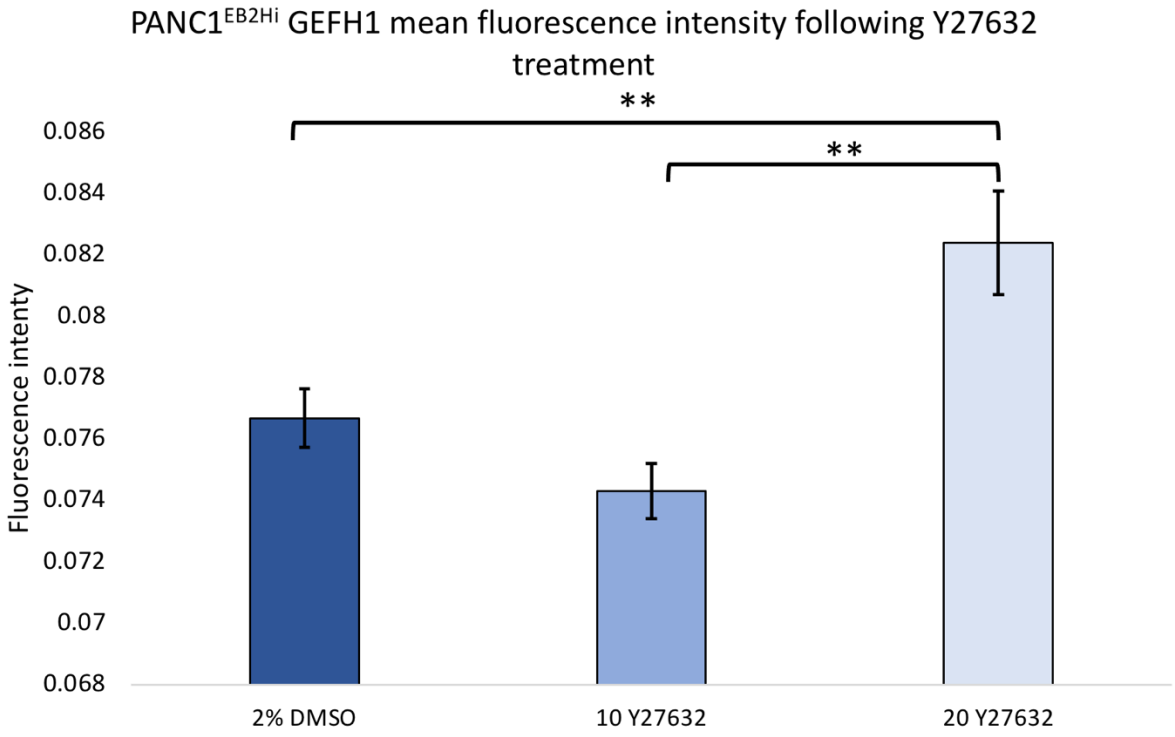

Figure 22. PANC1^{EB2Hi} cells incubated with either 2% DMSO, 10 µM or 20 µM Y27632 for 8 h and labelled for GEF-H1 (red) and the nucleus (DAPI, blue). Fluorescence intensity analysis of GEF-H1 showed that treatment with 20 µM Y27632 resulted in a significant increase in GEF-H1 fluorescence intensity compared to the control (2% DMSO) and treatment with 10 µM Y27632 (one-way ANOVA, $p < 0.01$) (based on 199 cells for 2% DMSO, 248 cells for 10 µM Y27632 and 206 cells for 20 µM Y27632). (Scale bar = 30 µm).

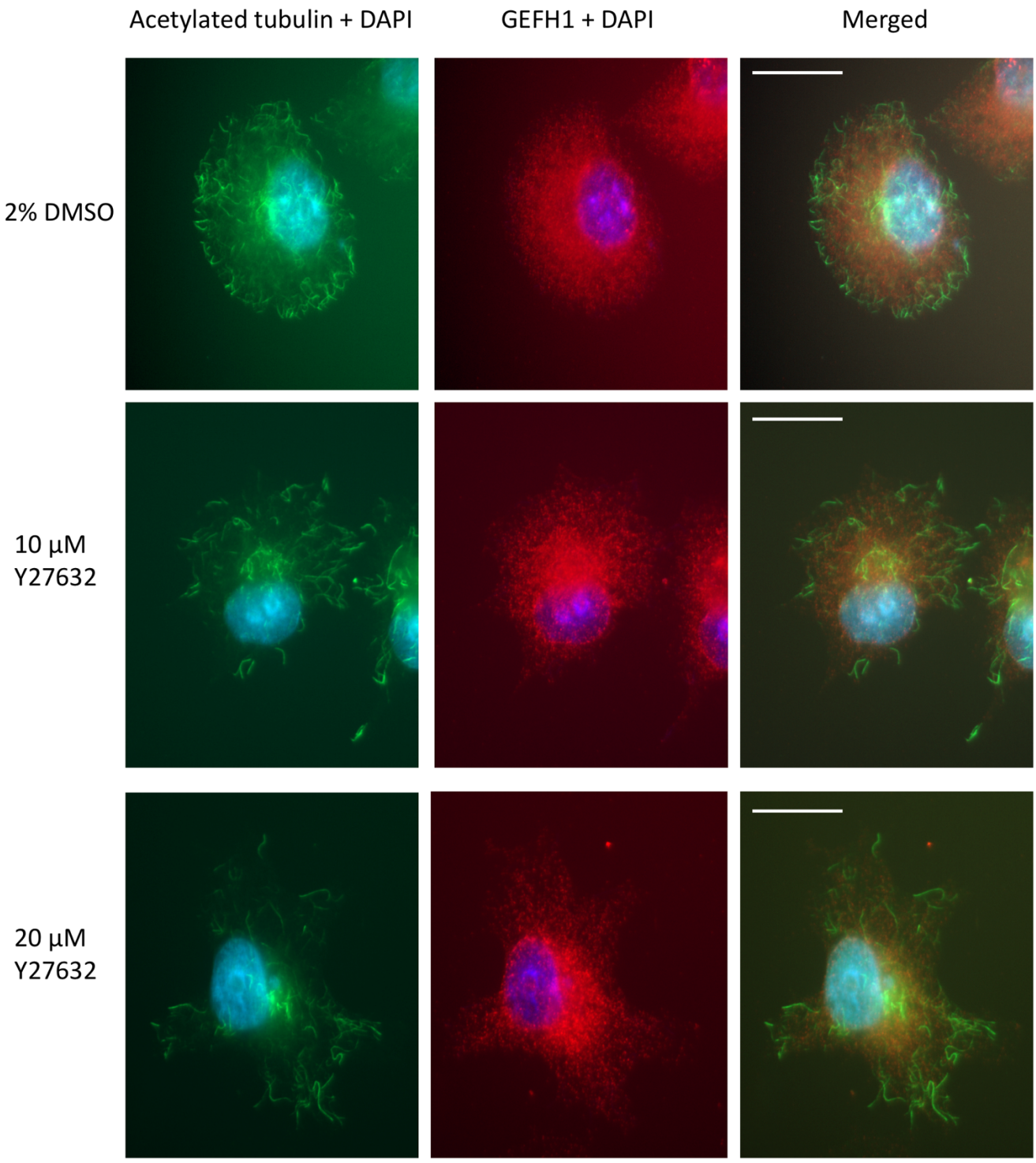

Figure 23. Random migrating PANC1^{EB2Hi} cells treated with the ROCK inhibitor Y27632 and labelled for acetylated tubulin (green), GEF-H1 (red) and the nucleus (DAPI, blue). GEF-H1 appears to be more concentrated in the cell cortex in the control and more widely distributed throughout the cell body in inhibited cells. ROCK inhibition appears to decrease acetylated tubulin. (Scale bar = 20 µm)

3.4.2 High and low EB2 expression in migrating MDA-MB-321 cells

EB2 fluorescence intensity analysis

The MDA^{EB2KO} cells were previously generated in the Mogensen lab by Ben Rix using CRISPR/Cas9, and to confirm the partial EB2 knockout in this study fluorescence intensity analysis was carried out. The MDA^{EB2KO} cells had a significantly decreased EB2 fluorescence intensity ($p < 0.01$) and this can be seen visually in the fluorescence images taken on set exposure (Figure 24).

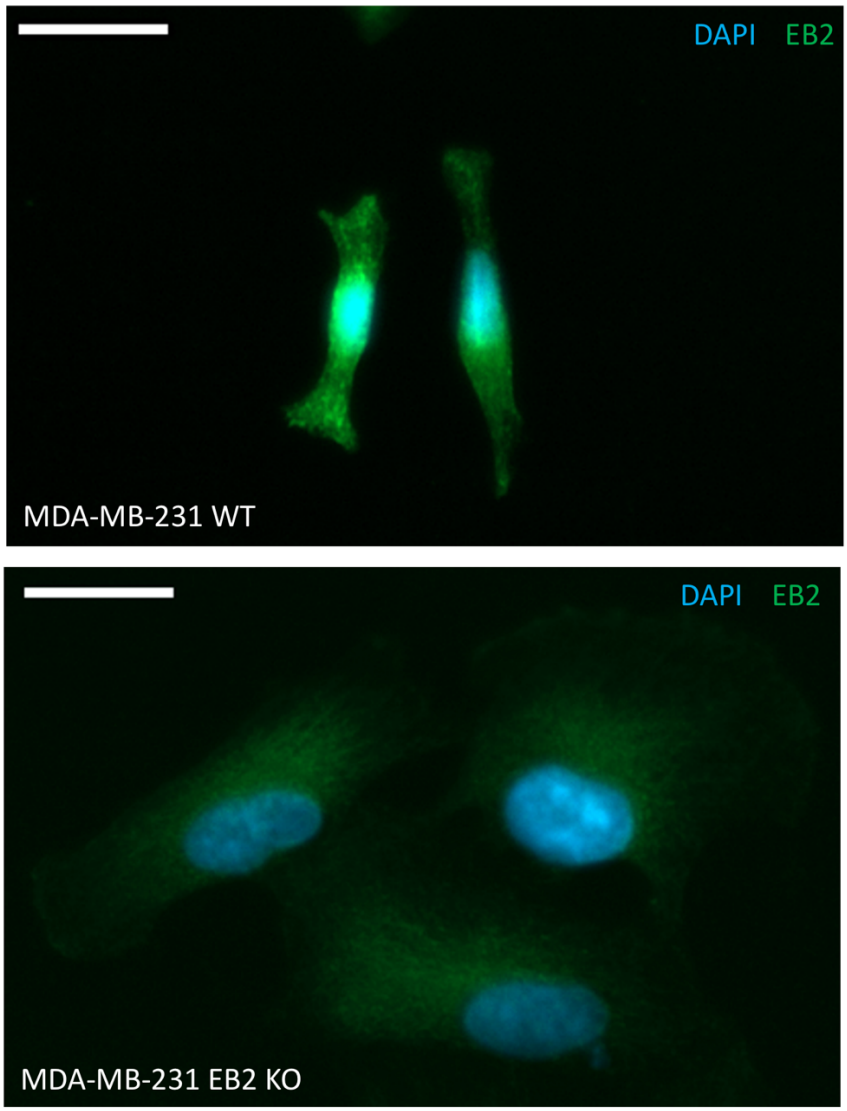

Figure 24. MDA^{WT} and MDA^{EB2KO} fluorescence intensity analysis. MDA^{EB2KO} cells have a significantly lower EB2 fluorescence intensity (* p = <0.01). Immunolabelling for EB2 shows that MDA^{WT} cells have more fluorescence that MDA^{EB2KO}, however, EB2 was still detected in these cells (scale bar = 20 µm).

Live migration

Previous work done in the Mogensen lab using PANC1^{EB2Hi} and PANC1^{EB2Low} clones has shown that cells expressing high levels of EB2 have an increased cell migration velocity (see Appendix). Therefore, live time-lapses of randomly migrating MDA^{WT} and MDA^{EB2KO} cells was performed to investigate whether this finding applies to other cell types.

Analysis of the live time-lapse movies in ImageJ using TrackMate found that MDA^{EB2KO} cells have a significantly decreased cell migration velocity compared to MDA^{WT} cells (Mann-Whitney U-test, $p < 0.001$). Additionally, the morphology of the migrating cells was also altered. Migrating MDA^{WT} cells displayed the elongated morphology typical of MDA-MB-231 cells, whereas MDA^{EB2KO} cells appeared larger and more rounded, with some cells displaying a completely circular morphology (Figure 25). This suggests that the decrease in cell migration velocity in MDA^{EB2KO} cells could be due to the lack of migratory phenotype displayed by these cells.

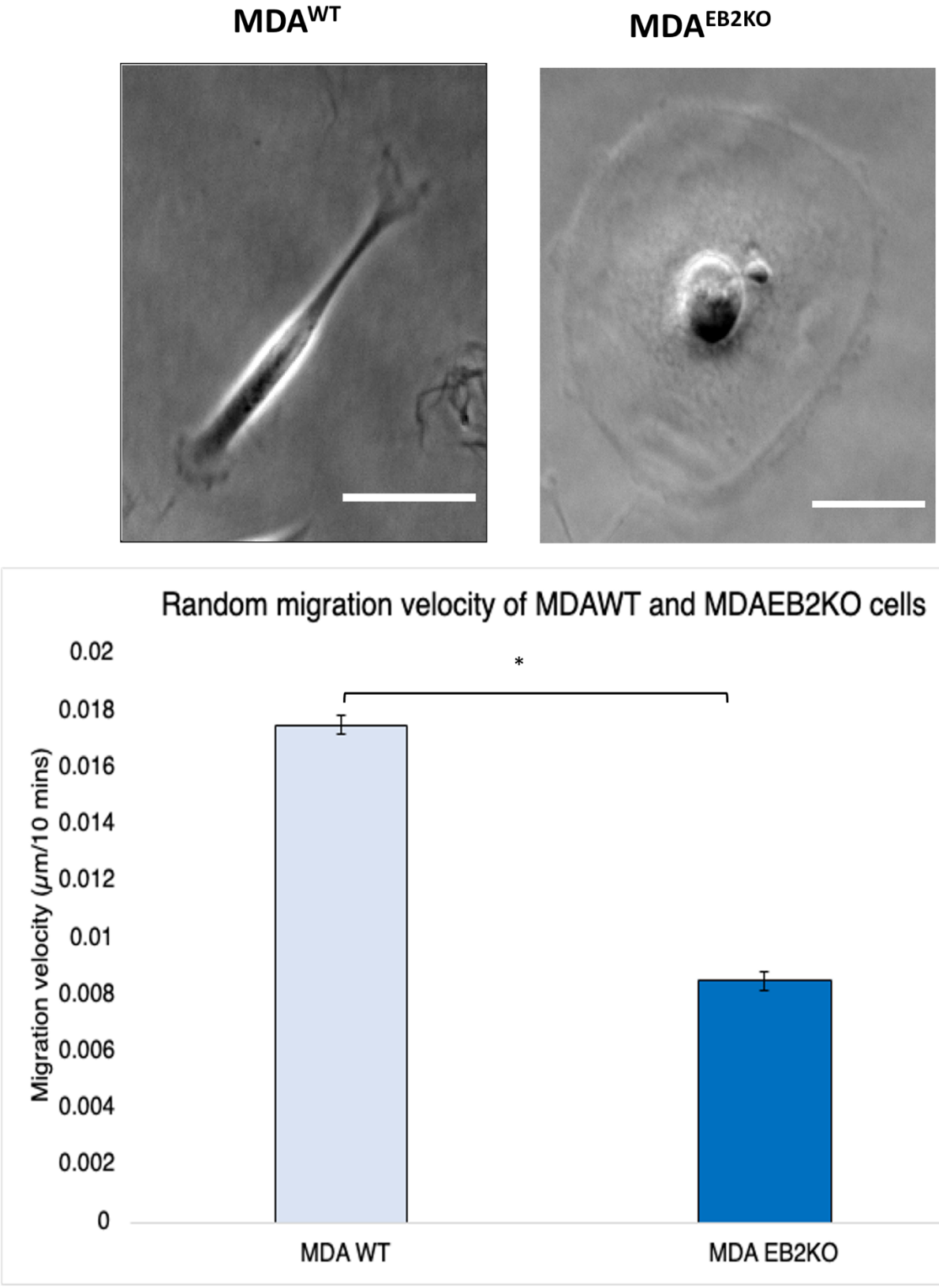

Figure 25. Live time-lapse of randomly migrating MDA^{WT} and MDA^{EB2KO} cells. MDA^{EB2KO} cells had a significantly decreased cell migration velocity compared to MDA^{WT} cells (Mann-Whitney U test, $p < 0.001$). Images from the cell migration time lapses show that the morphology of the migrating cells also varied, with the MDA^{WT} cells having an elongated morphology and the MDA^{EB2KO} cells having a rounded morphology (scale bar = 20 μm).

GEF-H1 in MDA^{WT} and MDA^{EB2KO} cells

As both EB2 and GEF-H1 are MT associated proteins that have been demonstrated to be involved in cell migration, the effect of EB2 expression on GEF-H1 was analysed. Migrating MDA^{WT} and MDA^{EB2KO} migrating cells were fluorescently labelled for GEF-H1 and the fluorescence was compared between the two cell lines. The fluorescence intensity analysis determined that MDA^{EB2KO} had a significantly higher GEFH1 intensity than MDA^{WT} cells (Mann-Whitney, $p < 0.01$) (Figure 26). However, this analysis was done manually in ImageJ and is based on a very small sample size and thus may not be representative. Additional experiments such as fluorescence intensity analysis with a larger number of cells and a Western blot need to be conducted in order to verify this result.

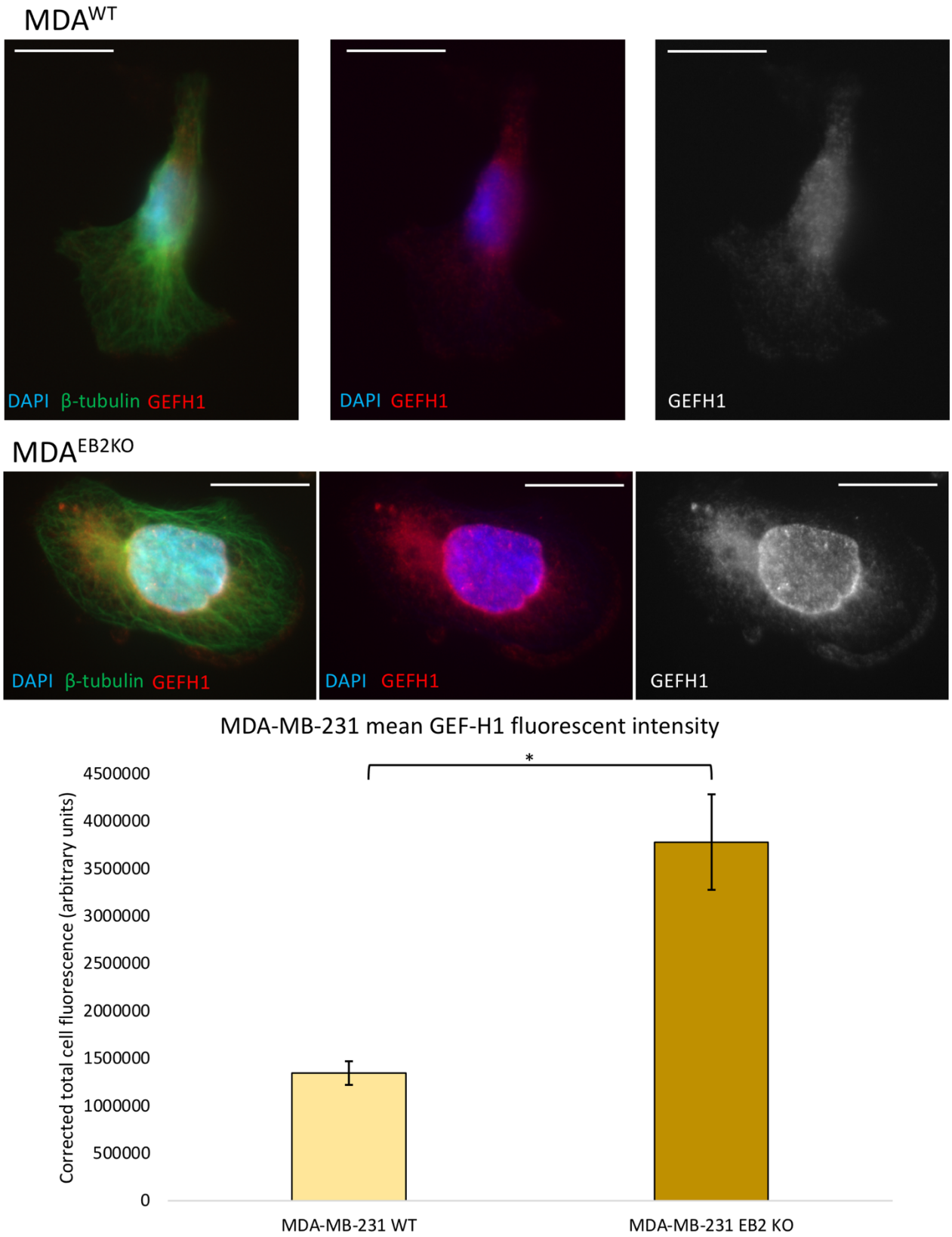

Figure 26. Randomly migrating MDA^{EB2KO} cells have increased GEF-H1 fluorescence compared to MDA^{WT} cells. The fluorescence images were taken on fixed settings and show that MDA^{EB2KO} cells have higher fluorescence. Additionally, the localisation of GEF-H1 seems to be primarily in the cell cortex, with a small amount of accumulation at the leading edge. The graph shows that the MDA^{EB2KO} cells have a significantly higher level of GEF-H1 fluorescence compared to MDAWT cells (Mann-Whitney, $p < 0.01$). However, this result is based on a very small sample (22 cells for MDA^{WT} and 20 cells for MDA^{EB2KO}) (scale bar = 10 µm).

Dynamin2 expression in MDA^{WT} and MDA^{EB2KO} cells

As previously mentioned, a co-immunoprecipitation assay in the Mogensen lab identified a potential interaction between EB2 and dynamin2, and consequently to further explore this the effects of decreased EB2 expression on dynamin2 expression were investigated. MDA^{WT} and MDA^{EB2KO} cells were fluorescently labelled for dynamin2 and the fluorescence intensity was analysed. The results showed that the MDA^{EB2KO} cells had a significantly increased fluorescence intensity compared to the MDA^{WT} cells (Mann-Whitney U, $p < 0.01$) (Figure 27). Additionally, from the migrating MDA^{WT} and MDA^{EB2KO} cells labelled for dynamin2 and paxillin, localisation of dynamin2 to the leading edge of migrating cells and colocalisation between these proteins can be observed. This suggests that dynamin2 localises to FAs.

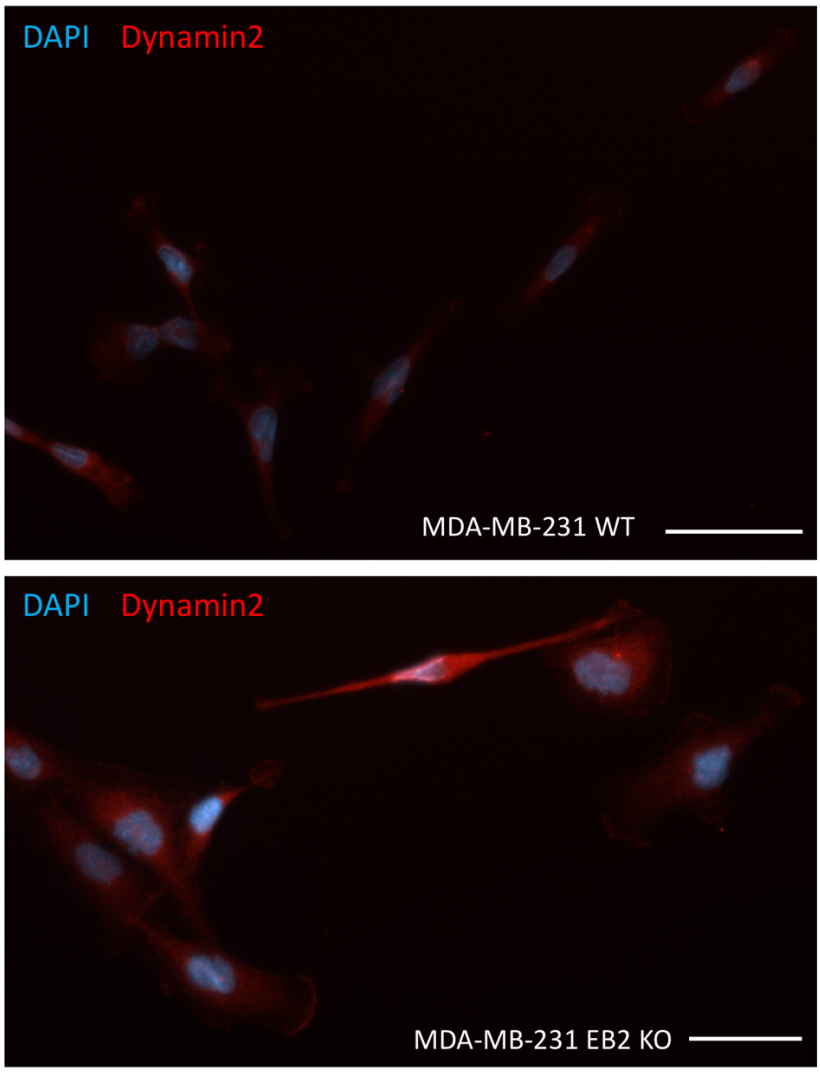

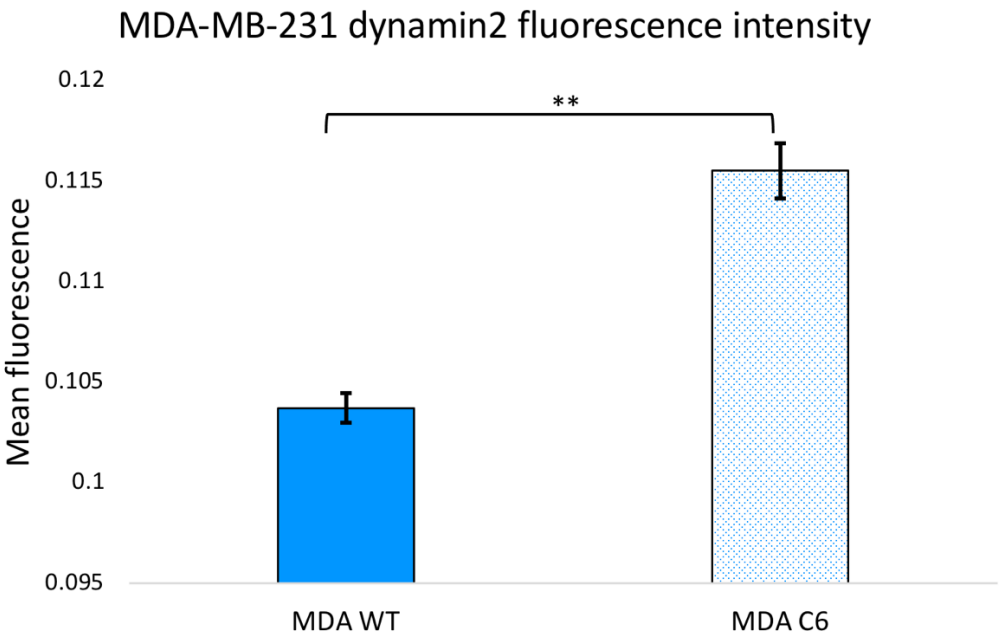

Figure 27. Dynamin2 fluorescence intensity analysis of MDA^{WT} and MDA^{EB2KO} cells. The fluorescence images taken on fixed settings show that MDA^{EB2KO} cells had higher dynamin2 fluorescence than MDA^{WT} cells, which was confirmed with fluorescence intensity analysis that showed that the fluorescence intensity was significantly higher in MDA^{EB2KO} cells (Mann-Whitney U test, $p < 0.01$) (Scale bar = 50 µm).

Chapter 4.
Discussion

Based on the results in this study the level of EB2 expression has a significant effect on several factors of cell migration in cancer cells. The differences in MT organisation between PANC1^{EB2Hi} and PANC1^{EB2Low} cells suggests that EB2 is important in MT organisation and that, when the expression of this protein is decreased, polarisation is lost. Generation of polarity is an important stage in cell migration, and therefore these cells would have a non-migratory phenotype, while cells expressing an increased level of EB2 are polarised and have a migratory phenotype. Goldspink et al. found a similar result, with EB2 depletion resulting in a loss of polarised MT organisation during apico-basal epithelial cell differentiation (Goldspink et al., 2013). Additionally, this is consistent with the finding that MDA^{EB2KO} cells had decreased cell migration velocity compared to MDA^{WT} cells. Moreover, PANC1^{EB2Low} cells had a more radial MT organisation, while PANC1^{EB2Hi} cells had a polarised MT organisation. This indicates that EB2 is essential for MT reorganisation during cell migration, which is key to providing migrating cells polarity. As EB2 localises to MT ends, it is possible that overexpression of EB2 leads to increased polarisation, which could play a part in increasing cell migration. Immunolabelling of MTs in PANC1^{EB2Hi} and PANC1^{EB2Low} cells show that PANC1^{EB2Low} cells have a more radial MT organisation compared to the PANC1^{EB2Hi}. This is evidence that the PANC1^{EB2Low} cells are not polarised whereas the PANC1^{EB2Hi} cells are.

The generation of cellular asymmetries, commonly referred to as cell polarity, is important for a myriad of functions, including morphogenesis, cytokinesis and cell migration (St Johnston and Ahringer, 2010) and this polarity is generated through the organisation of the cytoskeleton. Broadly, three types of cell polarity have been described: apical-basal, anterior-posterior and planar cell polarity (Dow and Humbert, 2007). Cell migration is a polarised process and the first stage in cell migration is the generation of front-rear polarity; cells not undergoing migration typically have a radial MT organisation and, in response to external stimuli, signalling pathways controlling cytoskeleton organisation are activated (Meiring et al., 2020). Gradual activation of Cdc42 and Rac at the leading edge control cytoskeleton organisation to promote lamellipodia formation, while Rho is activated at the rear of the cell and controls the retraction of the rear and cell body movement through inducing contraction of actomyosin (Etienne-Manneville, 2008).

Immunofluorescence labelling indicates that there is some accumulation of EB2 along the leading edge of migrating cells. This could potentially be attributed to the increased expression in these subcloned cells, however, it may also be due to the increased MT dynamics at the leading edge of migrating cells. The presence of EB2 at the leading edge of migrating cells, along with the potential colocalization between EB2 and pMLC, may indicate that this protein is not just involved in cell migration, but actively promotes migration and the migratory phenotype. However, it may be that the colocalisation of EB2 and pMLC is at FAs. Associations between FAs and pMLC have been identified, with one study showing that paxillin knockdown in 3D migrating breast cancer cells resulted in a decrease in pMLC (Deakin and Turner, 2011).

Previous work in the Mogensen lab identified dynamin2 as a potential binding partner of EB2, and Western blot analysis of PANC1^{EB2Hi} and PANC1^{EB2Low} clones suggested that PANC1^{EB2Low} cells have elevated EB2 expression compared to PANC1^{EB2Hi} cells (see Appendix). In line with this, fluorescence intensity analysis of MDA^{WT} and MDA^{EB2KO} cells revealed that MDA^{EB2KO} cells had increased fluorescence, suggesting an increased level of dynamin2 expression compared to MDA^{WT} cells. However, a Western blot needs to be carried out to confirm this result.

Dynamin2 has been found to be overexpressed in numerous cancer types (reviewed by (Trochet and Bitoun, 2021)) and has been demonstrated to be involved in cell migration in cancer cells, for example in pancreatic cancer cells, where silencing of dynamin2 resulted in decreased migration and dynamin2 depletion resulted in a decrease in lamellipodia formation (Razidlo et al., 2013). Additionally, dynamin2 overexpression has been identified in both breast and pancreatic cancer tissues (Sajed et al., 2020; Eppinga et al., 2012) and high levels of MAPRE2 expression has been identified in both breast (Heiser et al., 2012) and pancreatic cancer cells (Abiatari et al., 2009b). Both EB2 and dynamin2 are involved in cytoskeleton organisation in cell migration and so co-localisation of these proteins, as suggested by fluorescent staining in this study, could indicate an interaction between these proteins that causes changes in the cytoskeleton.

Moreover, identification of dynamin2 accumulation at the leading edge of migrating cells and localisation to FAs is consistent with Schafer et al., who found that dynamin2 localises where actin assembly occurs (Schafer et al., 2002). In addition to colocalising with EB2, dynamin2 colocalises with cortactin (Yamada et al., 2016). Cortactin binds to F-actin and has several binding sites for a variety of proteins, including an src homology 3 (SH3) domain that can bind to dynamin2, and through this dynamin2 is able to regulate actin organisation and cell shape; NIH/3T3 cells expressing dynamin2 missing the cortactin binding sequence exhibited a more elongated morphology and had a large increase in stress fibers along the long axis of the cells (McNiven et al., 2000). Therefore, this potentially suggests that EB2 could be involved in actin cytoskeleton organisation in addition to MT organisation. A potential mechanism of action may be an interaction between EB2 and dynamin2 that promotes cortactin activity, leading to increased actin reorganisation and an increase in cell migration.

As expected, GEF-H1 was found to localise along MTs in both PANC1 and MDA-MB-231 cells. Interestingly, the MDA^{EB2KO} cells were found to have a significantly higher level of GEF-H1 fluorescence, indicating that these cells have increased GEF-H1 expression compared to the MDA^{WT} cells. GEF-H1 expression has been linked to the stiffness of the ECM, with cells migrating through stiffer ECMs having higher levels of active GEF-H1 (Heck et al., 2012); while this finding was related to cells migrating through 3D ECMs, the surface that the cells were migrating across in this study could have contributed to the increased GEF-H1 expression. In this investigation the cells were migrating on collagen I coated glass coverslips, and while every effort was made to ensure all coverslips were coated the same way, there could have been variations in the thickness of the coating. Additionally, as this finding is based on a very small number of cells, no accurate conclusions can be taken from this result and further investigation, including fluorescence intensity analysis with a larger number of cells, PCR analysis and Western blot, needs to be carried out to provide confirmation.

Increased levels of GEF-H1 have been linked to cancer. GEF-H1 upregulation has been identified in colon cancer (Cao et al., 2019) and melanoma (Shi et al., 2016). Therefore, as EB2 upregulation has been identified in a number of cancers, it would be expected that the MDA^{WT} cells would have increased levels of GEF-H1, however the opposite was observed in this study. GEF-H1 upregulation causes increased phosphorylation of MLC by RhoA (Cao et al., 2019), which would indicate that these cells have more actomyosin contractility and thus increased cell migration. Indeed, Cao et al.

found that cells overexpressing GEF-H1 have increased migration and invasion (Cao et al., 2019). This contradicts the analysis of the MDA^{WT} and MDA^{EB2KO} cells from this study, wherein MDA^{EB2KO} had a decreased migration velocity compared to wildtype cells, but increased levels of GEF-H1 fluorescence intensity. As GEF-H1 is activated following MT depolymerisation, it may be that MDA^{EB2KO} cells have increased MT stability. While association between GEF-H1 and MTs was identified in both MDA^{WT} and MDA^{EB2KO} cells, GEF-H1 was not identified solely along MTs. Previous studies have indicated that the proper distribution of GEF-H1 in cells following the release from MTs is dependent upon GEF-H1 regulation and MT depolymerisation (Azoitei et al., 2019).

Moreover, the fluorescence intensity of GEF-H1 in $PANC1^{EB2Hi}$ cells following Y27632 treatment was investigated. Interestingly, in $PANC1^{EB2Hi}$ cells, 10 µM Y27632 slightly decreased GEF-H1 fluorescence intensity (although this was not significant) but 20 µM Y27632 significantly increased GEF-H1 intensity. Y27632 works to inhibit ROCK by competitively binding to the ATP-pocket in the active site (Ishizaki et al., 2000; Jacobs et al., 2006), thereby preventing ROCK from binding to ATP and becoming active. Furthermore, it was reported that Y27632 does not affect the levels of RhoA (Sahai et al., 1999). Thus, as there is reportedly no change in the level of RhoA following ROCK inhibition, it could be that there is a mechanism that prevents an accumulation of RhoA, which may result in an accumulation of GEF-H1, as this protein is responsible for activating RhoA.

Part of the hypothesis proposed in this study is that increased levels of EB2 expression may lead to an increase in amoeboid migration through the increase of MT dynamics, which would cause the release of GEFH1, thus suggesting that EB2 regulates GEFH1. Overall, there seems to be several contradictions between the existing literature and the results in this study regarding GEFH1.

While this study only investigated cells in 2D, there is evidence that migratory cell morphology in 2D can predict 3D morphology (although it cannot predict invasiveness) (Ziperstein et al., 2015). Therefore, it may be possible to draw some conclusions regarding 3D migratory types from the results of this investigation. We propose that EB2 expression affects the migratory phenotype in 3D environments, with increased EB2 expression leading to an amoeboid migration mode. The proposed mechanism of action is that increased EB2 expression leads to increased MT dynamics, resulting in the release of GEF-H1 from MTs. GEF-H1 is inactive when bound to MTs but is activated upon its release and this will result in RhoA activation, causing actomyosin contraction in the cortex of the cell and thus increased amoeboid migration.

To investigate this, $PANC1^{EB2Hi}$ cells were treated with the ROCK inhibitor Y27632. Several studies have treated 3D migrating cells with Y27632 and have found that this inhibitor suppresses the amoeboid migration mode. Huang et al. observed that glioma cells migrating in 3D hydrogels and treated with Y27632 underwent the amoeboid-to-mesenchymal (AMT) transition, while untreated cells underwent the mesenchymal-to-amoeboid (MAT) transition. Additionally, it was also found that cells treated with the ROCK inhibitor had higher integrin αVβ3 expression, indicating that these cells are forming FAs, which are not found in amoeboid migrating cells (Huang et al., 2017). A similar finding was observed by Weeks et al. in astrocytoma cells, wherein treatment with Y27632 inhibited membrane bleb formation and resulted in the mesenchymal migratory phenotype (Weeks et al., 2012).

When PANC1^{EB2Hi} cells were treated with Y27632, a change in cell morphology was observed. Analysis of the eccentricity in CellProfiler determined that the treated cells had increased eccentricity, which indicates that these cells have a more elongated morphology as opposed to spherical. This finding is in accordance with the previous studies, as a more elongated morphology is indicative of the mesenchymal migration mode as opposed to the amoeboid type. However, although the change in morphology was found to be significant ($p < 0.05$), there was not a dramatic change in eccentricity (mean eccentricity was 0.645 for 2% DMSO, and 0.673 for both 10 µM and 20 µM Y27632). Additionally, while the fluorescence intensity analysis of pMLC did show a significant decrease in pMLC following treatments with both Y27632 inhibitor concentrations, pMLC was still detected, therefore a future study using a higher concentration or a longer inhibitor incubation time followed by analysis of cell morphology could be carried out to determine whether this would have an effect on the eccentricity of the cells. However, a viability assay would need to be conducted to determine whether an increase in inhibitor concentration would be tolerated in these cells.

In a 3D environment, PANC1 cells have been shown to migrate using actin-rich protrusions called invadopodia (Kim et al., 2020). When RhoA/ROCK is inhibited, cells undergo a transition from amoeboid to the mesenchymal phenotype (Sahai and Marshall, 2003). While analysis of cell migration in 3D wasn't conducted here due to time constraints, cell morphology is a good indicator for migration mode. It is essential for cells to be able to change their migration mode based on the microenvironment and certain cell types are able to transition from mesenchymal to amoeboid migration. While mesenchymal migrating cells have cell protrusions in the form of lamellipodia, amoeboid cells generate spherical membrane bulges known as blebs (Schick and Raz, 2022). These blebs contain no F-actin and are mediated by hydrostatic pressure as a result of myosin II contraction (Schick and Raz, 2022). Adherent migrating cells treated with Y27632 (ROCK inhibitor) or blebbistatin (myosin inhibitor) had a significantly larger lamellipodia and, in addition, adherent cells possessing a constitutively active version of ROCK had a rounder cell morphology and the ability to form blebs, suggesting that the increasing actomyosin contractility is sufficient for cells to switch from lamellipodia to bleb formation (Bergert et al., 2012).

However, there is evidence to suggest that Rho/ROCK signalling is only essential for the early invasion stage of cell migration; MDA-MB-231 cells in aligned collagen matrices treated with either a Rho or ROCK inhibitor showed no significant alteration in 3D migration (Provenzano et al., 2009). This is supported by another study that found that when MDA-MB-231 cells migrating through a collagen microtrack were treated with either a Rho, ROCK or MCLK inhibitor, while cell traction forces were reduced, no effect on migration speed was observed (Carey et al., 2015).

Whereas Szarama et al. found that cochlea treated with SU5402 had a significant increase in MAPRE2 expression (Szarama et al., 2012), here there was no difference in EB2 fluorescence intensity in PANC1^{EB2Low} cells treated with SU5402, and only a slight decrease in EB2 intensity in PANC1^{EB2Hi} cells. However, this investigation was only carried out in the PANC1^{EB2Hi} and PANC1^{EB2Low} cells. Analysis of EB2 expression following inhibition of FGFRs would be interesting to carry out in the MDA^{WT} and MDA^{EB2KO} cells to determine whether FGF18-FGFR3 signalling could affect EB2 expression in other cell types. Furthermore, the link between FGFR3 and MAPRE2 was detected in the development of the organ of Corti (Szarama et al., 2012) and therefore, while no link between

FGFR3 and EB2 expression was detected here, it may be that there is a link between the two proteins during development or it may be cell type dependent.

Elucidating the functions of EB2 has implications beyond cell migration and cancer. Cyclin-dependent kinase-like 5 (CDKL5), expressed in the brain in the late embryonic stage, regulates neuronal morphogenesis, potentially through the association of this protein with F-actin (Chen et al., 2010) and MT +TIPs, including EB2. EB2 is a substrate of CDKL5 (Baltussen et al., 2018) and it has been suggested that CDKL5 influences MT dynamics through interactions with MT-associated proteins. However, while KO of CDKL5 did find reduced EB2 phosphorylation, no changes in MT stability and plasticity were detected (Di Nardo et al., 2022). Thus, while it seems that CDKL5 does regulate MT dynamics in neurons, the mechanism by which it does this through EB2 phosphorylation remains unknown. Because mutations in the CDKL5 gene results in a non-functional protein that is responsible for CDKL5 deficiency disorder, a neurological disorder that causes epileptic encephalopathy and developmental impairment (Jakimiec et al., 2020), it is important that all of the roles of CDKL5 be identified in order to find treatments for this disorder. Therefore, investigation of how EB2 regulates cell migration may also identify mechanisms and proteins that may be useful for determining the role of EB2 in neurons.

One element of cell migration that EB2 is involved in that wasn't focused on in this study is FA turnover. Mitogen-activated protein kinase kinase kinase kinase 4 (MAP4K4) is an EB2 binding partner and the FA disassembly rate decreases when either MAP4K4 is depleted or EB2 is knocked down (Yue et al., 2014). Similarly, HCLS1-associated protein X-1 (HAX1) has also been identified as an EB2 binding partner and Liu et al also showed that knockdown of either EB2 or HAX1 decreased the FA disassembly rate (Liu et al., 2015). MAP4K4 activates FA kinase (FAK) (Tripolitsioti et al., 2018; Migliavacca et al., 2022), a protein that is involved in several signalling pathways that promote cell migration, including FA turnover (Ren et al., 2000). EB2 knockdown results in a decrease in MAP4K4 in FAs and therefore it may be possible that EB2 recruits these proteins to FAs in order to carry out various roles in FA turnover. Furthermore, it has been identified that MAP4K4 phosphorylates vasodilator-stimulated phosphoprotein (VASP) in response to signalling through FGFR (Migliavacca et al., 2022) and therefore it would be interesting to see whether activation of this protein can also occur via FGFR3, as this could provide a possible explanation for the findings by Szarama et al. that FGFR3 regulates MAPRE2 expression (Szarama et al., 2012).

From this investigation it would seem that FGFRs do not affect EB2 expression, however, it may be that MAP4K4 regulates the expression of EB2. As MAP4K4 signalling occurs through a number of receptors, such as tumour necrosis factor α (TNFα) receptor 1 (Tesz et al., 2007) and epidermal growth factor receptor (EGFR) (Prolo et al., 2019), this may explain the finding in this study that FGFR inhibition had no effect on EB2 fluorescence intensity if EB2 is regulated via MAP4K4.

Moreover, through fluorescence immunolabelling in this study, evidence was found that EB2 and dynamin2 colocalise in addition to dynamin2 localisation to FAs. Dynamin2 and Hax1 are both binding partners of cortactin, a protein that regulates actin through binding to the Arp2/3 complex (Buday and Downward, 2007). Thus, through interactions with dynamin2 and Hax1, EB2 may be involved in regulating the actin cytoskeleton at FAs. In podocytes, downregulation of dynamin2 results in a loss of FAs, actin stress fibres and a dramatic change in cell shape (Gu et al., 2017). In this

same study, Gu et al. demonstrated that downregulation of mDia1 also resulted in the loss of FAs and stress fibres, and treatment of these knockdown cells with a dynamin inhibitor further decreased actin stress fibres and the number of FAs (Gu et al., 2017). Here, colocalisation of EB2 and mDia1 was identified, particularly at the leading edge of migrating cells. mDia1 knockdown impairs FA turnover, as shown in rat C6 glioma cells (Yamana et al., 2006) and further, co-expression of ROCK and mDia1 is required for evenly distributed FAs at the leading edge of HeLa cells, but expression of mDia1 alone was sufficient to marginally restore FAs in Rho inhibited HeLa cells (Watanabe et al., 1999). As actin stress fibres display a variety of morphologies and have differing associations with FAs, they can be separated into four categories: dorsal, ventral, transverse arcs and perinuclear actin cap (Tojikander et al., 2012). Human osteosarcoma mDia1 knockdown cells exhibited a reduction in dorsal stress fibre elongation as well as abnormal dorsal morphology (Hotulainen and Lappalainen, 2006), demonstrating that mDia1 is essential for the assembly of actin stress fibres. Additionally, Hotulainen and Lappalainen also found an accumulation of α-actinin, a protein initially responsible for cross-linking stress fibre bundles before being displaced by myosin II, which would further indicate the lack of proper stress fibre assembly in mDia1 knockdown cells (Hotulainen and Lappalainen, 2006). Therefore, there is evidence to suggest that there may be a FA turnover pathway involving FGFR3, MAP4K4, Hax1, EB2, dynamin2 and mDia1.

While this investigation presents some useful data regarding the effect that EB2 expression has on cell migration, it also highlights several avenues for future study. Here, PANC1 and MDA-MB-231 cell lines were used. A key cause of cancer is the development of mutations, and therefore it may be that some of the findings in this study could be attributed to a mutation in the cancer cells that is not present in non-cancerous cells. Thus, research into the effects of EB2 on cell migration in non-cancerous cells needs to be conducted to determine whether the results seen here are only due to changes in EB2 expression. Furthermore, due to time constraints, study of cell migration in a 3D environment was unable to be conducted. As 3D cell migration more accurately reflects a normal cellular environment, conducting research in a 3D environment, for example, through the use of spheroids, would provide further insight into the effects of EB2 expression on cell migration mode.

Conclusions

Overall, EB2 as a significant effect on cell migration through affecting the organisation of MTs. Additionally, EB2 expression does not appear to be regulated by FGFR3 in PANC1 cells and therefore the mechanism by which the expression of this protein is regulated still needs to be elucidated.

5. References

Abiatari, I., DeOliveira, T., Kerkadze, V., Schwager, C., Esposito, I., Giese, N., Huber, P., Bergman, F., Abdollahi, A., Friess, H. and Kleeff, J., 2009a. Consensus transcriptome signature of perineural invasion in pancreatic carcinoma. *Molecular Cancer Therapeutics*, 8(6), pp.1494–1504.

Abiatari, I., Gillen, S., DeOliveira, T., Klose, T., Bo, K., Giese, N., Friess, H. and Kleeff, J., 2009b. The microtubule-associated protein MAPRE2 is involved in perineural invasion of pancreatic cancer cells. *International Journal of Oncology*, 35(5), pp.1111-1116.

Akhmanova, A. and Hoogenraad, C., 2005. Microtubule plus-end-tracking proteins: mechanisms and functions. *Current Opinion in Cell Biology*, 17(1), pp.47-54.

Akhmanova, A. and Steinmetz, M., 2010. Microtubule +TIPs at a glance. *Journal of Cell Science*, 123(20), pp.3415-3419.

Amano, M., Ito, M., Kumura, K., Fukata, Y., Chihara, K., Nakano, T., Matsuura, Y. and Kaibuchi, K., 1996. Phosphorylation and Activation of Myosin by Rho-associated Kinase (Rho-kinase)*. *Journal of Biological Chemistry*, 271(34), pp.20246-20249.

Amin, E., Dubey, B., Zhang, S., Gremer, L., Dvorsky, R., Moll, J., Taha, M., Nagel-Steger, L., Piekorz, R., Somlyo, A. and Ahmadian, M., 2013. Rho-kinase: regulation, (dys)function, and inhibition. *Biological Chemistry*, 394 (11), pp. 1399-1410.

Azoitei, M., Noh, J., Marston, D., Roudot, P., Marshall, C., Daugird, T., Lisanza, S., Sandí, M., Ikura, M., Sondek, J., Rottapel, R., Hahn, K. and Danuser, G., 2019. Spatiotemporal dynamics of GEF-H1 activation controlled by microtubule- and Src-mediated pathways. *Journal of Cell Biology*, 218(9), pp.3077-3097.

Baltussen, L.L., Negraes, P.D., Silvestre, M., Claxton, S., Moeskops, M., Christodoulou, E., Flynn, H.R., Snijders, A.P., Muotri, A.R., and Ultanir, S.K., 2018. Chemical genetic identification of CDKL5 substrates reveals its role in neuronal microtubule dynamics. *The EMBO Journal*, 37 (24).

Barc J, Tadros R, Glinge C, Chiang DY, Jouni M, Simonet F, Jurgens SJ, Baudic M, Nicastro M, Potet F, Offerhaus JA, Walsh R, Choi SH, Verkerk AO, Mizusawa Y, Anys S, Minois D, Arnaud M, Duchateau J, Wijeyeratne YD, Muir A, Papadakis M, Castelletti S, Torchio M, Ortuño CG, Lacunza J, Giachino DF, Cerrato N, Martins RP, Campuzano O, Van Dooren S, Thollet A, Kyndt F, Mazzanti A, Clémenty N, Bisson A, Corveleyn A, Stallmeyer B, Dittmann S, Saenen J, Noël A, Honarbakhsh S, Rudic B, Marzak H, Rowe MK, Federspiel C, Le Page S, Placide L, Milhem A, Barajas-Martinez H, Beckmann BM, Krapels IP, Steinfurt J, Winkel BG, Jabbari R, Shoemaker MB, Boukens BJ, Škorić-Milosavljević D, Bikker H, Manevy F, Lichtner P, Ribasés M, Meitinger T, Müller-Nurasyid M; KORA-Study Group, Veldink JH, van den Berg LH, Van Damme P, Cusi D, Lanzani C, Rigade S, Charpentier E, Baron E, Bonnaud S, Lecointe S, Donnart A, Le Marec H, Chatel S, Karakachoff M, Bézieau S, London B, Tfelt-Hansen J, Roden D, Odening KE, Cerrone M, Chinitz LA, Volders PG, van de Berg MP, Laurent G, Faivre L, Antzelevitch C, Kääb S, Arnaout AA, Dupuis JM, Pasquie JL, Billon O, Roberts JD, Jesel L, Borggrefe M, Lambiase PD, Mansourati J, Loeys B, Leenhardt A, Guicheney P, Maury P, Schulze-Bahr E, Robyns T, Breckpot J, Babuty D, Priori SG, Napolitano C; Nantes Referral Center for inherited cardiac arrhythmia, de Asmundis C, Brugada P, Brugada R, Arbelo E, Brugada J, Mabo P, Behar N, Giustetto C, Molina MS, Gimeno JR, Hasdemir C, Schwartz PJ, Crotti L, McKeown PP, Sharma S, Behr ER, Haissaguerre M, Sacher F, Rooryck C, Tan HL, Remme CA, Postema PG, Delmar M, Ellinor PT, Lubitz SA, Gourraud JB, Tanck MW, George AL Jr, MacRae CA, Burridge PW, Dina C, Probst V, Wilde AA, Schott JJ, Redon R, Bezzina CR., 2022. Genome-wide association analyses identify new Brugada

syndrome risk loci and highlight a new mechanism of sodium channel regulation in disease susceptibility. *Nature Genetics*, 54(5):735.

Bear, J. and Haugh, J., 2014. Directed migration of mesenchymal cells: where signaling and the cytoskeleton meet. *Current Opinion in Cell Biology*, 30, pp.74-82.

Becker, A., Hernandez, Y., Frucht, H. and Lucas, A., 2014. Pancreatic ductal adenocarcinoma: Risk factors, screening, and early detection. *World Journal of Gastroenterology*, 20(32), pp.11182–11198.

Bergert, M., Chandradoss, S., Desai, R. and Paluch, E., 2012. Cell mechanics control rapid transitions between blebs and lamellipodia during migration. *Proceedings of the National Academy of Sciences*, 109(36), pp.14434-14439.

Böhler, A., Vermeulen, B., Würtz, M., Zupa, E., Pfeffer, S. and Schiebel, E., 2021. The gamma-tubulin ring complex: Deciphering the molecular organization and assembly mechanism of a major vertebrate microtubule nucleator. *BioEssays*, 43(8), p.2100114.

Bos, J., Rehmann, H. and Wittinghofer, A., 2007. GEFs and GAPs: Critical Elements in the Control of Small G Proteins. *Cell*, 129(5), pp.865-877.

Brito, C. and Sousa, S., 2020. Non-Muscle Myosin 2A (NM2A): Structure, Regulation and Function. *Cells*, 9(7).

Buday, L. and Downward, J., 2007. Roles of cortactin in tumor pathogenesis. *Biochimica et Biophysica Acta (BBA) - Reviews on Cancer*, 1775 (2), 263–273.

Campellone, K. and Welch, M., 2010. A nucleator arms race: cellular control of actin assembly. *Nature Reviews Molecular Cell Biology*, 11(4), pp.237-251.

Cao, J., Yang, T., Tang, D.H., Zhou, F., Qian, Y.X., and Zou, X.P., 2019. Increased expression of GEF-H1 promotes colon cancer progression by RhoA signaling. *Pathology - Research and Practice*, 215 (5), 1012–1019.

Carey, S.P., Rahman, A., Kraning-Rush, C.M., Romero, B., Somasegar, S., Torre, O.M., Williams, R.M., and Reinhart-King, C.A., 2015. Comparative mechanisms of cancer cell migration through 3D matrix and physiological microtracks. *American Journal of Physiology-Cell Physiology*, 308(6).

Carpenter, A.E., Jones, T.R., Lamprecht, M.R., Clarke, C., Kang, I., Friman, O., Guertin, D.A., Chang, J., Lindquist, R.A., Moffat, J., Golland, P., and Sabatini, D.M., 2006. *Genome Biology*, 7(10).

Chen, Q., Zhu, Y.-C., Yu, J., Miao, S., Zheng, J., Xu, L., Zhou, Y., Li, D., Zhang, C., Tao, J., and Xiong, Z.-Q., 2010. CDKL5, a protein associated with Rett syndrome, regulates neuronal morphogenesis via Rac1 signaling. *Journal of Neuroscience*, 30 (38), 12777–12786.

Conti, M. and Adelstein, R., 2008. Nonmuscle myosin II moves in new directions. *Journal of Cell Science*, 121(1), pp.11–18.

Coulombe, P. and Wong, P., 2004. Cytoplasmic intermediate filaments revealed as dynamic and multipurpose scaffolds. *Nature Cell Biology*, 6(8), 699–706.

Dai, X., Xiang, L., Li, T. and Bai, Z., 2016. Cancer Hallmarks, Biomarkers and Breast Cancer Molecular Subtypes. *Journal of Cancer*, 7(10), 1281–1294.

Deakin, N. O. and Turner, C. E., 2008. Paxillin comes of age. *Journal of Cell Science*, 121(15), 2435-2444.

Di Nardo, A., Rühmkorf, A., Award, P., Brennecke, A., Fagiolini, M., and Sahin, M., 2022. Phenotypic characterization of CDKL5-knockdown neurons establishes elongated cilia as a functional assay for CDKL5 deficiency disorder. *Neuroscience Research*, 176, 73–78.

Dominguez, R. and Holmes, K., 2011. Actin Structure and Function. *Annual Review of Biophysics*, 40, pp.169–186.

Dow, L.E., Humbert, P.O., 2007. Polarity regulators and the control of epithelial architecture, cell migration, and tumorigenesis, *International Review of Cytology*, 253–302.

Dvorsky, R., Blumenstein, L., Vetter, I.R., and Ahmadian, M.R., 2004. Structural insights into the interaction of Rocki with the switch regions of rhoa. *Journal of Biological Chemistry*, 279(8), 7098–7104.

El-Gendi, S., Abdelzaher, E., Mostafa, M. and Sheasha, G., 2015. FGF18 as a potential biomarker in serous and mucinous ovarian tumors. *Tumor Biology*, 37(3), 3173–3183.

Eppinga, R., Kreuger, E., Weller, S., Zhang, L., Cao, H. and McNiven, M., 2012. Increased Expression of the Large GTPase Dynamin 2 Potentiates Metastatic Migration and Invasion of Pancreatic Ductal Carcinoma. *Oncogene*, 31(10), 1228–1241.

Etienne-Manneville, S., 2013. Microtubules in Cell Migration. *Annual Review of Cell and Developmental Biology*, 29, 471 - 499.

Etienne-Manneville, S., 2008., Polarity proteins in migration and invasion. *Oncogene*, 27(55), 6970-6980.

Etienne-Manneville, S., Hall, A., 2001. Integrin-mediated activation of CDC42 controls cell polarity in migrating astrocytes through pkcζ, *Cell*, 106(4), 489–498.

Ferlay, J., Partensky, C. and Bray, F., 2016. More deaths from pancreatic cancer than breast cancer in the EU by 2017. *Acta Oncologica*, 55(9-10), 1158-1160.

Fletcher, D. and Mullins, R., 2010. Cell mechanics and the cytoskeleton. *Nature*, 463(7280), 485–492.

Fujiwara, I., Vavylonis, D. and Pollard, T., 2007. Polymerization kinetics of ADP- and ADP-Pi-actin determined by fluorescence microscopy. *Proceedings of the National Academy of Science of the United States of America*, 104(21), 8827–8832.

Gardner, M., Zanic, M. and Howard, J., 2013. Microtubule catastrophe and rescue. *Current Opinion in Cell Biology*, 25(1), 14-22.

Gauglhofer, C., Sagmeister, S., Schrottmaier, W., Fischer, C., Rodgarkia-Dara, C., Mohr, T., Stättner, S., Bichler, C., Kandioler, D., Wrba, F., Schulte-Hermann, R., Holzmann, K., Grusch, M., Marian, B., Berger,

W. and Grasl-Kraupp, B., 2011. Up-regulation of the fibroblast growth factor 8 subfamily in human hepatocellular carcinoma for cell survival and neoangiogenesis. *Hepatology*, 53(3), 854-864.

Goldspink, D., Gadsby, J., Bellett, G., Keynton, J., Tyrrell, B., Lund, E., Powell, P., Thomas, P. and Mogensen, M., 2013. The microtubule end-binding protein EB2 is a central regulator of microtubule reorganisation in apico-basal epithelial differentiation. *Journal of Cell Science*, 126(17), 4000–4014.

Gong, L., Xiao, M., He, D., Hu, Y., Zhu, Y., Xiang, L., Bao, Y., Liu, X., Zeng, Q., Liu, J., Zhou, M., Zhou, Y., Cheng, Y., Zhang, Y., Deng, L., Zhu, R., Lan, H. and Cao, K., 2020. WDHD1 Leads to Cisplatin Resistance by Promoting MAPRE2 Ubiquitination in Lung Adenocarcinoma. *Frontiers in Oncology*, 10, 461.

Gong, S., 2014. Isoforms of Receptors of Fibroblast Growth Factors. *Journal of Cellular Physiology*, 229(12), 1887-1895.

Goodson, H. and Jonasson, E., 2018. Microtubules and Microtubule-Associated Proteins. *Cold Spring Harbor Perspectives in Biology*, 10(6).

Gowda, V., Srinivasan, V., Reddy, V. and Bhat, M., 2021. Rare cause of west syndrome secondary to tubulinopathy due to congenital symmetric circumferential skin creases (CSCSC) kunze type due to a novel variant in MAPRE2 gene. *Annals of Indian Academy of Neurology*, 25(2), 283-285.

Griffiths, G. and Lucocq, J.M. 2014, Antibodies for immunolabeling by light and electron microscopy: Not for the faint hearted, *Histochemistry and Cell Biology*, 142(4), 347–360.

Gu, C., Lee, H., Garborcauskas, G., Reiser, J., Gupta, V. and Sever, S., 2017. Dynamin Autonomously Regulates Podocyte Focal Adhesion Maturation. *Journal of the American Society of Nephrology*, 28(2), 446-451.

Hartmann, S., Ridley, A. and Lutz, S., 2015. The Function of Rho-Associated Kinases ROCK1 and ROCK2 in the Pathogenesis of Cardiovascular Disease. *Frontiers in Pharmacology*, 6, 276.

Hartsthorne, D., Ito, M. and Erdödi, F., 1998. Myosin light chain phosphatase: subunit composition, interactions and regulation. *Journal of Muscle Research and Cell Motility*, 19(4), 325-41.

Heck, J., Ponik, S., Garcia-Mendoza, M., Pehlke, C., Inman, D., Eliceiri, K. and Keely, P., 2012. Microtubules regulate GEF-H1 in response to extracellular matrix stiffness. *Molecular Biology of the Cell*, 23(13), 2583–2592.

Heiser, L., Sadanandam, A., Kuo, W., Benz, S., Goldstein, T., Ng, S., Gibb, W., Wang, N., Ziyad, S., Tong, F., Bayani, N., Hu, Z., Billig, J., Dueregger, A., Lewis, S., Jakkula, L., Korkola, J., Durinck, S., Pepin, F., Guan, Y., Purdom, E., Neuvial, P., Bengtsson, H., Wood, K., Smith, P., Vassilev, L., Hennessy, B., Greshock, J., Bachman, K., Hardwicke, M., Park, J., Marton, L., Wolf, D., Collisson, E., Neve, R., Mills, G., Speed, T., Feiler, H., Wooster, R., Haussler, D., Stuart, J., Gray, J. and Spellman, P., 2011. Subtype and pathway specific responses to anticancer compounds in breast cancer. *Proceedings of the National Academy of Sciences*, 109(8), 2724-2729.

Higgs, H., 2013. Actin Assembly/Disassembly. In: *Encyclopedia of Biological Chemistry*, 2nd ed. London: Academic Press, 12-17.

Hotulainen, P., and Lappalainen, P., 2006. Stress fibers are generated by two distinct actin assembly mechanisms in motile cells. *Journal of Cell Biology*, 173(3), 383–394.

Huang, Y., Tong, L., Yi, L., Zhang, C., Hai, L., Li, T., Yu, S., Wang, W., Tao, Z., Ma, H., Liu, P., Xie, Y. and Yang, X., 2017. Three-dimensional hydrogel is suitable for targeted investigation of amoeboid migration of glioma cells. *Molecular Medicine Reports*, 17(1), 250-256.

Im, K., Mareninov, S., Diaz, M.F. and Yong, W.H. 2018, An introduction to performing immunofluorescence staining", *Methods in Molecular Biology*, 299–311.

Ishizaki, T., Uehata, M., Tamechika, I., Keel, J., Nonomura, K., Maekawa, M. and Narumiya, S., 2000. Pharmacological Properties of Y-27632, a Specific Inhibitor of Rho-Associated Kinases. *Molecular Pharmacology*, 57(5), 976-983.

Isrie, M., Breuss, M., Tian, G., Hansen, A., Cristofoli, F., Morandell, J., Kupchinsky, Z., Sifrim, A., Rodriguez-Rodriguez, C., Dapena, E., Doonanco, K., Leonard, N., Tinsa, F., Moortgat, S., Ulucan, H., Koparir, E., Karaca, E., Katsanis, N., Marton, V., Vermeesch, J., Davis, E., Cowan, N., Keays, D. and Esch, H., 2015. Mutations in Either TUBB or MAPRE2 Cause Circumferential Skin Creases Kunze Type. *American Journal of Human Genetics*, 97(6), 790–800.

Itoh, N. and Ornitz, D., 2004. Evolution of the Fgf and Fgfr gene families. *Trends in Genetics*, 20(11), 563-569.

Jacobs, M., Hayakawa, K., Swenson, L., Bellon, S., Fleming, M., Taslimi, P. and Doran, J., 2006. The Structure of Dimeric ROCK I Reveals the Mechanism for Ligand Selectivity. *Journal of Biological Chemistry*, 281(1), 260-268.

Jakimiec, M., Paprocka, J., and Śmigiel, R., 2020. CDKL5 deficiency disorder—a complex epileptic encephalopathy. *Brain Sciences*, 10(2), 107.

Jiang, H., Qu, L., Wang, Y., Con, J., Wang, W. and Yang, X., 2014. miR-99a promotes proliferation targeting FGFR3 in human epithelial ovarian cancer cells. *Biomedicine & Pharmacotherapy*, 68(2), 163-169.

Johnson, K., Conant, E. and Soo, M., 2021. Molecular Subtypes of Breast Cancer: A Review for Breast Radiologists. *Journal of Breast Imaging*, 3(1), 12–24.

Joshi, S. and Yu, D. 2017 Immunofluorescence, *Basic Science Methods for Clinical Researchers*, 135–150.

Katsuda, S., Okada, Y., Nakanishi, I., and Tanaka, J., 1988. Inhibitory effect of dimethyl sulfoxide on the proliferation of cultured arterial smooth muscle cells: Relationship to the cytoplasmic microtubules. *Experimental and Molecular Pathology*, 48(1), 48–58.

Kennecke, H., Yerushalmi, R., Woods, R., Cheang, M., Voduc, D., Speers, C., Nielsen, T. and Gelmon, K., 2010. Metastatic Behavior of Breast Cancer Subtypes. *Journal of Clinical Oncology*, 28(20), 3271-3277.

Kim, S., Jang, S., Kim, H., Chung, S., Park, J. and Kuh, H., 2020. Phenotypic Heterogeneity and Plasticity of Cancer Cell Migration in a Pancreatic Tumor Three-Dimensional Culture Model. *Cancers*, 12(5), 1305.

Klein, O., Krier-Burris, R.A., Lazki-Hagenbach, P., Gorzalczany, Y., Mei, Y., Ji, P., Bochner, B.S., and Sagi-Eisenberg, R., 2019. Mammalian diaphanous-related Formin 1 (MDIA1) coordinates mast cell migration and secretion through its actin-nucleating activity. *Journal of Allergy and Clinical Immunology*, 144(4), 1074–1090.

Kollman, J., Merdes, A., Mourey, L. and Agard, D., 2011. Microtubule nucleation by γ-tubulin complexes. *Nature Reviews Molecular Cell Biology*, 12(11), 709–721.

Krakhmal, N., Zavyalova, M., Denisov, E., Vtorushin, S. and Perelmuter, V. (2015). Cancer Invasion: Patterns and Mechanisms. *Acta Naturae*, 7(2), 17-28.

Krendel, M., Zenke, F.T., and Bokoch, G.M., 2002. Nucleotide exchange factor GEF-H1 mediates cross-talk between microtubules and the actin cytoskeleton. *Nature Cell Biology*, 4(4), 294–301.

Kuroso, K., Imai, Y., Kobayashi, M., Yanagimoto, K., Suzuki, T., Kojima, M. and Ueda, Y., 2010. Immunohistochemical Detection of Fibroblast Growth Factor Receptor 3 in Human Breast Cancer: Correlation with Clinicopathological/ Molecular Parameters and Prognosis. *Pathobiology*, 77(5), 231–240.

Lafitte, M., Moranvillier, I., Garcia, S., Peuchant, E., Iovanna, J., Rousseau, B., Dubus, P., Guyonnet-Dupérat, V., Belleannée, G., Ramos, j., Bedel, A., de Verneuil, H., Moreau-Gaudry, F. and Dabernat, S., 2013. FGFR3 has tumor suppressor properties in cells with epithelial phenotype. *Molecular Cancer*, 12.

Lambert, A., Pattabiraman, D. and Weinberg, R., 2017. Emerging Biological Principles of Metastasis. *Cell*, 168(4), 670-691.

Lawrence, E., 2016. Metastasis. In: *Henderson's Dictionary of Biology*, 16th ed. Harlow: Pearson, 351.

Lee, S., Hong, J., Kim, K., Kim, K., Kang, S., Lee, T., Kim, S., Park, S., Park, Y., Lim, H., Kang, W., Lee, J. and Park, J., 2020. Detection of Fusion Genes Using a Targeted RNA Sequencing Panel in Gastrointestinal and Rare Cancers. *Journal of Oncology*.

Lemmon, M. and Schlessinger, J., 2010. Cell signaling by receptor-tyrosine kinases. *Cell*, 141(7), 1117–1134.

L'Hôte, C. and Knowles, M., 2005. Cell responses to FGFR3 signalling: growth, differentiation and apoptosis. *Experimental Cell Research*, 304(2), 417-431.

Li, H., Qiu, Z., Li, F. and Wang, C., 2017. The relationship between MMP-2 and MMP-9 expression levels with breast cancer incidence and prognosis. Oncology Letters, 14(5), pp.5865–5870.

Li, L., Zhang, S., Li, H. and Chou, H., 2019. FGFR3 promotes the growth and malignancy of melanoma by influencing EMT and the phosphorylation of ERK, AKT, and EGFR. *BMC Cancer*, 19.

Lieber, M., Mazzetta, J., Nelson-Rees, W., Kaplan, M. and Todaro, G., 1975. Establishment of a continuous tumor-cell line (PANC-1) from a human carcinoma of the exocrine pancreas. *International Journal of Cancer*, 15(5), 741-747.

Liu, H., Yue, J., Huang, H., Gou, X., Chen, S., Zhao, Y. and Wu, X. (2015). Regulation of Focal Adhesion Dynamics and Cell Motility by the EB2 and Hax1 Protein Complex. *Journal of Biological Chemistry*, 290(52), 30771-30782.

Liu, X., Jing, X., Cheng, X., Ma, D., Jin, Z., Yang, W. and Qui, W., 2016. FGFR3 promotes angiogenesis-dependent metastasis of hepatocellular carcinoma via facilitating MCP-1-mediated vascular formation. *Medical Oncology*, 33(5).

Long, X., Shi, Y., Ye, P., Guo, J., Zhou, Q. and Tang, Y., 2020. MicroRNA-99a Suppresses Breast Cancer Progression by Targeting FGFR3. *Frontiers in Oncology*, 68(2), 163-169.

Maurer, S., Bieling, P., Cope, J., Hoenger, A. and Surrey, T., 2011. GTPγS microtubules mimic the growing microtubule end structure recognized by end-binding proteins (EBs). *Proceedings of the National Academy of Sciences*, 108(10), 3988-3993.

McIntyre, L.J., and Kim, Y.S., 1984. Effects of sodium butyrate and dimethylsulfoxide on human pancreatic tumor cell lines. *European Journal of Cancer and Clinical Oncology*, 20(2), 265–271.

McNiven, M., Kim, L., Kreuger, E., Orth, J., Cao, H. and Wong, T., 2000. Regulated Interactions between Dynamin and the Actin-Binding Protein Cortactin Modulate Cell Shape. *Journal of Cell Biology*, 151(1), 187–198.

Meiring, J., Shneyer, B. and Akhmanova, A., 2020. Generation and regulation of microtubule network asymmetry to drive cell polarity. *Current Opinion in Cell Biology*, 62, 86-95.

Migliavacca, J., Züllig, B., Capdeville, C., Grotzer, M., and Baumgartner, M., 2022. Cooperation of striatin 3 and MAP4K4 promotes growth and tissue invasion. *Communications Biology*, 5(1).

Mitchison, T. and Kirschner, M., 1984. Dynamic instability of microtubule growth. *Nature*, 312(5991), 237-242.

Mizuno, H. and Watanabe, N., 2012. mDia1 and formins: screw cap of the actin filament. *Biophysics*, 8, 95-102.

Mustacchi, G., Sormani, M., Bruzzi, P., Gennari, A., Zanconati, F., Bonifacio, D., Monzoni, A. and Morandi, L., 2013. Identification and Validation of a New Set of Five Genes for Prediction of Risk in Early Breast Cancer. *International Journal of Molecular Sciences*, 14(5), 9686-9702.

Odell, I.D. and Cook, D., 2013. Immunofluorescence techniques, *Journal of Investigative Dermatology*, 133(1), 1–4.

Ohbayashi, N., Shibayama, M., Kurotaki, Y., Imanishi, M., Fujimori, T., Itoh, N. and Takada, S., 2002. FGF18 is required for normal cell proliferation and differentiation during osteogenesis and chondrogenesis. *Genes & Development*, 16(7), 870–879.

Olsen, S., Garbi, M., Zampieri, N., Eliseenkova, A., Ornitz, D., Goldfarb, M. and Mohammadi, M., 2003. Fibroblast growth factor (FGF) homologous factors share structural but not functional homology with FGFs. *The Journal of Biological Chemistry*, 278(36), 34226–34236.

Ornitz, D. and Itoh, N., 2015. The Fibroblast Growth Factor signaling pathway. *Wiley Interdisciplinary Reviews Developmental Biology*, 4(3), 215–266.

Östman, A. and Böhmer, F., 2001. Regulation of receptor tyrosine kinase signaling by protein tyrosine phosphatases. *Trends in Cell Biology*, 11(6), 258-266.

Paluch, E., Aspalter, I. and Sixt, M., 2016. Focal Adhesion–Independent Cell Migration. *Annual Review of Cell and Developmental Biology*, 32, 469-490.

Paňková, K., Rösel, D., Novotný, M. and Brábek, J., 2010. The molecular mechanisms of transition between mesenchymal and amoeboid invasiveness in tumor cells. *Cellular and Molecular Life Sciences*, 67(1), 63-71.

Parry, D., Strelkov, S., Burkhard, P., Aebi, U. and Herrmann, H., 2007. Towards a molecular description of intermediate filament structure and assembly. *Experimental Cell Research*, 313(10), 2204-2216.

Paur, J., Nika, L., Maier, C., Moscu-Gregor, A., Kostka, J., Huber, D., Mohr, T., Heffeter, P., Schrottmaier, W., Kappel, S., Kandioler, D., Holzmann, K., Marian, B., Berger, W., Grusch, M. and Grasl-Kraupp, B., 2015. Fibroblast growth factor receptor 3 isoforms: Novel therapeutic targets for hepatocellular carcinoma. *Hepatology*, 62(6), 1767-1778.

Perez, T., Bergès, R., Maccario, H., Oddoux, S. and Honoré, S., 2021. Low concentrations of vorinostat decrease EB1 expression in GBM cells and affect microtubule dynamics, cell survival and migration. *Oncotarget*, 12(4), 304-315.

Petrie, R., Gavara, N., Chadwick, R. and Yamada, K., 2012. Nonpolarized signaling reveals two distinct modes of 3D cell migration. *Journal of Cell Biology*, 197(3), pp.439–455.

Rafiq, S., Rahman, H. and Amin, K., 2020. The Estimate of Cytokines and Fibroblast Growth Factors in Patients with Breast Cancer. *Journal of Zankoy Sulaimani*, 22(2), 9-16.

Prolo, L.M., Li, A., Owen, S.F., Parker, J.J., Foshay, K., Nitta, R.T., Morgens, D.W., Bolin, S., Wilson, C.M., Vega L, J.C., Luo, E.J., Nwagbo, G., Waziri, A., Li, G., Reimer, R.J., Bassik, M.C., and Grant, G.A., 2019. Targeted genomic CRISPR-Cas9 screen identifies MAP4K4 as essential for glioblastoma invasion. *Scientific Reports*, 9(1).

Provenzano, P.P., Inman, D.R., Eliceiri, K.W., and Keely, P.J., 2009. Matrix density-induced mechanoregulation of breast cell phenotype, signaling and gene expression through a FAK–Erk Linkage. *Oncogene*, 28(49), 4326–4343.

Razidlo, G., Wang, Y., Cheng, J., Krueger, E., Billadeau, D. and McNiven, M., 2013. Dynamin 2 \ Potentiates Invasive Migration of Pancreatic Tumor Cells through Stabilization of the Rac1 GEF Vav1. *Developmental Cell*, 24(6), 573-585.

Ren, X.D., Kiosses, W.B., Sieg, D.J., Otey, C.A., Schlaepfer, D.D., and Schwartz, M.A., 2000. Focal adhesion kinase suppresses rho activity to promote focal adhesion turnover. *Journal of Cell Science*, 113(20), 3673–3678.

Renner, C., Pfitzenmeier, J., Gerlach, K., Held, G., Ohnesorge, S., Sahin, U., Bauer, S. and Pfreundschuh, M., 1997. RP1, a new member of the adenomatous polyposis coli-binding EB1-like gene family, is differentially expressed in activated T cells. *The Journal of Immunology*, 159(3), 1276-1283.

Roostalu, J., Thomas, C., Cade, N., Kunzelmann, S., Taylor, I. and Surrey, T., 2020. The speed of GTP hydrolysis determines GTP cap size and controls microtubule stability. *eLife*, 9.

Roth, D., Fitton, B., Chmel, N., Wasiluk, N. and Straube, A., 2018. Spatial positioning of EB family proteins at microtubule tips involves distinct nucleotide-dependent binding properties. *Journal of Cell Science*, 132(4).

Rottner, K., Faix, J., Bogdan, S., Linder, S. and Kerkhoff, E., 2017. Actin assembly mechanisms at a glance. *Journal of Cell Science*, 130(20), 3427–3435.

Sahai, E. and Marshall, C.J., 2003. Differing modes of tumour cell invasion have distinct requirements for rho/rock signalling and extracellular proteolysis. *Nature Cell Biology*, 5(8), 711–719.

Sajed, R., Zanjani, L., Rahimi, M., Mansoori, M., Zarnani, A., Madjd, Z. and Ghods, R., 2020. Overexpression and translocation of dynamin 2 promotes tumor aggressiveness in breast carcinomas. *EXCLI Journal*, 19, 1423–1435.

Schafer, D., Weed, S., Binns, D., Karginov, A., Parsons, J. and Cooper, J., 2002. Dynamin2 and Cortactin Regulate Actin Assembly and Filament Organization. *Current Biology*, 12(21), 1852-1857.

Schick, J. and Raz, E., 2022. Blebs—formation, regulation, positioning, and role in amoeboid cell migration. *Frontiers in Cell and Developmental Biology*, 10.

Scotet, E. and Houssaint, E., 1998. Exon III splicing switch of fibroblast growth factor (FGF) receptor-2 and -3 can be induced by FGF-1 or FGF-2. *Oncogene*, 17(1), 67–76.

Seetharaman, S. and Etienne-Manneville, S., 2020. Cytoskeletal Crosstalk in Cell Migration. *Trends in Cell Biology*, 30(9), 720-73.

Shi, J., Guo, B., Zhang, Y., Hui, Q., Chang, P. and Tao, K., 2016. Guanine nucleotide exchange factor H1 can be a new biomarker of melanoma. *Biologics: Targets and Therapy*, 10, 89-98.

Siegel, R., Miller, K. and Jemal, A., 2020. Cancer statistics, 2020. *CA: A Cancer Journal for Clinicians*, 70(1), 7-30.

Song, N., Zhong, J., Hu, Q., Gu, T., Yang, B., Zhang, J., Yu, J., Ma, X., Chen, Q., Qi, J., Liu, Y., Su, W., Feng, Z., Wang, X. and Wang, H., 2018. FGF18 Enhances Migration and the Epithelial-Mesenchymal Transition in Breast Cancer by Regulating Akt/GSK3β/BCatenin Signaling. *Cellular Physiology and Biochemistry*, 49(3), 1060-1073.

Spano, D., Heck, C., Antonellis, P., Christofori, G. and Zollo, M., 2012. Molecular networks that regulate cancer metastasis. *Seminars in Cancer Biology*, 22(3), 234-249.

St Johnston, D. and Ahringer, J., 2010. Cell Polarity in Eggs and Epithelia: Parallels and Diversity. *Cell*, 141(5), 757-774.

Su, L. and Qi, Y., 2001. Characterization of Human MAPRE Genes and Their Proteins. *Genomics*, 71(2), 142-149.

Sulimenko, V., Hájková, Z., Klebanovych, A. and Dráber, P., 2017. Regulation of microtubule nucleation mediated by γ-tubulin complexes. *Protoplasma*, 254(3), 1187-1199.

Sung, H., Ferlay, J., Siegel, R., Laversanne, M., Soerjomataram, I., Jemal, A. and Bray, F., 2021. Global Cancer Statistics 2020: GLOBOCAN Estimates of Incidence and Mortality Worldwide for 36 Cancers in 185 Countries. *CA: A Cancer Journal for Clinicians*, 71(3), 209-249.

Szarama, K., Stepanyan, R., Petralia, R., Gavara, N., Frolenkov, G., Kelley, M. and Chadwick, R., 2012. Fibroblast growth factor receptor 3 regulates microtubule formation and cell surface mechanical properties in the developing organ of Corti. *Bioarchitecture*, 2(6), pp.214-219.

Taddei, M., Giannoni, E., Morandi, A., Ippolito, L., Ramazzotti, M., Callari, M., Gandellini, P. and Chiarugi, P., 2014. Mesenchymal to amoeboid transition is associated with stem-like features of melanoma cells. *Cell Communication and Signalling*, 12(24).

Tesz, G.J., Guilherme, A., Guntur, K.V.P., Hubbard, A.C., Tang, X., Chawla, A., and Czech, M.P., 2007. Tumor necrosis factor α (TNFA) stimulates MAP4K4 expression through TNFA receptor 1 signaling to C-jun and activating transcription factor 2. *Journal of Biological Chemistry*, 282 (27), 19302–19312.

Teixidó-Travesa, N., Roig, J. and Lüders, J., 2012. The where, when and how of microtubule nucleation – one ring to rule them all. *Journal of Cell Science*, 125(19), 4445-4456.

Thompson, S.B., Wigton, E.J., Krovi, S.H., Chung, J.W., Long, R.A., and Jacobelli, J., 2018. The formin MDIA1 regulates acute lymphoblastic leukemia engraftment, migration, and progression in vivo. *Frontiers in Oncology*, 8.

Tojkander, S., Gateva, G., and Lappalainen, P., 2012. Actin stress fibers – assembly, dynamics and biological roles. *Journal of Cell Science*.

Totsukawa, G., Wu, Y., Sasaki, Y., Hartsthorne, D., Yamakita, Y., Yamashiro, S. and Matsumura, F., 2004. Distinct roles of MLCK and ROCK in the regulation of membrane protrusions and focal adhesion dynamics during cell migration of fibroblasts. *Journal of Cell Biology*, 164(3), 427–439.

Tovey, C. and Conduit, P., 2018. Microtubule nucleation by γ-tubulin complexes and beyond. *Essays in Biochemistry*, 62(6), 765–780.

Trepat, X., Chen, Z. and Jacobson, K., 2012. Cell Migration. *Comprehensive Physiology*, 2(4), 2369–2392.

Tripolitsioti, D., Kumar, K.S., Neve, A., Migliavacca, J., Capdeville, C., Rushing, E.J., Ma, M., Kijima, N., Sharma, A., Pruschy, M., McComb, S., Taylor, M.D., Grotzer, M.A., and Baumgartner, M., 2018. MAP4K4 controlled integrin β1 activation and C-met endocytosis are associated with invasive behavior of medulloblastoma cells. *Oncotarget*, 9(33), 23220–23236.

Trochet, D. and Bitoun, M., 2021. A review of Dynamin 2 involvement in cancers highlights a promising therapeutic target. *Journal of Experimental & Clinical Cancer Research volume*, (238).

Umemoto, S., Bengur, A. and Sellers, J., 1989. Effect of Multiple Phosphorylations of Smooth Muscle and Cytoplasmic Myosins on Movement in an in Vitro Motility Assay. *The Journal of Biological Chemistry*, 64(3), 1431-1436.

Usui, H., Shibayama, M., Ohbayashi, N., Konishi, M., Takada, S. and Itoh, N., 2004. Fgf18 is required for embryonic lung alveolar development. *Biochemical and Biophysical Research Communications*, 322(3), 887-892.

van Haren, J. and Wittmann, T., 2019. Microtubule Plus End Dynamics − Do We Know How Microtubules Grow?. *BioEssays*, 41(3), 1800194.

Vicente-Manzanares, M., Ma, X., Adelstein, R.S., and Horwitz, A.R., 2009. Non-muscle myosin II takes centre stage in cell adhesion and migration. *Nature Reviews Molecular Cell Biology*, 10(11), 778–790.

Vinogradova, T., Paul, R., Grimaldi, A., Loncarek, J., Miller, P., Yampolsky, D., Magidson, V., Khodjakov, A., Mogilner, A. and Kaverina, I., 2012. Concerted effort of centrosomal and Golgi-derived microtubules is required for proper Golgi complex assembly but not for maintenance. *Molecular Biology of the Cell*, 23(5), 820-833.

Watanabe, N., Kato, T., Fujita, A., Ishizaki, T. and Narumiya, S., 1999. Cooperation between mDia1 and ROCK in Rho-induced actin reorganization. *Nature Cell Biology*, 1(3), 136–143.

Weeks, A., Okolowsky, N., Golbourn, B., Ivanchuk, S., Smith, C. and Rutka, J., 2012. ECT2 and RASAL2 Mediate Mesenchymal-Amoeboid Transition In Human Astrocytoma Cells. *The American Journal of Pathology*, 181(2), 662-674.

Wei, W., Mok, S., Oliva, E., Kim, S., Mohapatra, G. and Birrer, M., 2013. FGF18 as a prognostic and therapeutic biomarker in ovarian cancer. *Journal of Clinical Investigation*, 123(10), 4435–4448.

Wu, D., Zhou, Y., Pan, H., Qu, P. and Zhou, J., 2015. microRNA-99a inhibits cell proliferation, colony formation ability, migration and invasion by targeting fibroblast growth factor receptor 3 in prostate cancer. *Molecular Medicine Reports*, 11(2), 1469-1475.

Wu, D., Zhou, Y., Pan, H., Zhou, J., Fan, Y. and Qu, P., 2014. microRNA-99a inhibiting cell proliferation, migration and invasion by targeting fibroblast growth factor receptor 3 in bladder cancer. *Oncology Letters*, 7(4), 1219–1224.

Wu, Z., Chen, H., Liang, Y., Luo, W., Deng, F. and Zeng, F., 2020. Alternative splicing implicated in immunity and prognosis of colon adenocarcinoma. *International Immunopharmacology*, 89 Part B.

Xue, B. and Robinson, R., 2013. Guardians of the actin monomer. *European Journal of Cell Biology*, 92(10-11), 316-332.

Yamada, K. and Sixt, M., 2019. Mechanisms of 3D cell migration. *Nature Reviews Molecular Cell Biology*, 20(12), 738-752.

Yamana, N., Arakawa, Y., Nishino, T., Kurokawa, K., Tanji, M., Itoh, R.E., Monypenny, J., Ishizaki, T., Bito, H., Nozaki, K., Hashimoto, N., Matsuda, M., and Narumiya, S., 2006. The rho-MDIA1 pathway regulates cell polarity and focal adhesion turnover in migrating cells through mobilizing APC and c-src. *Molecular and Cellular Biology*, 26(18), 6844–6858.

Yoo, J., Jeong, M.-J., Cho, H.J., Oh, E.S., and Han, M.Y., 2005. Dynamin II interacts with syndecan-4, a regulator of focal adhesion and stress-fiber formation. *Biochemical and Biophysical Research Communications*, 328(2), 424–431.

Yue, J., Xie, M., Gou, X., Lee, P., Schneider, M. and Wu, X., 2014. Microtubules Regulate Focal Adhesion Dynamics through MAP4K4. *Developmental Cell*, 31(5), 572-585.

Yun, Y., Won, J., Jeon, E., Lee, S., Kang, W., Jo, H., Jang, J., Shin, U. and Kim, H., 2010. Fibroblast Growth Factors: Biology, Function, and Application for Tissue Regeneration. *Journal of Tissue Engineering*, 1(1).

Zhang, X., Ibrahimi, O., Olsen, S., Umemori, H., Mohammadi, M. and Ornitz, D., 2006. Receptor Specificity of the Fibroblast Growth Factor Family: The Complete Mammalian FGF Family. *Journal of Biological Chemistry*, 281(23), 15694–15700.

Zhong, F., Li, Y., Xu, C., Sun, B., Wang, J. and Yang, L., 2021. EB2 promotes hepatocellular carcinoma proliferation and metastasis via MAPK/ERK pathway by modulating microtubule dynamics. *Clinical Science*, 135(7), 847-864.

Zimmerman, N., Roy, I., Hauser, A., Wilson, J., Williams, C. and Dwinell, M., 2015. Cyclic AMP Regulates the Migration and Invasion Potential of Human Pancreatic Cancer Cells. *Molecular Carcinogenesis*, 54(3), 203-215.

Ziperstein, M., Guzman, A. and Kaufman, L., 2015. Breast Cancer Cell Line Aggregate Morphology Does Not Predict Invasive Capacity. *PLOS One*, 10(9).

Appendix

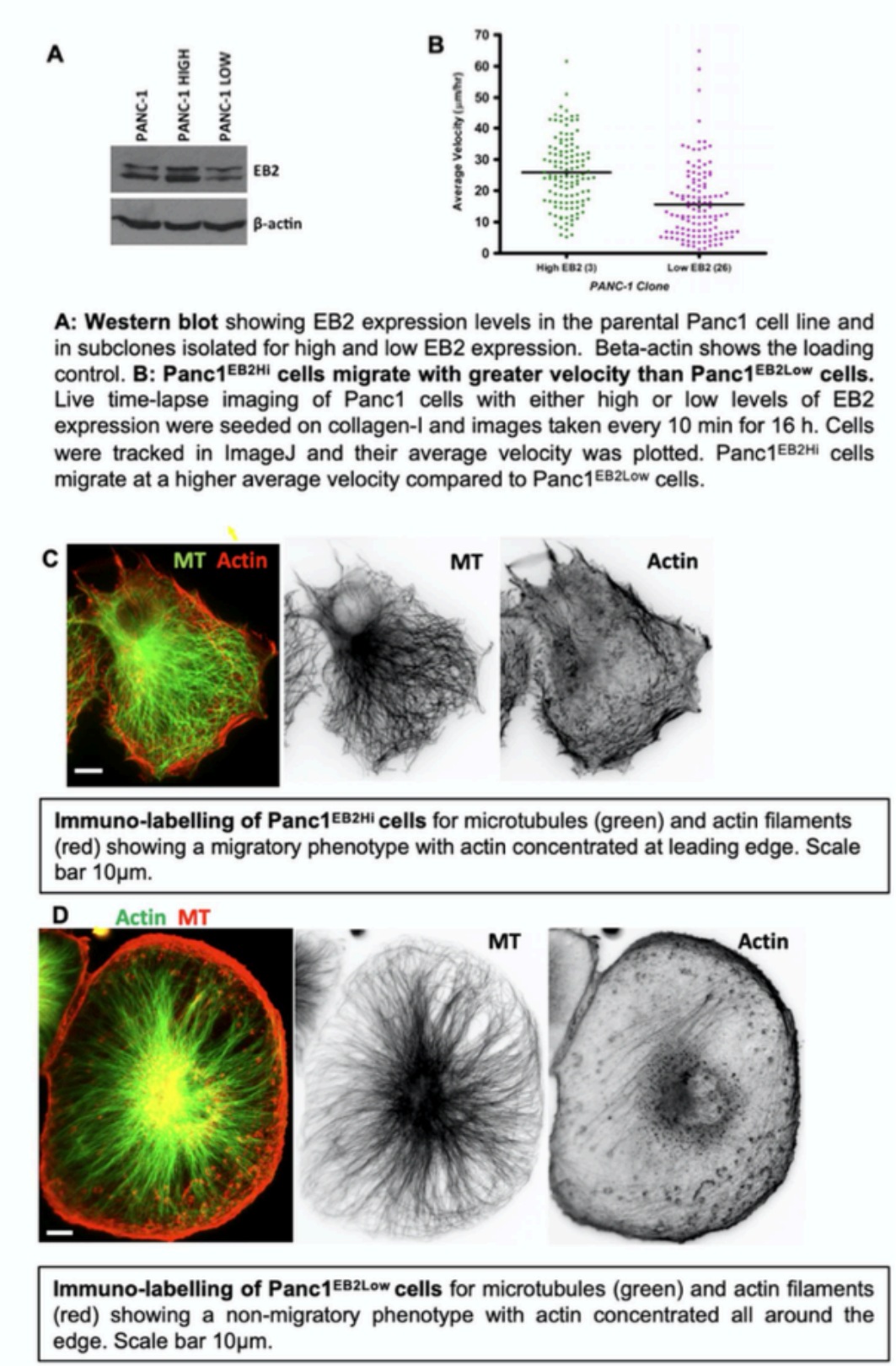

A: Western blot showing EB2 expression levels in the parental Panc1 cell line and in subclones isolated for high and low EB2 expression. Beta-actin shows the loading control. **B: Panc1^{EB2Hi} cells migrate with greater velocity than Panc1^{EB2Low} cells.** Live time-lapse imaging of Panc1 cells with either high or low levels of EB2 expression were seeded on collagen-I and images taken every 10 min for 16 h. Cells were tracked in ImageJ and their average velocity was plotted. Panc1^{EB2Hi} cells migrate at a higher average velocity compared to Panc1^{EB2Low} cells.

Immuno-labelling of Panc1^{EB2Hi} cells for microtubules (green) and actin filaments (red) showing a migratory phenotype with actin concentrated at leading edge. Scale bar 10μm.

Immuno-labelling of Panc1^{EB2Low} cells for microtubules (green) and actin filaments (red) showing a non-migratory phenotype with actin concentrated all around the edge. Scale bar 10μm.

Appendix 1. Preliminary data from the Mogensen lab showing the expression levels of EB2 in Panc-1^{EB2Hi} and Panc-1^{EB2Low} cells and its effect on random migration and cytoskeletal organisation.